USER- AND SPEED-ADAPTABILITY ENHANCEMENT OF USER GAIT PHASE

ESTIMATION FOR ROBOTIC TRANSFEMORAL PROSTHESIS CONTROL

A Dissertation

by

WOOLIM HONG

Submitted to the Graduate and Professional School of
Texas A&M University
in partial fulfillment of the requirements for the degree of

DOCTOR OF PHILOSOPHY

Chair of Committee,	Pilwon Hur
Co-Chair of Committee,	Reza Langari
Committee Members,	John J. Buchanan
	Kiju Lee
Head of Department,	Guillermo Aguilar

May 2022

Major Subject: Mechanical Engineering

ABSTRACT

Even if they are not aware of it, healthy humans walk stably and comfortably. Amputee patients, on the other hand, have difficulty performing stable and comfortable walking due to their missing limbs. Powered prostheses have been developed and studied by researchers for decades as a treatment to restore their gaits as closely as possible to those of healthy people. Nonetheless, amputees continue to have several gait deficiencies as a result of a lack of interaction between the users and their prostheses. The user's gait phase estimation is an important interacting factor. Because the user and the prosthesis should be treated as a coupled system, synchronized prosthesis control is required for stable walking and proper assistance. Researchers attempted to estimate user gait progression based on heel-strike, but this method is not adaptable to individual gait characteristics or speed change. As a result, the focus of this dissertation is on improving the adaptability of user gait phase estimation to individual gait traits and various walking speeds, allowing the powered prosthesis to provide a healthy human-like gait in a synchronized manner.

This dissertation makes three significant contributions to improving the estimation of the user gait phase during ambulation: i) phase-shifting method; ii) piecewise phase variable; and iii) machine learning-based estimation. First, we propose a custom-built powered transfemoral prosthesis and its underlying control framework capable of mimicking human behavior for stable and synchronized walking with the user. The first chapter then presents a phase-shifting method to improve the user adaptability of gait phase estimation. A phase variable is a kinematic variable that can be used in prosthesis control to estimate the user's gait phase. The thigh segment angle is particularly useful in calculating phase variables. Human data show that people have a cosine-like trend in their thigh segment movement while walking, which can be used to estimate their walking progression. However, a specific phase shift in the individual's thigh profile was discovered, reducing the gait phase estimation accuracy in the terminal swing phase. By compensating for this phase shift, the linearity of the phase variable was increased, and heel-strike detection was significantly improved. Furthermore, a piecewise phase variable is proposed to achieve better adaptation to different walk-

ing speeds. At different walking speeds, people have different toe-off timings. To account for this variable toe-off timing, we estimate toe-off at each gait cycle and adjust the slope of the phase variable based on the estimated toe-off timing. This allows for a more natural roll-over while walking. Additionally, while walking with the prosthesis, the enhanced and timely push-off was achieved. In the previous chapter, we investigated a learning-based gait phase estimation method to improve robustness and speed adaptability. Traditionally, in their model training, researchers provide a linearly interpolated label based on the heel-strike. This, however, cannot account for variable toe-off timing while training the given model. As a result, we propose a new piecewise linear label as the ground truth to improve the speed adaptability of gait phase estimation. As a result of the proposed method, we were able to obtain highly accurate gait phase prediction and heel-strike detection. As a result, it appears that compensating for phase shifts in the human thigh profile could improve user adaptability. We could also improve speed adaptability by reflecting variable toe-off timing at different walking speeds.

DEDICATION

This work is dedicated to my family. I also dedicate this work to my beloved Bomin Kim.

They have sincerely supported me with all their hearts and great care.

I couldn't have done this work without their patience, support and prayers.

Above all,

Glory to Almighty God, who always guides and rules my path.

ACKNOWLEDGMENTS

CONTRIBUTORS AND FUNDING SOURCES

NOMENCLATURE

OGAPS	Office of Graduate and Professional Studies at Texas A&M University
B/CS	Bryan and College Station
TAMU	Texas A&M University
IRB	Institutional Review Board
ACA	Amputee Coalition of America
MPC	Microprocessor-controlled
FSM	Finite state machine
CES	Cyber-expert system
WM	Wang and Mendel
HME	Human-expert
HIC	Human-inspired control
CWF	Canonical walking function
PHZD	Partial hybrid zero dynamics
GP	Gaussian process
DSR	Damping, stiffness, and re-positioning
SCSA	Stance-control, swing-assist
PD	Proportional-derivative
AVT	Active variable transmission
CESR	Controlled energy storage and return
COM	Center of mass
COP	Center of Pressure
HS	Heel-strike

FF	Flat-foot
HO	Heel-off
TO	Toe-off
IMU	Inertial measurement unit
LSTM	Long short-term memory
AMPRO II	A&M Prosthesis II
ROS	Robot operating system
PV	Phase variable
PS-PV	Phase-shifted phase variable
PW-PV	Piecewise phase variable
RMSE	Root-mean-square error
MSE	Mean-squared error
SD	Standard deviation
LE	Lyapunov exponent
GRF	Ground reaction force
ANOVA	Analysis of variance
GPE	Gait phase estimation
GM	General model
SM	Slow model
NFM	Normal-fast model
CNN	Convolutional neural network

TABLE OF CONTENTS

LIST OF FIGURES

LIST OF TABLES

1. INTRODUCTION

1.1 Motivation

According to [17], approximately 600,000 people in the United States had a major lower-limb amputation in 2005, and the amputee growth is predicted to double by 2050. According to the Amputee Coalition of America (ACA), approximately 185,000 new lower extremity amputations are performed each year [18]. Worldwide, this number reaches more than a million due to the global prevalence of diabetes by 2030 [19]. Lower-limb amputation is known to reduce amputees' mobility and dexterity in daily living, leaving patients vulnerable to fall and injury [20–24]. It also prevents amputees from participating in social activities due to reduced mobility [21, 25]. Lower-limb amputation, as a result, would have a significant psychological and physical impact on patients. Lower-limb amputations are classified according to the type of amputation [26]. The population with transfemoral (i.e., above-knee) amputation accounts for approximately 18.5% of the total amputee population [27], which is the second-largest group in the major lower-limb amputee population after the transtibial (i.e., below-knee) amputee population [18, 28]. It is worth noting that toe amputation is commonly excluded from major lower-limb amputation. Between these two most common amputee groups, the transfemoral amputee group typically faces more mobility challenges and is more prone to falling than the transtibial amputee group due to its larger portion of loss [22, 23]. This motivates us to focus on restoring transfemoral amputees' natural mobility by proposing an advanced treatment using a robotic prosthesis.

1.2 Transfemoral Prostheses

Lower-limb prostheses have evolved and are widely used to replace missing limbs in order to restore amputees' mobility, stability, and community participation [21, 25]. According to references [25, 29, 30], approximately 68% of amputees use a prosthesis for at least seven hours a day to aid their mobility and perform daily activities. Lower-limb prostheses are commonly categorized into three types: passive, microprocessor-controlled (MPC), and robotic (i.e., powered) prosthesis.

1.2.1 Passive prostheses

Passive prostheses (Figure 1.1.A) are widely regarded as the primary substitute for amputee locomotion due to their low cost and ease of use. Passive devices, on the other hand, do not provide an adequate substitute for compensating the power loss associated with a missing limb, which can result in an expensive metabolic cost [31]. This energy inefficiency worsens in complex walking scenarios, such as slope walking [32] or stair walking [33, 34]. Furthermore, they do not provide user-adaptive behavior (which is inherently stable and symmetric), potentially causing secondary impairment on the residual bodies of amputees in their long-term use [35, 36].
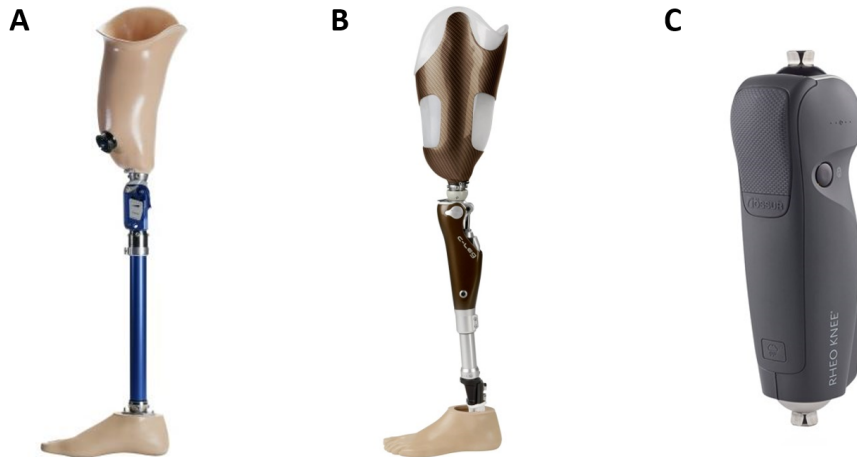
Figure 1.1: (A) Ottobock aqualine waterproof passive prosthesis. (B) Ottobock C-Leg. (C) Ossur Rheo Knee. "Adapted from [1–3]."

1.2.2 Microprocessor-controlled (MPC) prostheses

More advanced prostheses (e.g., Figures 1.1.B and C) are on the market for providing more compliant support to the user by modulating damping on the joint [2, 3, 37]. They also provide a swing motion via an inertial coupling-based mechanism between the thigh and the shank. This mechanism enables the knee joint to naturally coordinate with the user's movement. This device, however, has limited functional capability in a variety of ambulation scenarios, such as slope

2

or stair walking. Furthermore, such devices lack interactive control based on the users' walking condition or the users themselves, resulting in an atypical gait when compared to healthy people, according to [36]. According to [36], having a more human-like gait (i.e., symmetric gait) reduces asymmetry in terms of mechanical loading and muscle activation on the low back and lower extremity muscles.

1.2.3 Robotic prostheses

There have been several studies on robotic transfemoral prostheses due to their potential abilities to achieve a more natural human gait in broader walking scenarios: level walking [38–40], slope walking [41–43], stair walking [5, 44], and stumble recovery [45, 46]. Several control strategies can be used to operate the robotic prosthesis, including indirect control for optimum prosthesis performance or direct control of the prosthesis' joint kinematics.
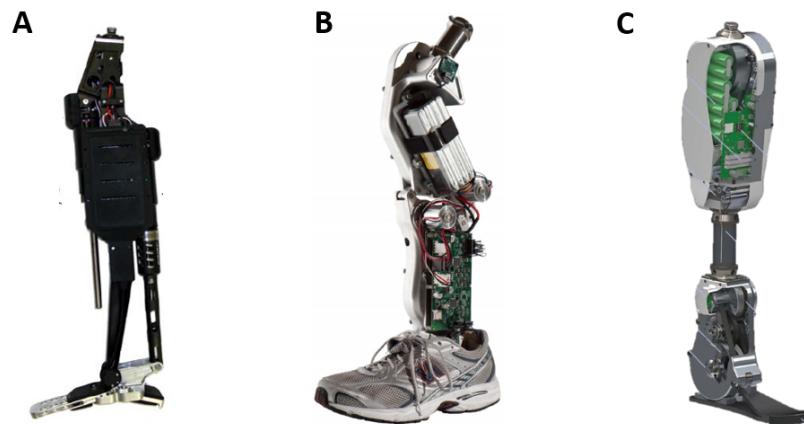
Figure 1.2: Three evolved versions of a robotic prosthesis by Vanderbilt University: (A) Vanderbilt Leg 1.0. (B) Vanderbilt Leg 2.0. (C) Vanderbilt Leg 3.0. "Adapted from [4–6]."

The impedance-based controller is well known for its adaptability and human-robot interaction in prosthesis control [39, 47–49]. Vanderbilt University researchers created robotic prostheses (Figure 1.2) that are controlled by a set of impedance parameters (e.g., stiffness K, damping D, and equilibrium angle θ_{eq}) as well as the user's walking progression for both ankle and knee [4,

39]. These impedance parameter sets are obtained by fitting the ankle and knee torque curves from human data to a non-linear spring-damper impedance model. They divide a gait cycle into several sub-phases and assign different parameter sets to improve such fits [4, 39]. Furthermore, they apply this concept to various walking scenarios, such as incline walking [41], stair walking [5], and sit-to-stand and vice versa [50]. This can be accomplished by incorporating different locomotion modes (i.e., finite-state machines (FSMs)) based on walking conditions. Their devices (Figure 1.2) perform admirably in all walking conditions with transfemoral amputees. However, difficulties arise when incorporating user feedback and joint sensors during walking trials [5, 41]. The more locomotion modes a prosthesis has, the more parameters must be tuned, resulting in a time-consuming tuning process. Because these control parameters must be personalized for each individual, the extensive tuning required prior to operation may limit amputees' practical use of the prosthesis. Several attempts have been made to use an automatic process rather than manual tuning by the prosthetist to reduce the burdensome tuning process [48, 49]. Researchers at the Georgia Institute of Technology proposed a 3-dimensional simulation framework implementation to reduce the burden of experimental tuning in the early stages of development, according to [49]. They use a stochastic optimization process to minimize the error according to the desired joint kinematics by tuning the impedance parameters (i.e., K, D, and θ_{eq}) on the simulation platform during the swing phase. Furthermore, Huang et al. proposed an auto-tuning method called cyber-expert system (CES) to reduce the effort of impedance parameter tuning for their robotic knee prosthesis [48]. Using the Wang and Mendel (WM) approach [51], they attempted to tune the parameters using CES based on three gait parameters: maximum knee flexion, gait phase duration, and maximum angular velocity. They evaluated CES performance by comparing pre- and post-tuning results for step length, gait symmetry, and trunk motion. Furthermore, human-expert (HME) pre- and post-tuning results were provided to validate their proposed method.

Human-inspired control (HIC) was proposed as an alternative to impedance control to force the prosthesis to track mathematically optimized human walking functions known as canonical walking functions (CWFs) [7, 8, 38, 52]. This control scheme guarantees the prosthesis's stability
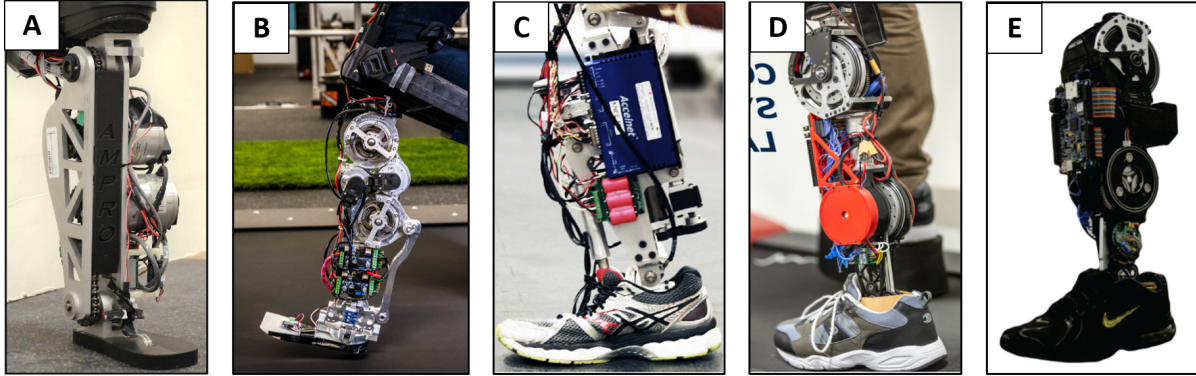
Figure 1.3: Robotic transfemoral prostheses developed at AMBER lab: (A) AMPRO I, (B) AM-PRO III, and at Locomotor Control Systems Laboratory: (C) Generation 1.0, (D) Generation 2.0, (E) Generation 3.0. "Adapted from [7–10]."

due to partial hybrid zero dynamics (PHZD), regardless of the impact from the heel-strike (see Figures 1.3.A and B). Furthermore, they do not require the discretized gait cycle (i.e., sub-phases) by using the parameterized gait cycle (i.e., phase variable), reducing the number of parameters and eliminating the possibility of phase switching malfunction. This control framework can be further extended to achieve more complex walking by proposing appropriate walking trajectories based on human data (e.g., incline walking [42], stair walking [44], and 3D walking [53]). However, in order to generate trajectories for various walking scenarios that satisfy PHZD constraints, a highly demanding optimization process is required, which cannot be done in real-time. As a result, depending on the environment, this hinders adaptive control of the prosthesis. Furthermore, because of its control property to intensively track the desired trajectories without user interaction, adhering control to kinematic trajectories is relatively less interactive. Gregg et al. reported another tracking method that used desired trajectories based on virtual constraints (see Figure 1.3.C) [9, 40]. This control method allows the prosthesis to have constrained joint trajectories, which can be used to achieve stable prosthetic walking [54–56]. Then, they utilized a model-free torque control using output proportional-derivative (PD) control. Since virtual constraints are obtained in relation to walking progression, it is critical in this framework to have a robust virtual constraint to reflect the user's walking [9, 57]. This approach further developed to perform a stable walking under the

perturbation [58], incline walking [59], and even non-rhythmic behaviors using different FSMs (e.g., backward walking, obstacle avoidance, and kicking [60]). High gain tracking, as previously indicated, inhibits the users' ability to keep compliant contact with the ground. To provide ground compliance and a free-swing for power reduction, a robotic transfemoral prosthesis incorporating high-torque, low-impedance actuators was recently designed (see Figures 1.3.D and E) [10].
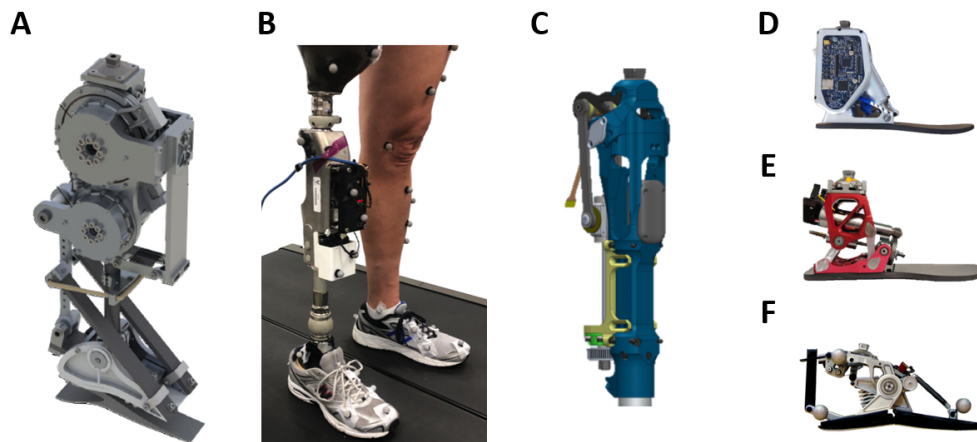
Figure 1.4: (A) Robotic prosthesis developed at Carnegie Mellon University. Semi-powered prosthesis by Vanderbilt University: (B) Knee and (D) Ankle. Powered prosthesis by University of Utah: (C) Knee and (E) Ankle. (F) Controlled energy storage and return (CESR) foot. "Adapted from [11–16]."

Several researchers have recently attempted to combine the aforementioned methods (i.e., impedance and tracking control) in order to reap the benefits of both methods at the same time [6, 12, 13, 43, 61, 62]. They used the impedance control during the stance phase to maintain a better interaction and the tracking control during the swing phase to improve tracking ability (e.g., sufficient dorsiflexion for stumble avoidance). This was motivated by the fact that impedance control requires careful attention during the swing phase because the prosthesis is not in contact with the ground, resulting in a lack of control during this phase. According to [63], this may induce foot-drop owing to gravity and stumbling if it does not give enough dorsiflexion on the ankle. However,

both control methods that use a predefined trajectory or impedance information have very limited action on the swing leg motion for maintaining the amputee's stability in the face of a large disturbance. Lawson et al. newly provide the desired trajectory with sufficient clearance, given from human data, when the large disturbance is detected, to improve recovery from stumbling [45]. This framework, on the other hand, necessitates the use of a separate stumble recognizer to respond to disturbances. Rather than using predefined information, a swing leg control using the target position based on local feedback was proposed at Carnegie Mellon University [64, 65]. Starting from the human-like double pendulum model [64], they developed a neuromuscular lower-limb model focusing on the modular control with local muscle reflexes [65]. Using this model, they successfully achieve a robust swing leg placement into various landing points and mimic the human joint torques and muscle activation [65]. They, further, develop the amputated human model combined with their prosthesis to investigate the prosthesis control based on muscle reflexes and local feedback [61]. The joint torques are generated by implementing a neuromuscular virtual model controller that simulates five muscles around the ankle and knee (e.g., a soleus, gastrocnemius, tibialis anterior, vastus, and biarticular hamstring), thereby actuating series elastic actuators on the prosthetic joints [61, 66]. Notably, both simulation studies [61, 64] and experimental studies [11, 46] demonstrate the robustness of local reflex control under perturbation. The proposed swing leg control can adapt and guide the foot placement into the new target position when disturbances (e.g., horizontal impulse on the foot [61, 64] or sudden changes in the target angle [64]) occur during the swing phase, according to [64]. These findings are assessed using their custom-built prosthesis, as shown in Figure 1.4.A, by varying the timing of the disturbances [11, 46]. It is reported that when the early- and late-disturbance are given during the swing, the subject's balance is reasonably recovered; however, it is not successful when the mid-disturbance is given. Thatte et al. add a distance sensor (e.g., LIDAR) to have environment-related information to estimate the device configuration for more robust trip avoidance [11]. This lets the prosthesis predict the hip trajectory using Gaussian Process (GP) model and provide reactive control to follow the newly generated trajectories. Their method reduces the probability of tripping, but there is still room for

7

testing different types of trip trigger with more subjects.

Despite the benefits of the aforementioned robotic prostheses, there is a trade-off against the increased size and weight of the prosthesis. Weight reduction has recently been attempted in the development of powered prostheses to incorporate the functional advantages of a robotic device as well as the benefit of a lightweight passive device. Vanderbilt University researchers propose a semi-powered ankle [13], knee [12] prosthesis. Damping, stiffness, and re-positioning (DSR) ankle prosthesis (Figure 1.4.D) can provide a human-like ankle modulation with sufficient swing-phase dorsiflexion despite its lightweight [13]. This achievement can be done by using a hybrid of hydraulic and electrical actuation. This proposed hybrid actuation is also utilized on their knee prosthesis, called stance-control, swing-assist (SCSA) prosthesis, depicted in Figure 1.4.B [12]. SCSA prosthesis allows the hydraulic stance control and PD swing control to provide stance knee stability and knee flexion/extension, respectively. They can, thus, achieve an energy-efficient performance due to their optimized mechanism design and lightweight while forgoing the substantial push-off by the prosthesis [12, 13]. Lenzi et al. also proposed a lightweight powered ankle-foot prosthesis based on polycentric mechanism in Figure 1.4.E [15]. The pylon (i.e., shank part) and the foot are connected with a seven-bar mechanism, combining one rotation and two translations. In conjunction with an actuation system, this mechanism could improve static stability and reduce socket torque. During the stance phase, they imposed a virtual impedance using either quasi-stiffness or impedance parameters (i.e., stiffness and damping) from the able-bodied subjects [15]. Further, they proposed a lightweight powered knee prosthesis, named Utah Knee (Figure 1.4.C), based on a slider-crank mechanism with an active variable transmission (AVT) [14, 67]. AVT adapts motor torque and speed output based on the demands of various ambulation activities, allowing the prosthesis to function in both active and passive modes. Utah Knee is only actively controlled for swing and ramp ambulation, while it is passively controlled during the stance phase via a spring-damper system. A stance energy injection, on the other hand, is thought to help with power swings and stair ambulation. This framework enables them to save motor power and select a smaller motor for weight reduction. Consequently, these powered devices are chosen to provide a lighter prosthesis

8

to the user while sacrificing the actuation power injection into the gait cycle [12–14, 62, 67]. They have, however, used a commercial prosthetic foot and are less concerned with developing a new foot for energy compensation during the stance phase. Collins et al. developed a controlled energy storage and return (CESR) prototype foot (Figure 1.4.F), which is able to regulate energy storage and return of a coil spring by using a contained active control element [16]. According to [68], the CESR foot can achieve greater energy storage/return, push-off power/work, and center of mass (COM) push-off than the conventional prosthetic foot. However, it has been reported that when they walk with CESR, their metabolic economy increases; they believe this is due to the weight of their prosthetic foot. [69] discovered that the softest spring has the highest energy storage/return value and prosthesis COM push-off work. However, in the metabolic economy, an intermediate spring condition has the lowest cost. In this regard, we can conclude that there is room for further investigation into the optimality of the prosthetic foot in terms of both energy storage/return and metabolic economy. This is difficult to achieve in the current approach due to the system's unavoidable weight limit. Furthermore, while a semi-powered prosthesis can lower the barrier to using an active-controlled prosthesis, it is still unclear whether a more interactive-controlled prosthesis that can communicate with the user and react to the environment around the user is possible. One obvious fact is that, regardless of the control scheme, estimating the user's walking state is critical for interactive control of the prosthesis in various situations.

1.3 User Gait Phase Estimation

User gait phase estimation has been widely studied due to its importance to control the lower-limb assistive devices, such as exoskeletons [70–73] or powered prostheses [40, 59, 74–77]. Such robotic devices should be real-time controlled and kept in sync with the user's walking state. Failure to synchronize with the user can result in instability and failure to provide adequate assistance to the user while walking [72, 77]. In order for wearable devices to provide synchronized control with the user, accurate gait phase estimation is required. There are two kinds of gait phase estimation studies. The first is a discrete gait phase estimation (also known as gait event detection), and the second is a continuous gait phase estimation.
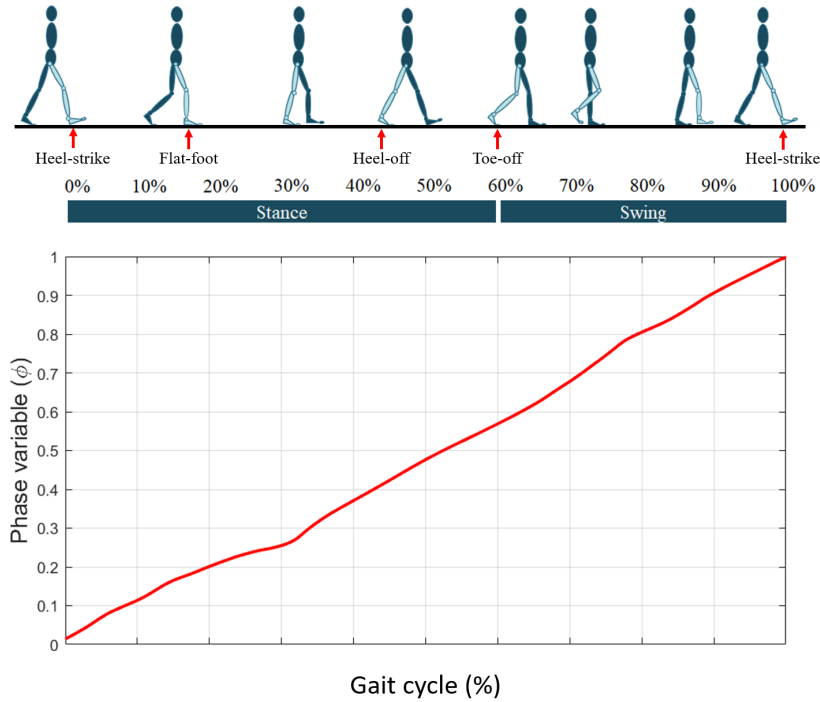
Figure 1.5: Human walking consists of several gait events depends on the contact constraints: heel-strike (HS), flat-foot (FF), heel-off (HO), and toe-off (TO). A discrete gait phase model is introduced based on theses events. The human walking phase also can be referred to the percentage of a gait cycle, resulting in a continuous gait phase.

A discrete gait phase is a common way to represent human walking using various wearable sensor sets [78]. Several gait phase models have been introduced in discrete gait phase estimation studies to divide a gait cycle into a different number of phases [79–83]. For example, based on heel-strike and toe-off detection, each gait cycle can be divided into two basic phases (stance and swing). [79, 80] proposed a rule-based algorithm for detecting heel-strike and toe-off using multiple sensor combinations. Furthermore, Kotiadis et al. detected heel-off based on shank information to add more phases to the gait cycle [81]. Hidden markov models have also been used by researchers to improve detection accuracy [82–84]. For controlling the wearable devices, these discrete gait phase estimators are typically combined with a finite-state machine (FSM) control scheme [39]. In this control scheme, a set of control parameters were given to a specific gait phase for proper control to the user, requiring a tedious tuning for each individual [63].

Because humans exhibit continuously varying joint kinematics/kinetics trends, having a continuous gait phase estimation would be more effective in the seamless control of wearable devices [43, 63, 85–87]. One method for estimating the user gait phase is to use a kinematic variable (i.e., phase variable) that changes only during locomotion [42, 43, 53, 58, 59, 88]. By parameterizing the entire gait cycle based on kinematic changes, this variable can tell the user's walking progression regardless of time. As a result, the phase variable allows the prosthesis to track the user's walking state and provide the appropriate control signals. The phase variable was calculated using the following kinematic data: tibia angle [88], linearized hip position [42, 53], and thigh angle [58, 59]. According to related studies, the phase variable must be i) strictly monotonic and bounded on [0,1] over time [58, 59, 89–91] and ii) purely controlled by the user [42, 53, 90]. The strict monotonicity and boundedness ensure a bijective mapping from the phase variable to 0-100% of the gait cycle (see Figure 1.5). To have full user authority, a phase variable must be determined by the user's actions rather than by the prosthetic. The following are notable computations of phase variables for prosthesis control using various types of kinematic data.

- **Tibia angle:** The tibia angle profile, as introduced by Holgate et al. [88], can be divided into two parts at roughly 70% of the gait cycle. Each divided part satisfies the user autonomy, monotonicity, and boundedness requirements. This phase variable allows the user to continuously control the prosthesis. The tibia information, however, can only be used with transtibial (below knee) amputees and not with transfemoral (above knee) amputees. As a result, this phase variable is restricted to transtibial prostheses.

- **Linearized hip position:** The researchers used a linearized hip position as the phase variable in transfemoral prosthesis control [38, 42, 53]. This variable is determined by inverse kinematics using the user's shank and thigh information and is a function of the user's horizontal hip position. The user's hip position exhibits a monotonic trend while walking. However, in order to measure the shank and thigh angles, users must wear sensors (e.g., IMUs) on their intact side, which is inconvenient. Furthermore, by using data from the intact leg to control the prosthesis, the prosthetic limb's autonomy is severely limited.

11

- **Thigh angle:** The residual leg's thigh angle shows a periodic movement during the gait cycle [58, 59, 89–91]. The residual thigh angle, unlike the tibia angle, can be controlled by both transtibial and transfemoral amputees. This eliminates the need for sensors on the intact limb as well. The resulting phase variable has shown reasonable estimation across different walking conditions: various speed [59], sloped terrains [43, 59], obstacle [92], and robustness under perturbations [58]. The thigh angle has been widely used in computing the phase variable for transfemoral prosthesis control due to its ease of implementation and consistency at different walking speeds.

Another approach is a learning-based gait phase estimation. As machine learning is currently being studied, many researchers attempted to use this technique to improve the accuracy and robustness of gait phase estimation [71, 72, 75, 76]. Because the machine-learning techniques used diverse kinematics/kinetics data from multiple sensors for model training, they were able to more precisely present human gait behavior. For instance, Seo et al. estimated the user gait phase in a continuous manner for their ankle exoskeleton [71]. For model training, they used shank-mounted inertial measurement units (IMUs) and additional foot pressure sensors. Researchers presented a learning-based gait phase estimator for their hip exoskeleton in [72]. Their neural network model was trained using data from several sensors, including hip encoder angles and Euler angles from the thigh IMU. They both achieved a robust and accurate estimation at dynamic walking speeds. [75, 76] attempted user gait phase estimation using the learning algorithm for the prosthesis application. Vu et al. proposed the new gait phase estimation algorithm to mitigate the accuracy reduction while achieving a densely discretized gait phase detection [75]. They trained their model using lower-shank data, predicting a full gait cycle within 1% interval [75]. Lee et al. made a more precise estimation using long short-term memory (LSTM) based on IMUs at thigh and torso information in a continuous manner at various walking speeds [76]. In [77], researchers proposed an online learning scheme based on individual user gait kinematics (i.e., thigh kinematics) to improve the gait phase estimator. Starting with a pre-trained general model, their model automatically refined the features based on individual gait kinematics. Weigand et al. applied their

gait phase estimation algorithm to stair walking with a single IMU at the shank [93]. They further compared the model-free estimation approach and the model-based estimation approach.

1.4 Contributions of the Dissertation

Even though many different studies have investigated user gait phase estimation for controlling the lower-limb assistive devices, there is still a gap when it is utilized with different users and at different speeds. Being adaptive to different users and to different speeds is more than necessary for providing proper control of the lower-limb robotic devices. In this dissertation, we focus on achieving gait phase estimation that can be adaptive to different individuals and to different walking speeds. We firstly aim to enhance the user adaptability of gait phase estimation. We focus on the inherent phase-shift of an individual's thigh kinematics and compensate for this shift to enhance the user adaptability in gait phase estimation. So, a phase-shifted phase variable is newly proposed in this chapter. We tested two variants of the proposed phase-shifted phase variable on a transfemoral prosthesis in an emulator study. Phase-shifting improves heel-strike detection, according to the results. Furthermore, phase-shifting improves the linearity of the phase variable throughout the gait cycle. Phase-shifting results in fewer deviations from the limit cycle, according to analysis of the knee and ankle phase portraits. In the second chapter, we attempt to be more adaptable to varying walking speeds while estimating the user's gait phase. The conventional phase variable cannot reflect variable toe-off timing at different speeds, despite the fact that people's toe-off timing varies with walking speed. Motivated by this discovery, we propose a new piecewise phase variable that can be adjusted for different toe-off timing at different walking speeds in order to maximize gait performance with a prosthesis. In a prosthetic walking experiment with an able-bodied and an amputee subject, we validated the proposed idea. The effects of the piecewise phase variable on gait performance (e.g., joint kinematics/kinetics and ground reaction forces) were measured and analyzed. As a result, both subjects show a faster load transfer with the piecewise phase variable. This allows the subjects to have a longer push-off duration with more push-off work during their walking. Furthermore, when the piecewise phase variable is used, both subjects have higher ground reaction forces at their prosthesis-side legs. This implies that

they had more trust in the given prosthesis with the proposed phase variable. In the final chapter, we focus on increasing the robustness of gait phase estimation at different walking speeds using a learning-based approach. In the learning-based gait phase estimation scheme, a linearly interpolated function based on heel-strike is the conventional way to generate the ground truth for the model training. However, this labeling method cannot reflect variable toe-off timing at different walking speeds while training the model. Thus, we propose a new labeling method (i.e., piecewise linear label) to train the estimator based on variable toe-off onset at different walking speeds. Using long short-term memory (LSTM), we obtained three different trained models (general, slow, and normal-fast). These models are compared in order to determine the effects of the piecewise linear label at various walking speeds. As a result, when the piecewise linear label was used in model training, the accuracy increased significantly. According to the findings of this chapter, the proposed labeling method could improve the adaptability of speed change in gait phase estimation, resulting in significantly higher accuracy.

1.5 Structure of the Dissertation

This section describes the dissertation's flow. The main objectives of the research, as well as the related research questions, are described in Chapter 2. Background knowledge is explained in Chapter 3 to help you understand the following content. Chapter 4 describes a new phase-shifting method for improving the user adaptability of gait phase estimation. In Chapter 5, a new piecewise phase variable is proposed to improve adaptation to different walking speeds while estimating the user gait phase. In Chapter 6, a learning-based gait phase estimation method is proposed to improve estimation robustness at different speeds. Furthermore, a new labeling method (i.e., piecewise label) is proposed to make gait phase estimation more adaptable to different speeds. We conclude all the remarks of the dissertation in Chapter 7.

2.   RESEARCH OBJECTIVES

User gait phase estimation is one of the most important aspects in the control of the robotic prosthesis. This is due to the fact that, when using the prosthesis, synchronization with the user must be guaranteed in order to avoid instability and maximize gait performance, which necessitates an accurate and adaptive estimation of the user's gait phase. In this dissertation, we thus focus on achieving more adaptive gait phase estimation for different individuals and to different walking speeds. Thus, the goal of this dissertation is to achieve more adaptive gait phase estimation for different individuals and walking speeds. First and foremost, we aim to improve different people's adaptability in gait phase estimation. Second, we aim to be able to estimate gait phase more adaptably to different walking speeds. We also aim to improve the robustness of gait phase estimation at various walking speeds. To achieve the stated goals, we can develop the four research questions listed below. It is worth noting that we begin to question how humans behave in the given situation.

1. While walking, humans have complex dynamics. How can this complex walking be represented as a walking progression, and how can it be used to control prosthetics?

2. Humans walk in a predictable pattern. Nonetheless, each individual may have a unique characteristic in their ambulation. If so, how can we measure them and apply them when estimating an individual's gait phase?

3. Humans can freely change their leg movement while walking at different speeds. So, how can we estimate the user's gait phase adaptively and provide interactive control to the user at different speeds?

4. Human dynamics change at different walking speeds. How can we ensure the robustness of gait phase estimation at various speeds?

3. BACKGROUNDS*

In this chapter, we explain a preliminary knowledge of human gait and our prosthetic system to help understand this dissertation better. We begin with a brief overview of human locomotion and gait phases. In addition, we describe the traditional method for computing the phase variable using human thigh data. This section also introduces the custom-built transfemoral prosthesis. We describe briefly the hardware of the prosthetic system as well as the control framework that we used in this dissertation.

3.1 Human Gait Phases
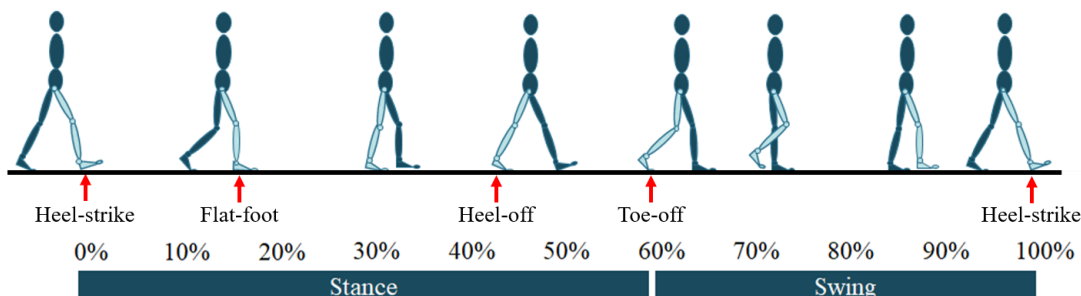
Figure 3.1: Human locomotion is a complex behavior comprised of several events such as heel-strike (HS), flat-foot (FF), heel-off (HO), and toe-off (TO).

To study human gait patterns, it is necessary to first comprehend what gait phases are and how they are defined. Human locomotion, as depicted in Figure 3.1, is a complex behavior consisting of several events such as heel-strike (HS), flat-foot (FF), heel-off (HO), and toe-off (TO) [78, 94].

When these events are considered, human gait can be divided into finite phases. The number of phases depends on how a single gait cycle is discretized, but human walking is simply considered to consist of two walking phases in this study: i) stance phase (from HS to TO) and ii) swing phase (from TO to another HS) (see Figure 3.1). In general, the stance phase is specified from 0% to 60% of the gait cycle, while the swing phase is specified for the remainder of the gait cycle [94]. The duration of the stance and swing phases, on the other hand, varies with walking speed because TO occurs at different timings at different walking speeds [95, 96].

3.2 Phase Variable Computation

As stated in Section 1.3, one approach to user gait phase estimation is the phase variable. Among several candidates for phase variable computation, thigh information is one of the most popular [58, 59, 89–91]. The conventional method of computing phase variables with thigh information will be covered in this section. When using the thigh information, the researchers made two assumptions below [58, 59, 89–91].

Assumption 1: A thigh angle profile (i.e., $\theta(t)$) is a cosine-like function.

Assumption 2: A thigh angle integral (i.e., $\Theta(t) = \int \theta(t) \, dt$) is a sine-like function.

Based on these assumptions, the phase portrait of thigh segment angle profile and its integral can be represented as an ellipse. As a result, the arc-tangent function can be used to calculate a phase variable, as shown below.

$$\Phi(t) = \frac{1}{2\pi} \operatorname{atan2}(k(\Theta(t) - \alpha), (\theta(t) - \beta)) \tag{3.1}$$

where the normalizing factors including the scale coefficient k, the amplitude shift of thigh integral α, and that of thigh angle β are defined by

$$k = \frac{|\theta_{max} - \theta_{min}|}{|\Theta_{max} - \Theta_{min}|}, \quad \alpha = \frac{|\Theta_{max} + \Theta_{min}|}{2}, \quad \beta = \frac{|\theta_{max} + \theta_{min}|}{2}. \tag{3.2}$$

17

To make $\Phi(t)$ bounded on [0,1], the final $\Phi(t)$ is generated as below:

$$\Phi(t) = \begin{cases} \Phi(t) & \text{for } \Phi(t) \geq 0 \\ \Phi(t) + 1 & \text{for } \Phi(t) < 0 \end{cases} \tag{3.3}$$

The normalizing factors (k, α, and β) help center the phase portrait ($\theta(t)$ vs. $\Theta(t)$) around the origin, reducing the non-linearity of the phase variable. The integral value is initialized when the heel-strike occurs, and the normalizing factors are updated every quarter gait cycle to maintain the orbital radius in the gait cycle [58, 59]. We will refer to the phase variable produced by this procedure as PV and denote it as $\Phi(t)$ throughout this paper.

3.3 A&M Powered Prosthetic System
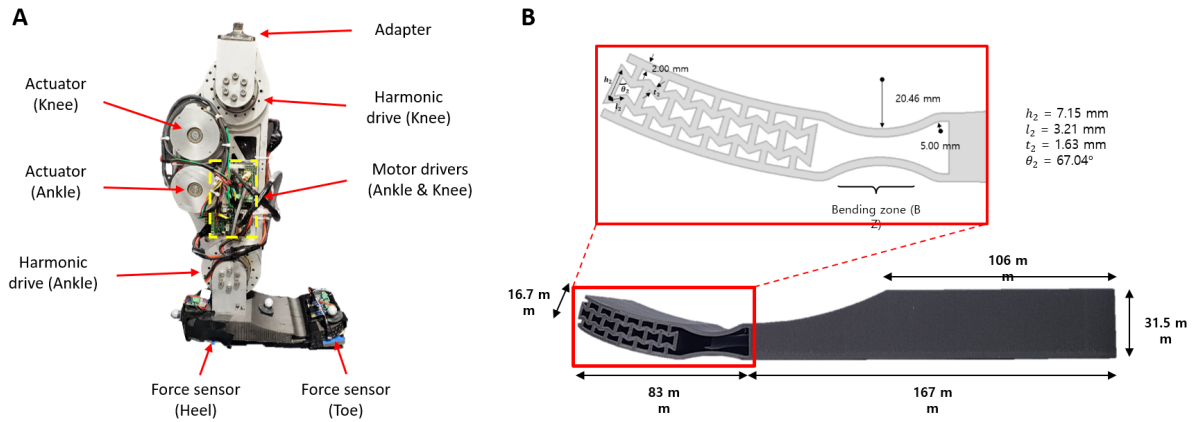
Figure 3.2: (A) AMPRO II is comprised of an actuated ankle, knee, and a passive toe joint. (B) Human-like toe joint using re-entrant structure and bending zone.

3.3.1 Hardware

The A&M Powered Prosthesis II (AMPRO II) is the second generation of Texas A&M University's custom-designed powered transfemoral prosthesis (see Figure 3.5.A). This device is fully actuated with two brushless DC (BLDC) motors (BN28, MOOG) positioned at the ankle and knee.

18

The AMPRO II is controlled by a three-tiered control framework that provides human-like joint control in accordance with the user's gait progression, which is estimated by a phase variable based on global thigh movement measured by a 9-axis IMU on the prosthesis. Force sensors (FlexiForce A502, Tekscan) are also used beneath the prosthetic foot to detect walking events (i.e., HS or PO) for switching from stance to swing phase, and vice versa. The IMU processor and high-level control (implemented by two BeagleBone Black boards, element14 operating at 200 Hz) are used to calculate the phase variable and detect the corresponding walking state during operation. The mid-level controller calculates and transmits the desired joint torques to the motor drivers (G-SOLWHI, ELMO) based on the detected walking state; these motor drivers control the two actuators at the lowest level via the Controller Area Network (CAN) protocol. Two high-resolution optical encoders (E5, US Digital) on the prosthesis measure the actual joint angles. All the joint kinematics and motor outputs were recorded in real-time using the rosbag function [97] (see Figure 3.3).
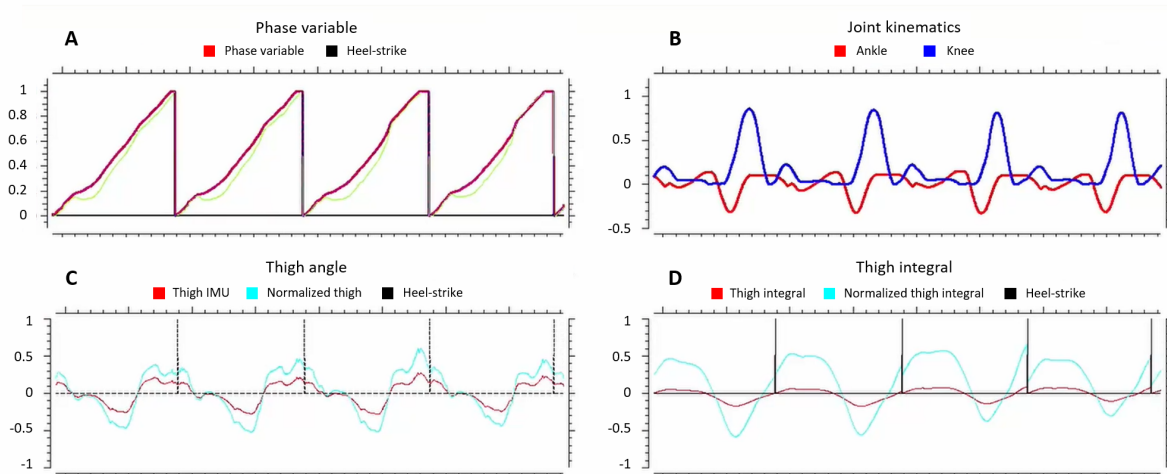
Figure 3.3: Real-time data recording. (A) Resulting phase variable using thigh kinematics. (B) Prosthetic ankle/knee kinematics from motor driver. (C) Thigh segment angle measured by IMU. (D) Thigh segment angular velocity measured by IMU.

Foot characteristics are also important in human walking because they interact with the ground during the stance phase [16, 69, 98–100]. Thus, we designed a new prosthetic foot using compliant

materials and structures (see Figure 3.5.B) to provide more human-like performance [101]. To maximize gait performance while walking, we specifically focus on mimicking human toe joint characteristics. To provide enough toe flexion and nonlinear toe joint characteristics, we used an auxetic structure (e.g., a re-entrant structure) and a bending zone. The toe joint was created as a single 3D printable part and was printed with short carbon fiber reinforced polymer filament (e.g., onyx). The printed foot was validated by comparing with the human walking data [102, 103] in the simulation. The simulation was conducted to investigate toe characteristics during the stance phase [101]. As shown in Figure 3.4.A, when human HO occurred during the stance phase, the ground reaction force (GRF) began to slowly decrease, and then the GRF decreased more rapidly as the COP decreased. The simulation result shows the similar trends during the stance phase. However, some discrepancies were found in the last period of the stance phase due to the gap between the re-entrant structure at the toe part. The ankle kinematics was also analyzed to validate the fixed condition of the ankle part in the simulation. When human TO occurred during the stance phase, the ankle torque-angle decreased as shown in Figure 3.4.B. The simulation result shows a similar trend compared to the human gait and is well in line with the maximum torque of human data.
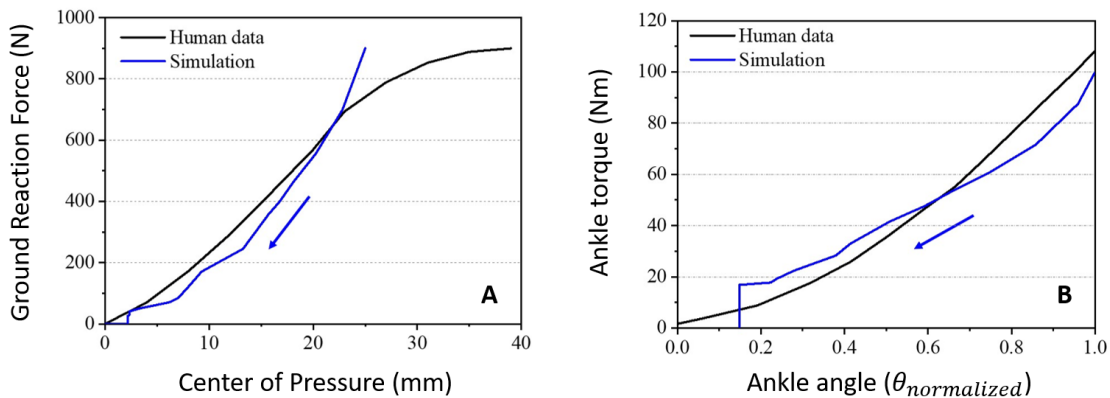
Figure 3.4: Comparison between simulation result and human data. (A) Ground reaction force according to the center of pressure (COP) (B) Ankle torque according to the normalized ankle angle.

3.3.2 Control framework

AMPRO II is controlled by a hybrid control framework that combines an impedance control and a tracking control [43, 74, 104]. In the stance phase, the impedance control framework is used to maximize interaction between the prosthesis and the user. During the swing phase, the tracking control framework is used to ensure foot clearance by tracking the human-like desired trajectories.
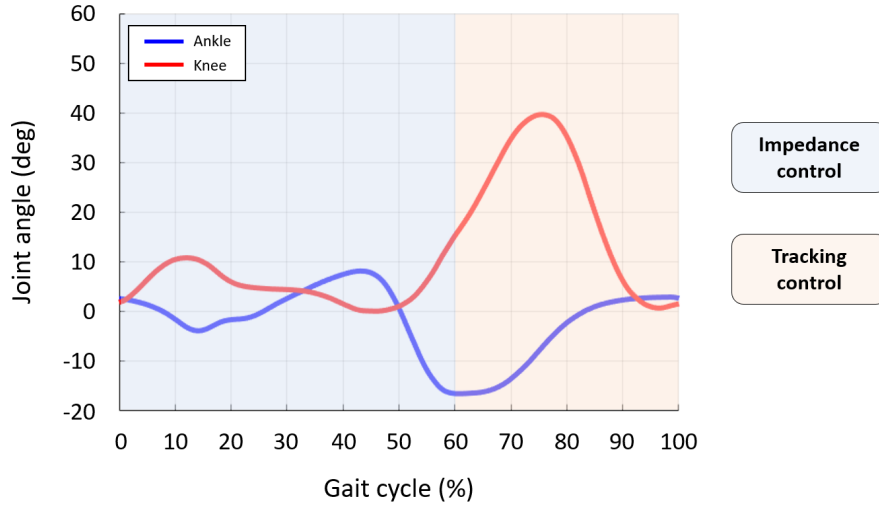
Figure 3.5: Hybrid control framework: impedance control (stance) and tracking control (swing).

3.3.2.1 Stance phase: impedance control

By interacting with the ground during the stance phase, we were able to simulate the various joint kinematics using an impedance control. Impedance control is a common strategy in which the control input to the joint is defined by the equation below.

$$\tau = K(\theta - \theta_{eq}) + D\dot{\theta} \tag{3.4}$$

The terms K and D represent the stiffness and damping parameters of the joint, respectively, while

θ and $\dot{\theta}$ represent the joint's angular position and velocity. The equilibrium angle of the joint is denoted by θ_{eq}. K, D, and θ_{eq} are referring to as impedance parameters. Impedance control with these parameters allows the prosthesis to adapt to the ground more interactively as the user's COM moves forward. The lower-limb joints (i.e., ankle and knee) in this framework were modeled as a spring-damper system, as in previous works [39, 47–49]. The majority of studies use a finite-state machine (FSM), which divides the gait cycle into several gait phases. Then, for each phase, a proper set of impedance parameters (i.e., K, D, and θ_{eq}) should be assigned. In other words, as more gait phases are added, the number of tuning parameters grows. This necessitates a time-consuming tuning procedure, which is a disadvantage of impedance control. Thus, we reduce the effort of the impedance control tuning process even further by implementing continuously varying impedance parameters that are virtually constrained depending on the phase variable [63, 104].

$$K^j(t) = \sum_{i=0}^{m} k_i^j t^i \quad \text{for} \quad 0 \le t < \phi_{TO} \tag{3.5}$$

$$D^j(t) = \sum_{i=0}^{n} d_i^j t^i \quad \text{for} \quad 0 \le t < \phi_{TO} \tag{3.6}$$

The ankle and knee modulation curves in our framework were generated using a least-square fit to the ankle and knee joint moment curves found in healthy human walking data, respectively [103]. During the stance phase of the given optimization problem, both stiffness and damping parameters were given by fourth-order polynomials to allow for continuous variation of both parameters, as described in Equations 3.5 and 3.6, where $j \in \{\mathbf{a}nkle, \mathbf{k}nee\}$.

Table 3.1: Stiffness and damping coefficients for ankle and knee joints.

i^{th} order	4	3	2	1	0
Ankle stiffness (k_i^a)	-23891	24295	-6882	611	24
Ankle damping (d_i^a)	56	-51	11	-1	0
Knee stiffness (k_i^k)	7039	-667	-4401	1311	98
Knee damping (d_i^k)	-1093	1356	-525	65	-0

Table 3.1 shows the stiffness and damping function coefficients. Impedance parameters given in Equations 3.5 and 3.6 represent the nominal stiffness and damping functions. These parameters should be tuned to provide gait performance according to the individual user by using normalizing and offset factors as follows in Equation 3.8. The actual tuned parameters are given in Table 3.2.

$$K_{tuned}^{j}(t) = \alpha^{j} K^{j}(t) + \gamma^{j} \tag{3.7}$$

$$D_{tuned}^{j}(t) = \beta^{j} D^{j}(t) \tag{3.8}$$

Table 3.2: Tuned parameters for ankle and knee.

$j \in \{a, k\}$	α^j	β^j	γ^j
Ankle tuning ($j = a$)	1	50	1
Knee tuning ($j = k$)	1	50	1

We varied three equilibrium angles based on gait phases (HS, FF, HO, and TO) while maintaining a single function for each stiffness and damping parameter (see Table 3.3). The resulting stiffness and damping functions of ankle and knee are illustrated in Figure 3.6. This ankle impedance trends obtained (see Figure 3.6.A) are well in line with previous studies [85, 86, 105].

Table 3.3: Equilibrium angles. Phase 1: HS–FF, Phase 2: FF–HO, and Phase 3: HO–TO.

Slope	Ankle equilibrium angles (deg)		
	Phase 1	Phase 2	Phase 3
0°	5.60	-11.06	-16.00
Slope	Knee equilibrium angles (deg)		
	Phase 1	Phase 2	Phase 3
0°	10.26	5.83	13.86
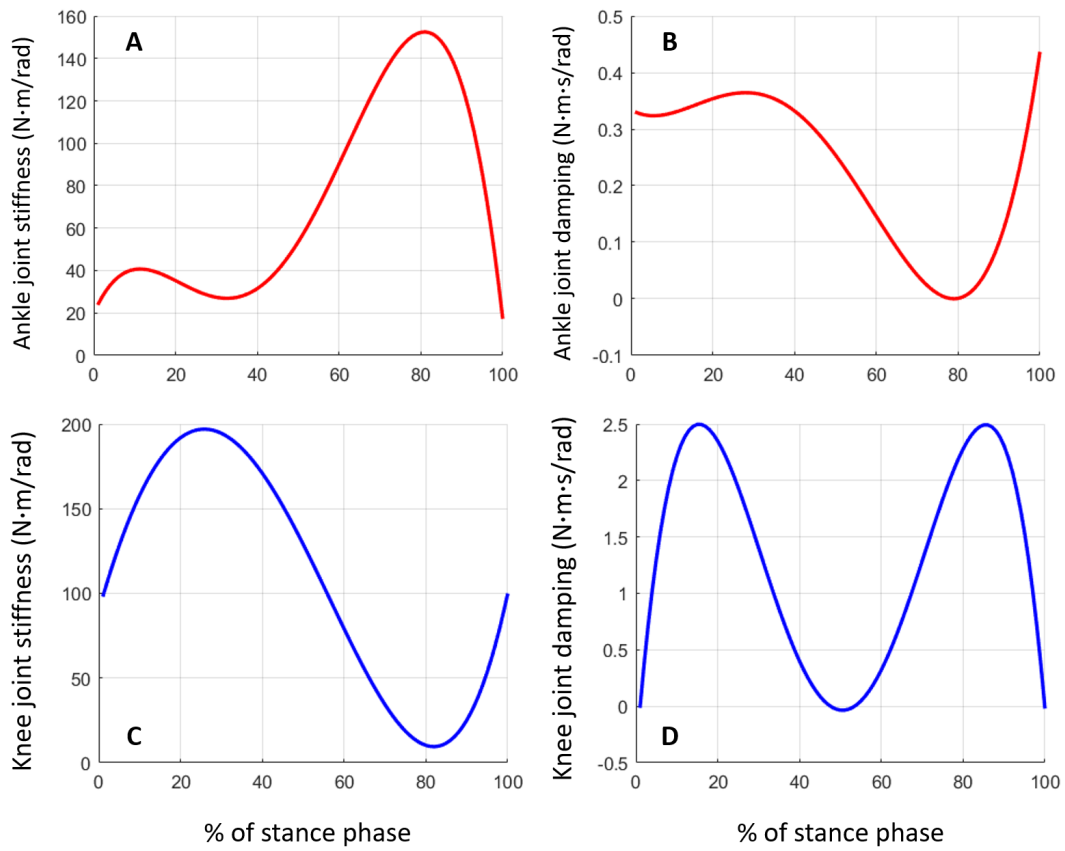
Figure 3.6: Resulting impedance parameters. (A) Ankle joint stiffness. (B) Ankle joint damping. (C) Knee joint stiffness. (D) Knee joint damping.

3.3.2.2   Swing phase: tracking control
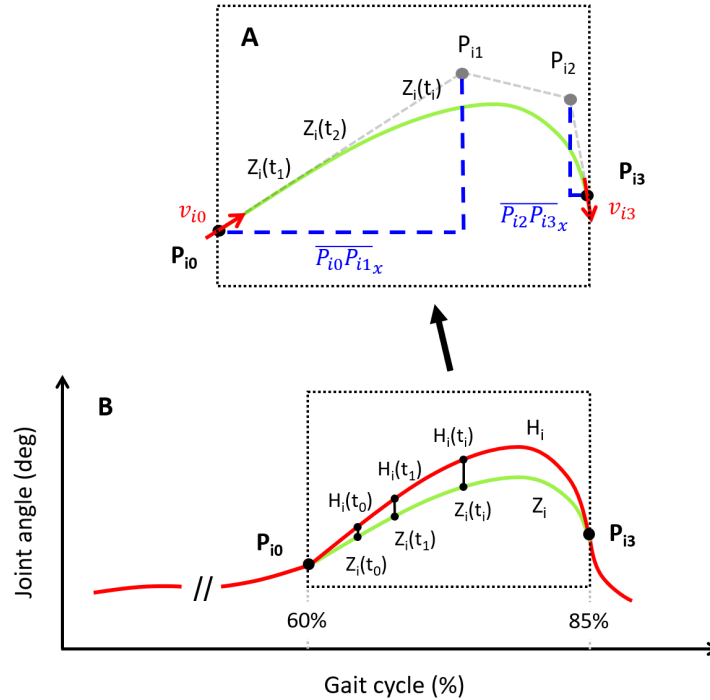
Figure 3.7: (A) Cubic Bezier polynomial with four control points ($P_{i0} - P_{i3}$). When P_{i0} and P_{i3} are fixed, the final curvature $Z_i(t)$ varies dramatically depending on the control points P_{i1} and P_{i2}. (B) Based on $Z_i(t)$, human walking optimization was performed comparing to the human data (H_i) for both joints, where $i \in \{\mathbf{a}\text{nkle}, \mathbf{k}\text{nee}\}$. It should be noted that the trajectory depicted in the figure is not a specific joint, but rather an arbitrary trajectory used to demonstrate the concept.

We used a tracking control during the swing phase to avoid tripping by following pre-defined ankle and knee trajectories [43,90]. This ensures a sufficient foot clearance during the swing phase. Cubic Bezier polynomials were used as the base function to generate the proper trajectories, where $t \in [0, 1]$ is related to the gait cycle (60–85%) and the control points ($P_{i0} - P_{i3}$) correspond to the proper joint angles:

$$Z_i(t) = (1 - t)^3 P_{i0} + 3t(1 - t)^2 P_{i1} + 3t^2(1 - t)P_{i2} + t^3 P_{i3} \tag{3.9}$$

The geometric relationship between the control points of Bezier polynomials is shown in Fig. 3.7.A. P_{i1} and P_{i2} can be re-described as follows using $P_{i0}, P_{i3}, v_{i0}, v_{i3}$, where $\overline{P_{i0}P_{i1}}_x$ and $\overline{P_{i2}P_{i3}}_x$ are the horizontal projections of $\overline{P_{i0}P_{i1}}$ and $\overline{P_{i2}P_{i3}}$, respectively.

$$
\begin{aligned}
P_{i1} &= (P_{i0} + \overline{P_{i0}P_{i1}}_x \cdot v_{i0}) \\
P_{i2} &= (P_{i3} - \overline{P_{i2}P_{i3}}_x \cdot v_{i3})
\end{aligned}
\tag{3.10}
$$

A least-square fit to the healthy human walking trajectories was used to generate both ankle and knee desired trajectories. As shown in Equation 3.11, the ankle and knee trajectories in the optimization problem were given by cubic Bezier polynomials to minimize the error between the Bezier curves (Z_i) and the human data (H_i) (see Figure 3.7.B).

$$
\begin{aligned}
\min_{x_{i1},\, x_{i2}} \; f &= ||Z_i(t) - H_i(\phi)|| \\
s.t \quad Z_i(0) &= H_i(0.60) = P_{i0} \\
Z_i(1) &= H_i(0.85) = P_{i3} \\
\dot{Z}_i(0) &= \dot{H}_i(0.60) = v_{i0} \\
\dot{Z}_i(1) &= \dot{H}_i(0.85) = v_{i3}
\end{aligned}
\tag{3.11}
$$

While satisfying the boundary conditions, Euclidean norm was utilized to find the optimal values which can minimize the defined objective function in Equation 3.11. In this problem, from the vector $X_i := [x_{i0},\ x_{i1},\ x_{i2},\ x_{i3}]^T = [P_{i0},\ \overline{P_{i0}P_{i1}}_x,\ \overline{P_{i2}P_{i3}}_x,\ P_{i3}]^T$, only x_{i1} and x_{i2} were treated as the free variables since $[x_{i0}, x_{i3}]^T = [P_{i0}, P_{i3}]^T$ were given by the assumption. MATLAB was used to solve Equation 3.11 as an offline optimization problem. Table 3.4 displays the optimal coefficients from the optimization problem. While operating the prosthesis, P_{i3} and v_{i3} are provided by the human data, whereas the initial point (P_{i0}) and velocity (v_{i0}) are updated using the measured joint angle and angular velocity at TO for each gait cycle (Table 3.4). Bezier curve trajectories can be generated in real-time using these coefficients, without the need for online optimization. Level walking trajectories of healthy humans were given as desired trajectories from 85% to 100% of

Table 3.4: Optimal coefficients for Bezier curve during 60–85% of the gait cycle.

Coefficients	Ankle (i=a)	Knee (i=k)
x_{i1}	0.1122	0.0617
x_{i2}	0.1170	0.0568

the gait cycle [106]. The resulting trajectories were validated against healthy human data given by [106]. The proportional–derivative (PD) controller was used to control the prosthesis to track the given trajectories, while lower PD gains were given during the terminal swing phase (85–100% of the gait cycle) for smoother adaptation to the ground.

4. USER ADAPTABILITY ENHANCEMENT OF GAIT PHASE ESTIMATION[*]

As stated in Section 3.2, the phase variable is commonly represented as a function of the thigh angle [40, 43, 59]. This method assumes that the thigh angle profile and integral are sinusoids. However, this assumption still differs from the ideal sinusoids, resulting in inaccurate gait phase estimation at the end of the gait cycle, particularly at slower walking speeds. We show in this chapter that the thigh angle and its integral are phase-shifted from the ideal sinusoids by analyzing walking data from both able-bodied and amputee subjects. Then, we propose a new phase variable that incorporates phase-shift and is accurate even at slower walking speeds. In an emulator study, we test two variants of the proposed phase-shifted phase variable on a transfemoral prosthesis.

4.1 Methods

Figure 4.1 depicts the healthy human thigh data, the shifted thigh data, and the ideal sinusoids. The shifted thigh information is clearly closer to the ideal sinusoids than the original thigh information. Based on this observation, we propose a phase-shifted phase variable (PS-PV), which is calculated using the previously mentioned PV and a novel phase-shifting method. First, we will present some hypotheses that will serve as the foundation for the proposed method. These hypotheses are supported by an offline analysis of walking data from both able-bodied and amputee subjects. Finally, a real-time PS-PV implementation for the powered prosthesis is described.

Hypothesis 1: A thigh angle profile is a phase-shifted cosine-like function (see Figure 4.1.A).

Hypothesis 2: A thigh integral is a phase-shifted sine-like function (see Figure 4.1.B).

Hypothesis 3: A phase-shifting method achieves the strict monotonicity of the phase variable[†].

Hypothesis 4: A phase-shifting method reduces the heel-strike detection error.

[†]When the ideal sinusoidal functions are used in the phase variable calculation, a strictly monotonic phase variable is resulted.
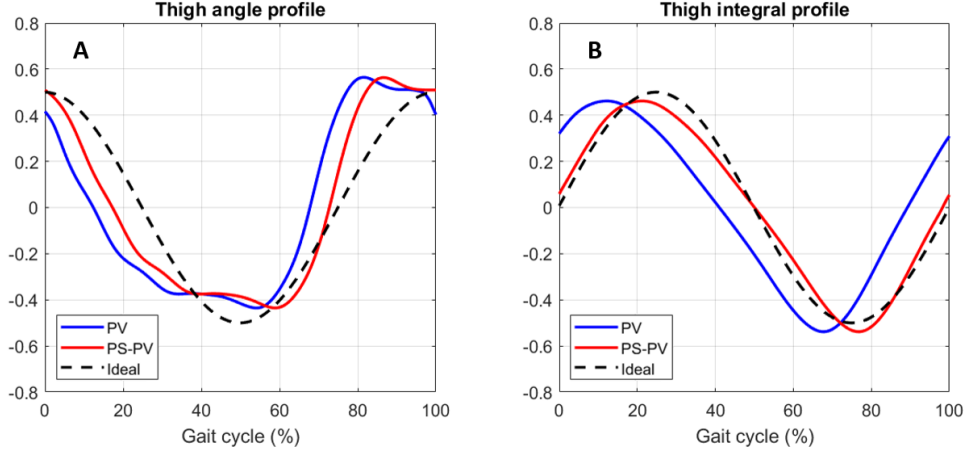
Figure 4.1: An example of a healthy subject's thigh angle and integral profile during the gait cycle. The ideal sinusoidal functions are represented by black dashed lines, while the conventional thigh information and the phase-shifted thigh information are represented by blue and red lines, respectively. (A) Two thigh angle profiles (PV vs. PS-PV) and a cosine function. (B) Two thigh integral profiles (PV vs. PS-PV) and a sine function.

4.1.1 Phase-shifting method

To validate the given hypotheses, we checked whether the thigh profile and its integral are phase-shifted from ideal sinusoids. We used a cross-correlation technique, which is widely used in signal processing for time delay detection, to find the desired phase-shift for the best fitting to the ideal sinusoids. The obtained phase-shifts (thigh: φ_{thigh} and thigh integral: φ_{integ}) were used to calculate the phase-shifted thigh angle $\hat{\theta}(\hat{t})$ and phase-shifted thigh integral $\hat{\Theta}(\bar{t})$ in Equations 4.1 and 4.2 (see Figure 4.2). The phase-shifted phase variable (PS-PV: $\hat{\Phi}(t)$) is calculated in the following way. The normalization factors (k, α, and β) are the same as PV (as calculated in Equation 3.2).

$$\hat{\theta}(\hat{t}) = \theta(t + \varphi_{thigh}) \tag{4.1}$$

$$\hat{\Theta}(\bar{t}) = \Theta(t + \varphi_{integ}) \tag{4.2}$$

$$\hat{\Phi}(t) = \frac{1}{2\pi} \, \mathrm{atan2}(k(\hat{\Theta}(\bar{t}) - \alpha), (\hat{\theta}(\hat{t}) - \beta)) \tag{4.3}$$

29
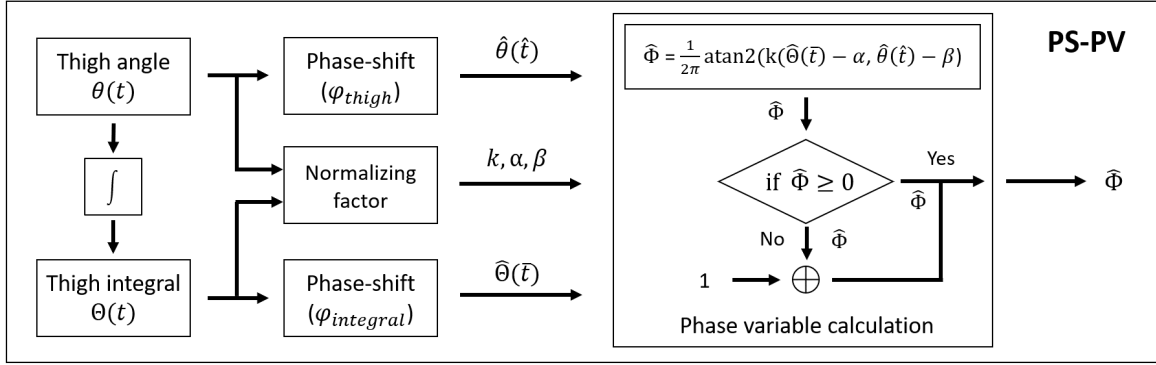
Figure 4.2: Overview of phase-shifted phase variable (PS-PV) computation using thigh information. Phase-shifts for thigh (φ_{thigh}) and its integral (φ_{integ}) are respectively implemented.

4.1.2 Method validation

We compare our method to the conventional method using offline analysis on both able-bodied and amputee subject walking data. Each method is evaluated using four metrics: i) cross-correlation between thigh angle and cosine function, ii) cross-correlation between thigh integral and sine function, iii) linearity of the phase variable, and iv) heel-strike detection error. The cross-correlation result indicates how similar the two functions are. The result is 1.0 if and only if the thigh angle profile (or its integral) is identical to the ideal cosine (or sine) function. We compare the root-mean-square error (RMSE) between the phase variable and a linear function over the gait cycle that is bounded on [0,1] to determine the linearity of the resulting phase variable of each method. The heel-strike detection error represents the temporal difference between the actual heel-strike and when the phase variable reaches its maximum (i.e., 1.0). This is represented as the percentage of the gait cycle.

4.1.2.1 *Healthy subject walking*

We collected data on walking from three healthy subjects (males, 28.3±1.5 yrs, 1.70±0.15 m, 65.0±3.0 kg). The Texas A&M University Institutional Review Board (IRB) approved the experiment protocol (IRB2015-0607F). The subjects were asked to walk at four different speeds on a treadmill: 0.5, 1.0, 1.5, and 2.0 m/s. Their thigh angles were measured using an Inertia

Measurement Unit (IMU) mounted on the thigh. The subjects' actual heel-strikes were detected using a force sensor attached to their heels, and the walking data set was segmented based on these heel-strikes. Each trial included more than 50 consecutive gaits.

Table 4.1: Method comparison: results of four metrics in four different walking speeds. Mean and ± 1 SD across 50 consecutive gaits for three subjects.

	Speed (m/s)	PV	PS-PV
Thigh angle correlation	0.5	0.862 ± 0.033	0.913 ± 0.014
	1.0	0.859 ± 0.037	0.935 ± 0.011
	1.5	0.783 ± 0.035	0.950 ± 0.008
	2.0	0.700 ± 0.036	0.949 ± 0.008
Thigh integral correlation	0.5	0.894 ± 0.036	0.988 ± 0.003
	1.0	0.876 ± 0.038	0.994 ± 0.002
	1.5	0.801 ± 0.035	0.993 ± 0.002
	2.0	0.720 ± 0.037	0.990 ± 0.002
Linearity RMSE	0.5	0.040 ± 0.009	0.035 ± 0.007
	1.0	0.029 ± 0.006	0.024 ± 0.005
	1.5	0.025 ± 0.005	0.028 ± 0.007
	2.0	0.044 ± 0.007	0.046 ± 0.005
Heel-strike detection error	0.5	0.793 ± 0.760	0.736 ± 0.350
	1.0	0.706 ± 0.719	0.540 ± 0.272
	1.5	1.073 ± 0.949	0.667 ± 0.264
	2.0	2.063 ± 2.188	1.642 ± 0.411

Figure 4.1 presents one subject's thigh angle and thigh integral data. The phase-lag is visible in both the thigh angle and its integral when compared to the ideal cosine and sine functions. As a result, a leading phase for both the thigh angle and the thigh integral should improve correlation with the ideal sinusoidal functions. This notion is supported by the processed results shown in Table. 4.1. Using two-way repeated ANOVA in RStudio statistical software, we discovered a significant effect of walking speed on the method (PV or PS-PV) and a significant difference between the methods (RStudio, Boston, MA, USA). Walking speed has a significant effect on two correlation metrics, the linearity error, and the heel-strike detection error in both PV and

31

PS-PV (p < 0.05). The correlation metrics, in particular, decreased as walking speed increased, while both errors (i.e., linearity and heel-strike detection) increased. Across all walking speeds, the correlation metrics increased significantly from PV to PS-PV (p < 0.05). Furthermore, this effect is even higher when the walking speed is increased. The implementation of phase-shifting consistently reduced the heel-strike detection error, but this reduction was not significant. The linearity errors, on the other hand, improved only at slower walking speeds when phase-shifting was used.

4.1.2.2   *Amputee subject walking*

Walking kinematics of amputees differ greatly from those of healthy humans. As a result, the analysis of amputee walking data can provide strong support for the proposed idea. We conducted a biomechanical analysis for amputee walking using a publicly available biomechanics dataset from the University of Utah [107]. This dataset contains the walking of 18 unilateral transfemoral amputees at five different speeds. The amputee subjects were divided into two groups based on their comfortable walking speed (0.8 m/s): K2 (limited community ambulators) and K3 (full community ambulators) [107]. Each group consisted of nine people who walked at different speeds: K2: 0.4, 0.5, 0.6, 0.7, 0.8 m/s and K3: 0.6, 0.8, 1.0, 1.2, 1.4 m/s. The four metrics were evaluated using the provided dataset.

A three-way mixed ANOVA was performed for each result to find significant differences between given factors (i.e., group, walking speed, and method). We chose the overlapped walking speed (0.6 and 0.8 m/s) for the statistical analysis to include two groups. One of the subjects in the K2 group had no walking data at 0.8 m/s [107], so he was excluded. According to the findings, there was no interaction effect between each given factor (p > 0.05). For all metrics, there was no significant difference between the two groups (p > 0.05). As depicted in Figure 4.3, we found significant differences between two methods (PV vs. PS-PV) for all four metrics (A*: p=0.004, B*: p=0.001, C*: p=0.02, D*: p=2.58e-05). Significant differences in linearity error and heel-strike detection error were found between walking speeds of 0.6 and 0.8 m/s (see Figures 4.3.C**: p=0.002 and D**: p=0.002). In other words, phase-shifting improved all four metrics significantly.
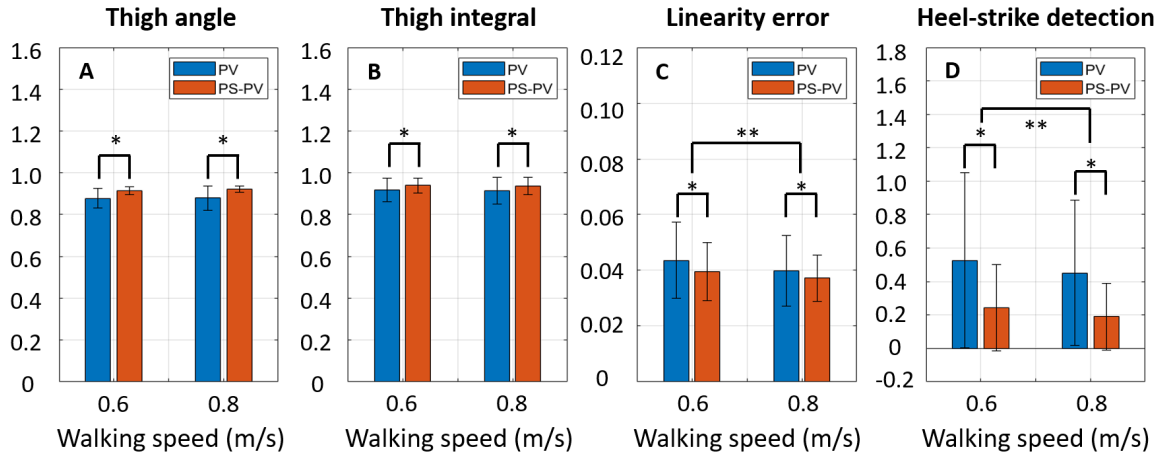
Figure 4.3: Bar indicates mean value of each metric while error bar is given with ± 1 SD (Blue: PV, Red: PS-PV). (A) Cross-correlation between thigh profile and ideal cosine function. (B) Cross-correlation between thigh integral and ideal sine function. (C) RMSE between the phase variable and a linear function. (D) Heel-strike detection error. * indicates a significant difference between PV and PS-PV while ** indicates a significant difference between two walking speeds.

i) At two different walking speeds, the thigh angle correlation increased by 4.2% and 4.8%, respectively (Figure 4.3.A). ii) In Figure 4.3.B, thigh integral correlation also increased by 2.4% and 2.5% at each walking speed. iii) Figure 4.3.C shows that the linearity errors are reduced by 9.5% and 6.9%, respectively. iv) Heel-strike detection errors are drastically reduced by 53.8% and 58.0% for each walking speed (see Figure 4.3.D). As a result, Hypotheses 1 and 2 (Section 4.1) are validated across all walking speeds in both able-bodied and amputee subjects. Hypothesis 4 is also supported by the results of both healthy and amputee walking data analysis. In the case of Hypothesis 3, we discovered that after implementing phase-shifting in an amputee subject, the linearity error decreased. When phase-shifting was used on a healthy subject, the linearity error decreased at 0.5 and 1.0 m/s but increased at faster walking speeds (1.5 and 2.0 m/s).

4.1.3 Real-time phase-shifting implementation

4.1.3.1 *Phase-shift detection*

In Section 4.1.2, we determined the best phase-shift by performing a cross-correlation on the best-fitting sinusoidal functions. This, however, cannot be accomplished during real-time pros-

33

thetic control. As a result, we must detect the phase delay during the operation of the prosthetic. We propose two references for phase delay, as shown in Figure 4.4.
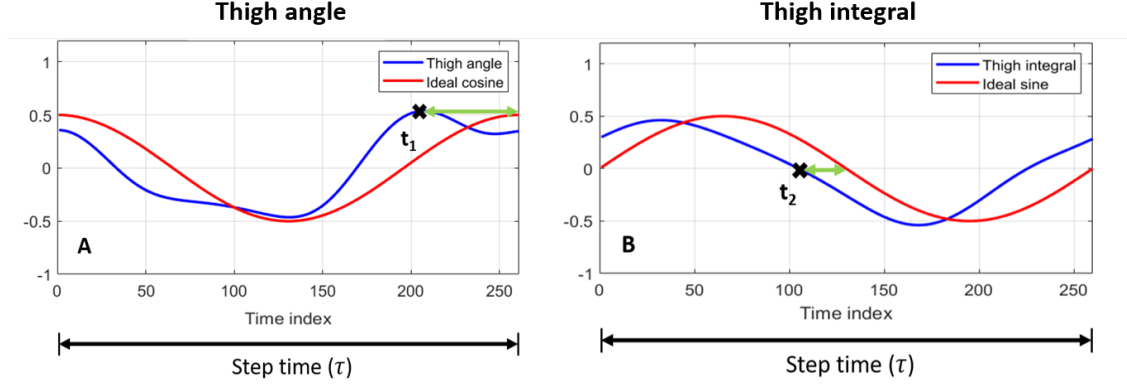
Figure 4.4: (A) Phase-shift in thigh angle: $\varphi_1 = \tau - t_1$. (B) Phase-shift in thigh integral: $\varphi_2 = \tau/2 - t_2$. Blue lines indicate thigh information, while red lines indicate ideal sinusoids.

Reference 1: The phase-shift (φ_1) between the peaks in the thigh angle profile (t_1 in Figure 4.4.A) and the ideal cosine function (corresponds to actual heel-strike) is determined.

Reference 2: The phase-shift (φ_2) between the zero-crossing point from positive to negative in the thigh integral (t_2) and the half-way mark (or half the step time) is determined (refer Figure 4.4.B).

$$\varphi_1 = \tau - t_1, \quad \varphi_2 = \frac{1}{2}\tau - t_2 \tag{4.4}$$

4.1.3.2 *Phase-shifted phase variable computation*

We update Equation 4.1 using φ_1 as shown in Equation 4.5. Note that the phase-shifted thigh integral can be computed in two ways: i) by using the phase-shift φ_2 to get $\hat{\Theta}_1(\bar{t})$ (refer Equation 4.6), ii) by integrating the shifted thigh angle $\hat{\theta}(\hat{t})$ (refer Equation 4.7). Because the thigh angle $\theta(t)$ is not an ideal cosine function, these two methods would differ. Thus, we utilize these two variants of phase-shifted thigh integral when we compute the phase variable (see Figure 4.5).

34

$$\hat{\theta}(\hat{t}) = \theta(t + \varphi_1) \tag{4.5}$$

$$\hat{\Theta}_1(\bar{t}) = \Theta(t + \varphi_2) \tag{4.6}$$

$$\hat{\Theta}_2(\hat{t}) = \int \hat{\theta}(\hat{t}) \, d\hat{t} \tag{4.7}$$
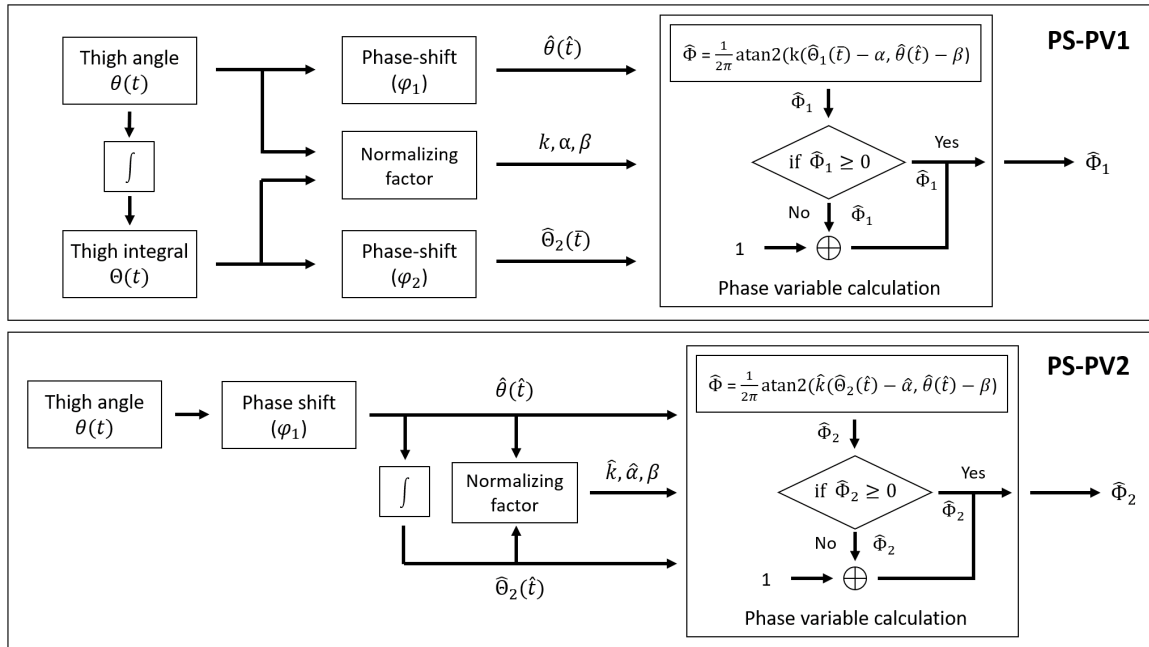
Figure 4.5: Overview of phase variable computation using the proposed phase-shift method. Resulting phase variables are PS-PV1: $\hat{\Phi}_1(t)$ and PS-PV2: $\hat{\Phi}_2(t)$

The phase variable using Equation 4.6 is called PS-PV1 and denoted by $\hat{\Phi}_1(t)$, while the one using Equation 4.7 is called PS-PV2 and denoted by $\hat{\Phi}_2(t)$.

$$\hat{\Phi}_1(t) = \frac{1}{2\pi} \operatorname{atan2}(k(\hat{\Theta}_1(\bar{t}) - \alpha), (\hat{\theta}(\hat{t}) - \beta)) \tag{4.8}$$

$$\hat{\Phi}_2(t) = \frac{1}{2\pi} \operatorname{atan2}(\hat{k}(\hat{\Theta}_2(\hat{t}) - \hat{\alpha}), (\hat{\theta}(\hat{t}) - \beta)) \tag{4.9}$$

In the case of PS-PV2, we must use different normalization factors for the thigh integral $\hat{\Theta}_2(\hat{t})$:

$$\hat{k} = \frac{|\hat{\theta}_{max} - \hat{\theta}_{min}|}{|\hat{\Theta}_{2,max} - \hat{\Theta}_{2,min}|}, \qquad \hat{\alpha} = \frac{|\hat{\Theta}_{2,max} + \hat{\Theta}_{2,min}|}{2} \qquad (4.10)$$

All normalizing factors are updated via a weighted sum of their prior values (computed during previous gait cycles). Taking into account the history of these factors allows for more stable walking. The weighting is a forgetting factor $e^{-\Delta t}$, where Δt is the time elapsed since the corresponding value was recorded.

4.1.4 Experimental protocol

A healthy young subject (male, 1.70 m, 70 kg) took part in the experiment, which used an L-shape adapter to simulate prosthetic walking (see Figure 4.6). The subject was instructed to walk on the treadmill at his preferred pace (0.80 m/s). Handrails on either side of the treadmill ensured safety during the experiment. This prosthetic experiment protocol was approved by the Institutional Review Board (IRB) at Texas A&M University (IRB2015-0607F).
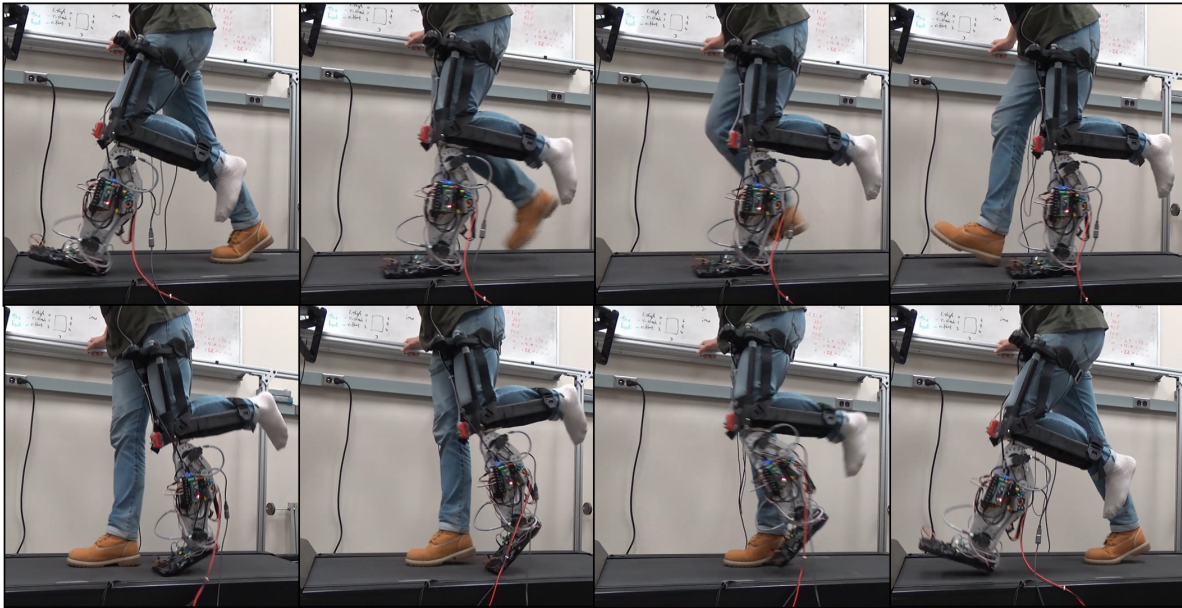
Figure 4.6: The healthy subject walked with AMPRO II using the L-shape emulator.

4.2 Results
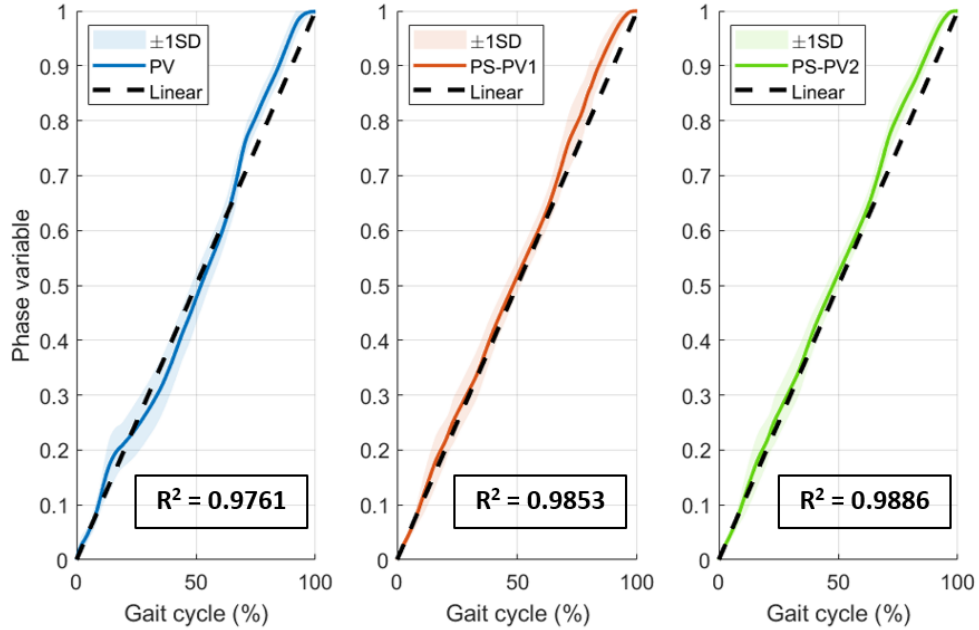
Figure 4.7: Resulting phase variable using three different methods (Blue: PV, Red: PS-PV1, Green: PS-PV2). While the solid lines represent the mean of 15 consecutive steps, the shaded regions indicate ± 1 SD. Black dashed lines indicate the linear function over the gait cycle.

4.2.1 Method comparison

As shown in Table. 4.2, when phase-shifting methods (PS-PV1 and PS-PV2) were used for prosthetic control, the correlation results of both the thigh angle and its integral increased. The

Table 4.2: Correlation results of thigh angle and its integral using three different methods: PV, PS-PV1, and PS-PV2.

	PV	PS-PV1	PS-PV2
Thigh angle	0.858 ± 0.025	0.888 ± 0.020	
Thigh integral	0.895 ± 0.048	0.899 ± 0.059	0.906 ± 0.050
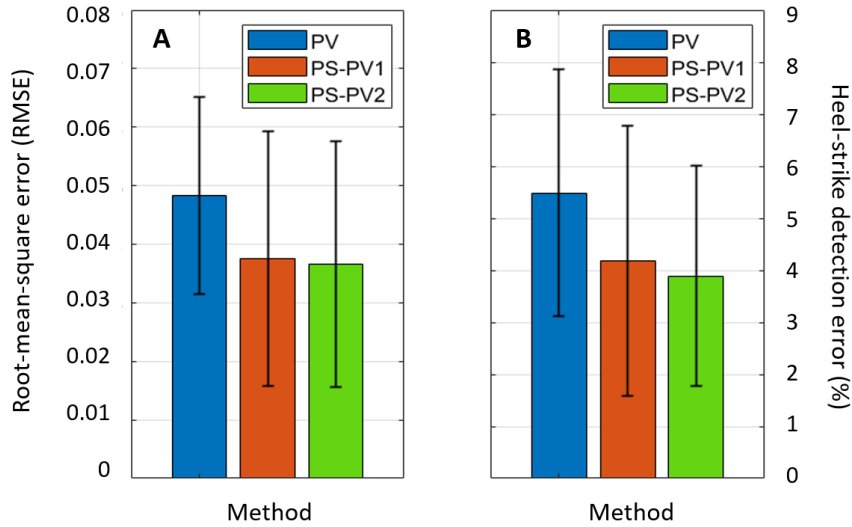
Figure 4.8: (A) RMSE between the phase variable and a linear function. (B) Heel-strike detection error in the percentage. (Blue: PV, Red: PS-PV1, Green: PS-PV2). Error bars indicate ± 1 SD.

phase variables that resulted (i.e., PV, PS-PV1, and PS-PV2) are shown in Figure 4.7. First, all three phase variables provide a reliable estimation result throughout the gait cycle while adhering to the aforementioned properties (Section 1.3). In comparison to the previous method (PV: R^2 = 0.9761), the phase-shifting method produces higher linearity (PS-PV1: R^2 = 0.9853, PS-PV2: R^2 = 0.9886). This fact also can be seen in Figure 4.8.A; when phase-shifting is used, the RMSE between the resulting phase variable and a linear function decreases. The heel-strike detection error in PV is 5.5%, while those of PS-PV1 and PS-PV2 are 4.2% and 3.9%, respectively (see Figure 4.8.B).

4.2.2 Joint kinematics/kinetics comparison

The prosthetic joint kinematics/kinetics results are shown in Figure 4.9. PV shows greater ankle dorsiflexion and knee flexion than the other two phase-shifting methods (see Figures 4.9.A and D). Figures 4.9.C and F show significant push-off power in PV. Surprisingly, these results can be attributed to the phase variable's aforementioned linearity. According to the results in Figure 4.7, PV has a steeper slope than others from 65% to 70% of the gait cycle. Due to the fact that this

region is in the middle of the swing phase, the steeper slope causes accelerated joint movements

and an uncomfortably high push-off. This is demonstrated clearly in the supplemental video [108].

The slope of PS-PV2 is slightly steeper than that of PS-PV1 (see Figure 4.7). As a result, PS-PV2

has slightly higher knee flexion than PS-PV1.
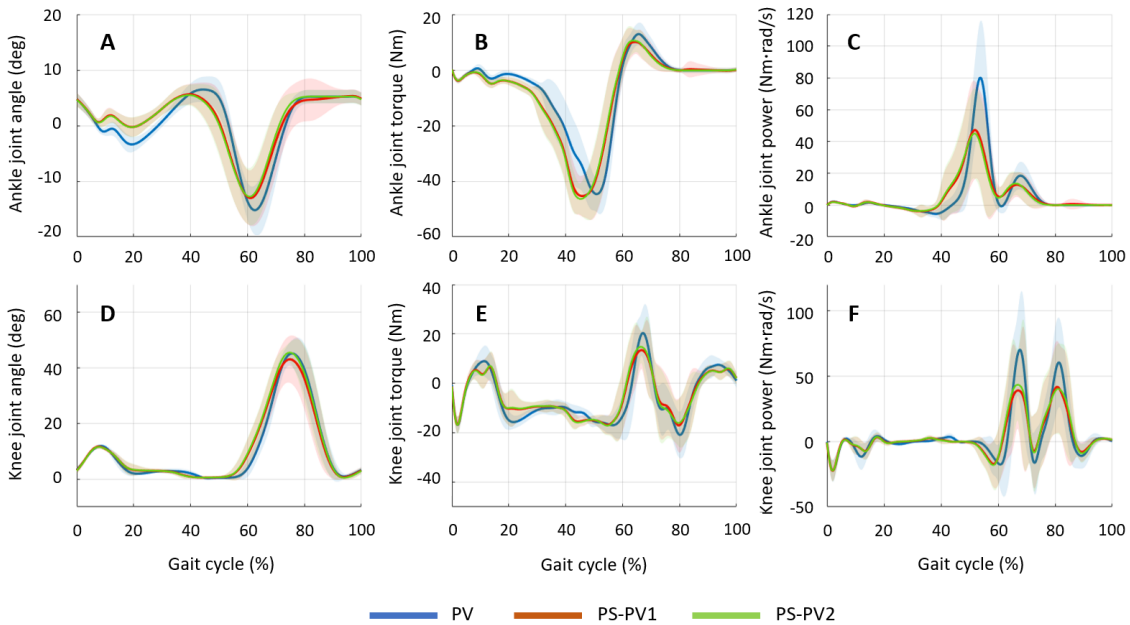
Figure 4.9: Joint kinematics/kinetics results (Top: Ankle, Bottom: Knee) using the three phase variables: Blue: PV, Red: PS-PV1, Green: PS-PV2. The solid lines and the shaded regions indicate the mean and ± 1 SD of 15 consecutive steps, respectively.

4.3 Discussion

The phase portraits of the knee joint were analyzed to assess the stability of each method (see

Figure 4.10). Each phase portrait contains a distinct limit cycle. Interestingly, PS-PV1 and PS-PV2

had lower deviations from the limit cycle. In terms of qualitative deviation from the limit cycle,

PS-PV2 had the least, followed by PS-PV1, and PV had the most. We also attempted to quantify

this result with the Lyapunov exponent (LE). LE quantifies the trajectory's exponential rates of
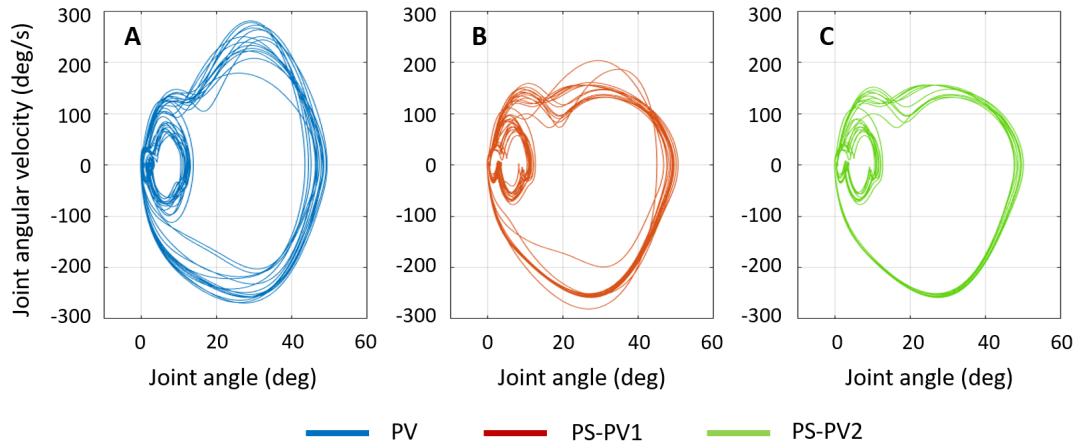
Figure 4.10: Phase portrait (joint angle vs. joint angular velocity) of the knee joint for 15 consecutive gaits (Blue: PV, Red: PS-PV1, Green: PS-PV2)

convergence (or divergence) to determine its sensitivity to initial conditions [109, 110]. When LE is negative, for example, the deviation from the limit cycle converges to zero. The rate of convergence is referred to by the magnitude of LE. As a result, the largest LE (the dominant value) is frequently used as a measure of the system's local instability [111–113]. To calculate the maximum LE based on the Euclidean distance from the limit cycle, we used the Kantz algorithm [113, 114]. The limit cycle is defined as the averaged phase portrait of 15 gaits. PS-PV2 had the lowest LE (ankle: -0.0340, knee: -0.0805), followed by PS-PV1 (ankle: 0.0185, knee: -0.0205), and finally PV (ankle: 0.0244, knee: 0.0123)[‡]. Because of the small number of subjects, it is difficult to draw any statistical conclusions. We could, however, highlight some obvious trends. PS-PV1 and PS-PV2 had lower LE values than PV, implying that they provide more stable and robust control than PV.

Due to the limited torque of the motors, we limited the walking speed to 0.80 m/s, which is slower than normal human walking. In the future, more walking experiments will be carried out at various walking speeds. Because of the use of an L-shape simulator and the difference in height between the two limbs, slightly higher hip extensions were observed on the prosthesis side during

---

[‡]It is important to note that a positive LE value for PV does not easily refer to the instability in this case. This is due to the fact that human walking is known to be stable, even if their phase portrait does not always show a perfect convergence to the limit cycle.

the experiment. This may have an impact on thigh kinematics and the resulting phase variable. The affected thigh angle, however, still has a phase shift from the ideal cosine function, so the proposed method is still valid. Because individuals have different joint kinematics while walking, the amount of phase-shift may vary depending on the user. [106, 107]. As a result, it is reasonable to assert that the required phase shift is user-specific. Using the proposed phase-shifted phase variable, we could create a learning-based gait phase estimation model.

4.4 Conclusion

We focus on user adaptability for gait phase estimation in this chapter. We propose a phase-shifted phase variable based on the user's thigh information. The thigh angle and its integral profiles are shown to be phase-shifted sinusoids. When phase-shifts are applied to the thigh angle and integral profiles, the resulting phase variable improves its linearity and heel-strike detection. In an emulator study, a real-time implementation of this phase variable was proposed and tested on a transfemoral prosthesis. The application of phase-shifting, like the offline analysis, made the resulting phase variable more linear. A significant advantage of a linear phase variable is more controlled push-off assistance (as shown in the supplemental video [108]). When the proposed method was applied to the phase portrait of the knee and ankle, the phase-shifted phase variables had fewer deviations from the limit cycle. Preliminary results suggest that the phase variable should be computed using the integral of the phase-shifted thigh angle rather than having a dedicated thigh integral phase-shift for real-time implementation. We conclude that the proposed phase-shifted phase variable allows for more accurate gait progress detection and, consequently, more robust walking. Because it has been demonstrated that each individual has their own phase-shift, we could improve user adaptability by utilizing this phase-shift information. We anticipate that having user-adaptive control of the prosthesis with the phase-shifted phase variable will result in better gait performance for each individual.

5. SPEED ADAPTABILITY ENHANCEMENT IN GAIT PHASE ESTIMATION

When controlling the prosthesis at different walking speeds, speed adaptability is an important property to have. Because the prosthesis is controlled by the user's walking state, speed adaptability in the user's gait phase estimation should be achieved. The conventional phase variable (i.e., PV) can adapt to different walking speeds based on thigh movement during the gait cycle [40, 43, 59]. The duration of heel-strike (i.e., stride time) can be also used to estimate the walking speed. However, this existing phase variable cannot reflect variable toe-off (TO) timing at different speeds, despite the fact that people are prone to having different TO timing at different walking speeds [95, 96]. Motivated by this finding, we newly propose a piecewise phase variable that can be adjusted for different TO timing at different walking speeds to maximize the prosthesis's gait performance. This chapter's goal is to validate the piecewise phase variable in a prosthetic walking experiment with both able-bodied and amputee subjects. The effects of the piecewise phase variable on joint kinematics, kinetics, gait symmetry, and ground reaction forces are measured and analyzed. The biomechanical results of the piecewise phase variable are compared to those of the conventional phase variable (shown in Section 3.2).

5.1 Methods

5.1.1 Piecewise phase variable

The best thing about using phase variables is that they can represent the user's walking state in percentage regardless of walking speed by using user kinematics (e.g., thigh information) [59, 74]. So, when the user walks faster or slower, this is reflected in the user kinematics, adapting to varying walking speeds. However, one downside is that the phase variable has a limitation in detecting some important events (i.e., HO and TO) at varying speeds because it is computed solely on kinematics information. According to [95, 96], human HO and TO are known to occur at different timings at various speeds. For example, as walking speed decreases, the stance phase lengthens and the swing phase shortens. This is due to the fact that people tend to have a longer stance phase

at slow speeds in order to maintain their balance. To account for these varying TO onset timings in phase variable computation at different walking speeds, we propose a new piecewise phase variable, named PW-PV. In contrast to the conventional phase variable (i.e., PV), we continue to track TO onset timings and use the estimated TO timing to implement speed-adaptation when computing the piecewise phase variable.
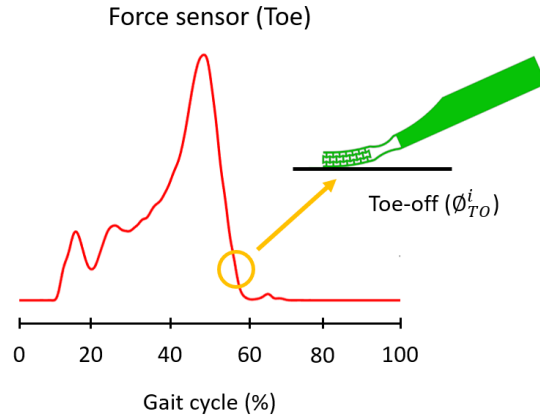
Figure 5.1: Toe-off estimation based on toe force sensor. A total of five toe-off timings (including current toe-off) are utilized to estimate the next toe-off timing.

The TO onset timing estimation procedure is depicted in Figure 5.1. We continued to detect TO with a force sensor attached to the toe and saved the detected TO timings from five previous gaits. The TO estimation was performed using a weighted average of these five prior TO values, as shown in Equation 5.1. The weighting is expressed as a forgetting factor e^{-i}, where i represents the ith prior TO value.

$$\phi_{TO}^{EST} = \frac{\sum_{i=1}^{5} e^{-i} \cdot \phi_{TO}^{i}}{\sum_{i=1}^{5} e^{-i}} \tag{5.1}$$

The estimated TO timing (ϕ_{TO}^{EST}) includes the variable TO timings and is used to adjust the PV slope, resulting in PW-PV. Figure 5.2 depicts the slope-adjustment based on the estimated TO

timing. The blue line in this figure represents the conventional phase variable (i.e., PV) throughout the gait cycle. This PV lost its strict monotonicity around 90% of the gait cycle, implying that the knee is already fully extended at this point and the actual heel-strike happens 10% later. If the knee is fully extended in the middle of the swing, this early saturation in PV may cause tripping. By adjusting the slope of the given phase variable, this can be improved. As a result, we apply the slope-adjustment of the phase variable based on the estimated TO timing, expecting to the red line (PW-PV in Figure 5.2). We could reflect the variable TO at different walking speeds by adjusting the phase variable slope. We followed the same procedure as described in Section 3.2 to obtain PV
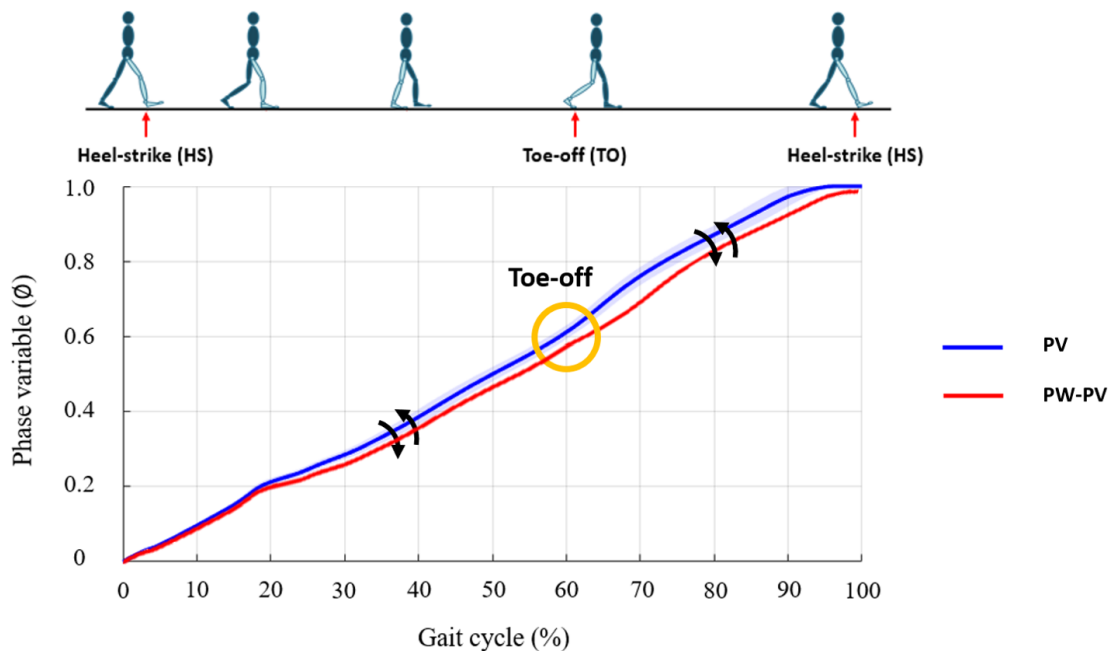
Figure 5.2: After obtaining PV (Blue), slope-adjustment is applied based on the estimated TO timing (ϕ_{TO}^{EST}), resulting in PW-PV (Red).

(denoted by ϕ), but we used slope-adjustment based on the estimated TO timing (ϕ_{TO}^{EST}) to compute the piecewise phase variable (i.e., PW-PV, denoted by ϕ_{PW}). The initial condition of TO timing was set to 0.6, referring to 60% of the gait cycle. Starting with 0.6, TO timing is updated every gait cycle and used to estimate the user's TO timing (ϕ_{TO}^{EST}) based on five previous gait cycles.

Equation 5.2 explains the PV slope-adjustment and the PW-PV computation. The resulting ϕ_{PW} function is a real-valued continuous function with a range of [0,1]. This PW-PV is used directly to control the prosthesis. Based on our control framework, TO is the starting point for using tracking control, so we can anticipate a proper swing to avoid tripping due to an early extended knee.

$$\phi_{PW} = \begin{cases} \frac{0.6}{\phi_{TO}^{EST}}\phi & \phi < \phi_{TO}^{EST} \\ \frac{0.4(\phi - \phi_{TO}^{EST})}{1 - \phi_{TO}^{EST}} + 0.6 & \phi \geq \phi_{TO} \end{cases} \tag{5.2}$$

5.1.2 Experimental protocol
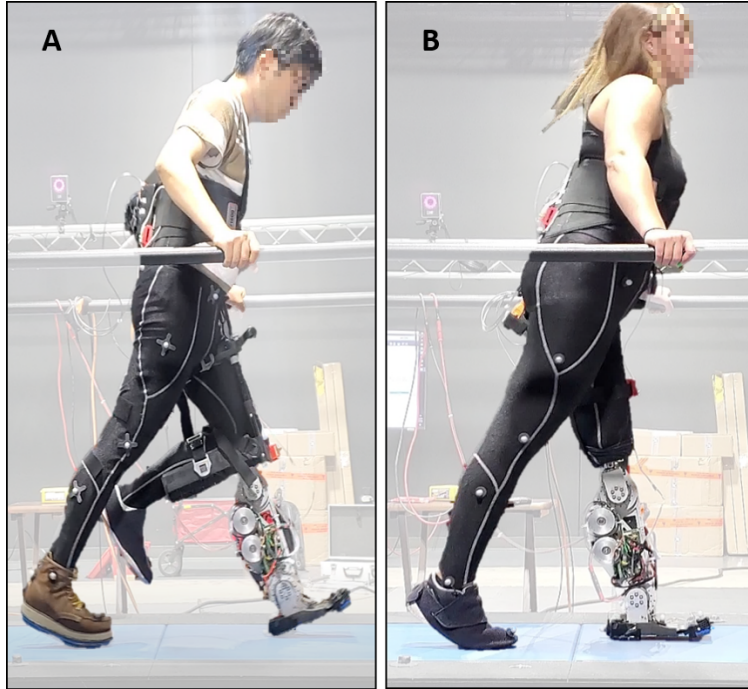
Figure 5.3: (A) An able-bodied subject wears the prosthesis using L-shape simulator. (B) An amputee subject wears the prosthesis with her own socket.

An indoor experiment was conducted with both an able-bodied subject (male, 170 cm, 70 kg) and a unilateral transfemoral amputee subject (female, 164 cm, 66 kg w/o prosthesis) for experimental validation. The able-bodied subject was participated in prosthetic walking experiment

45

using L-shape simulator (Figure 5.3.A), while the amputee subject was participated with her own socket (Figure 5.3.B). She has been using a X3 Knee with a Freedom Runway Foot (Ottobock) in her daily life. All trials was conducted on an instrumented treadmill (Tandem treadmill, AMTI) with 44 camera-based motion capture system (Vantage V5, Vicon). The amputee subject chose her preferred speed (i.e., 0.54 m/s) while the able-bodied subject walked at 0.67 m/s. These speed was decided to avoid subjects' fatigue and any potential safety issue. The chosen speed condition was fixed across all trials. Each walking trial lasted 90 seconds, and a sufficient break time was given to the participant between each trial. The participants' safety was assured with handrails located on either side of the treadmill. This experiment was reviewed and approved by the Institutional Review Board (IRB) at Texas A&M University (IRB2015-0607F).

5.1.3 Data analysis

In Vicon Nexus, motion capture data were collected and gap-filled, and the associated anthropomorphic model was reconstructed using Visual3D. (C-Motion). The marker and ground reaction force data were filtered with a third-order Butterworth low-pass filter with cutoff frequencies of 10 and 20 Hz, respectively. The sagittal plane was used for all joint kinematics and kinetics computations. In RStudio statistical software, a paired t-test was used to determine the significance of the difference between two methods for statistical analysis (RStudio version 1.3.1093). Statistical significance was denoted as follows: * = $p \leq 0.05$, ** = $p \leq 0.01$, *** = $p \leq 0.001$.

5.2 Results

Figures 5.4 and 5.5 depict the able-bodied and healthy subjects walking on the treadmill while wearing the powered prosthesis (i.e., AMPRO II). During the walking experiment, joint kinematics/kinetics of both prosthesis- and contralateral-side were recorded in real-time using the motion capture system and the motor drivers. The results are explained in detail below.

5.2.1 Prosthesis-side kinematics/kinetics

Figure 5.6 depicts the HO and TO timings, which were captured using force sensors under the prosthetic foot. According to the results, both able-bodied and amputee subjects ($p < 0.001$)
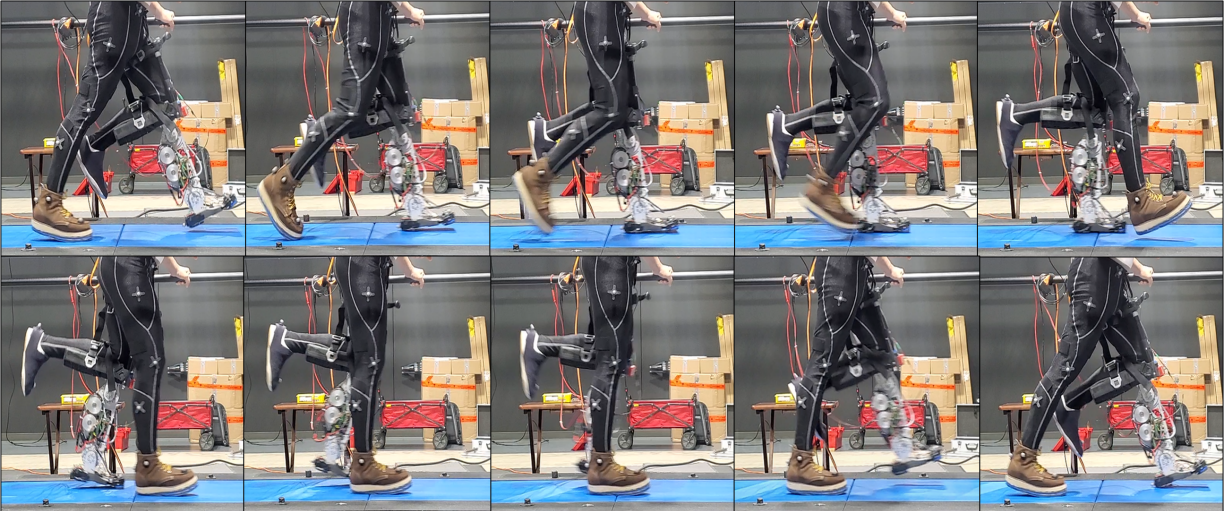
Figure 5.4: The healthy subject walk with AMPRO II using the L-shape emulator.
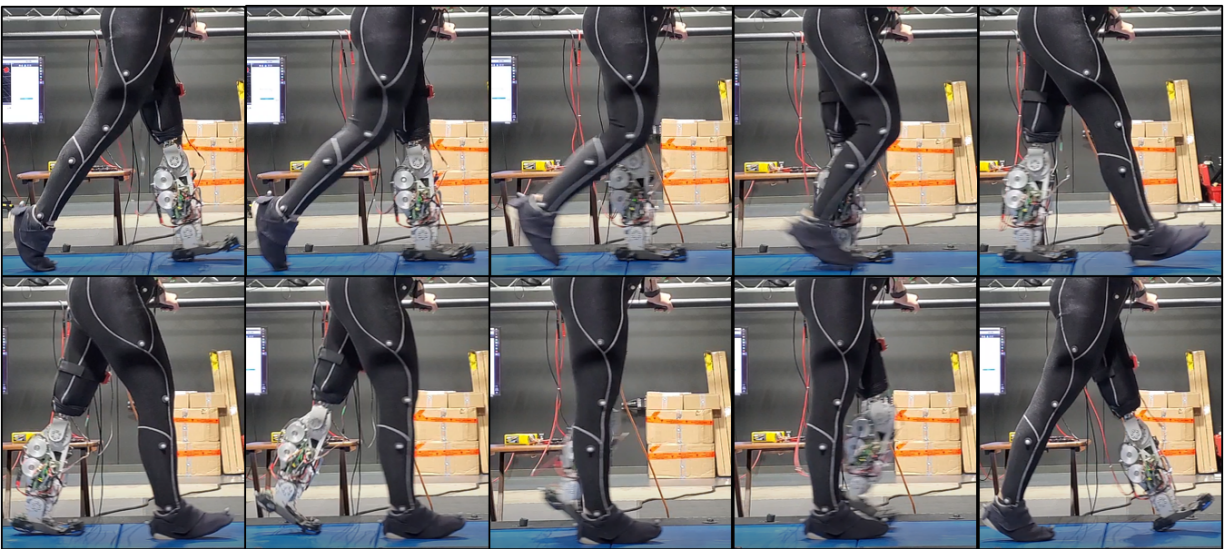
Figure 5.5: The amputee subject walk with AMPRO II using her own socket.

clearly made earlier HOs with PW-PV. Furthermore, the able-bodied subject made his HO around 30% of the gait cycle (Figure 5.6.A), which is a more timely HO based on human data [115, 116]. In terms of TO, the amputee subject showed no significant difference, whereas the able-bodied subject showed a slightly later TO (p=0.021) with PW-PV. According to human data [115, 116], both PV and PW-PV produced a proper TO onset timings. These results imply that a faster load

47
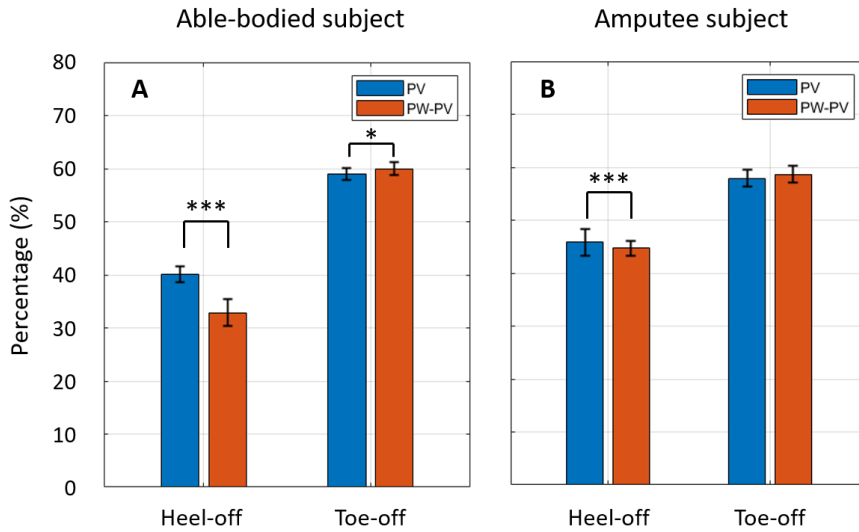
Figure 5.6: Gait event detection in the percentage. (A) Able-bodied subject. (B) Amputee subject. Blue line indicates PV result while red line indicates PW-PV result.

transfer occurred due to phase variable adjustment using PW-PV. This is also supported by the kinematics results in Figures 5.7 and 5.8. Both subjects showed earlier ankle dorsiflexion before 20% of the gait cycle when PW-PV was used (see Figures 5.7.A and 5.8.A). Figures 5.7.B and 5.8.B show that knee flexions occur earlier in comparison to PV.

In Figures 5.7.F and 5.8.F, the prosthesis knee torque showed an apparent difference between two methods (i.e., PV vs. PW-PV) for both subjects. To be specific, in Figure 5.7.F, knee extension torque was seen with PW-PV, while PV exhibited knee flexion torque during 20–40% of the gait cycle. The amputee subject had knee extension torque during this region regardless of the method, but PW-PV exhibited a more extension torque (see Figure 5.8.F). Due to the faster load transfer with PW-PV, an extension torque was offered to support the body weight during mid-stance, making the subject move forward with the extended knee. The identical torque trend can be found in human data [117, 118]. According to Figure 5.7.G, there was no apparent different between the average ankle peak power of PV (1.6800 ± 0.2531 W/kg) and that of PW-PV (1.6511 ± 0.1874 W/kg). No significant difference was also found in the timing of ankle peak power (PV: 49.35 ± 1.65 % vs. PW-PV: 48.70 ± 1.53 %). In the case of the amputee subject, PW-PV showed 13.89% greater
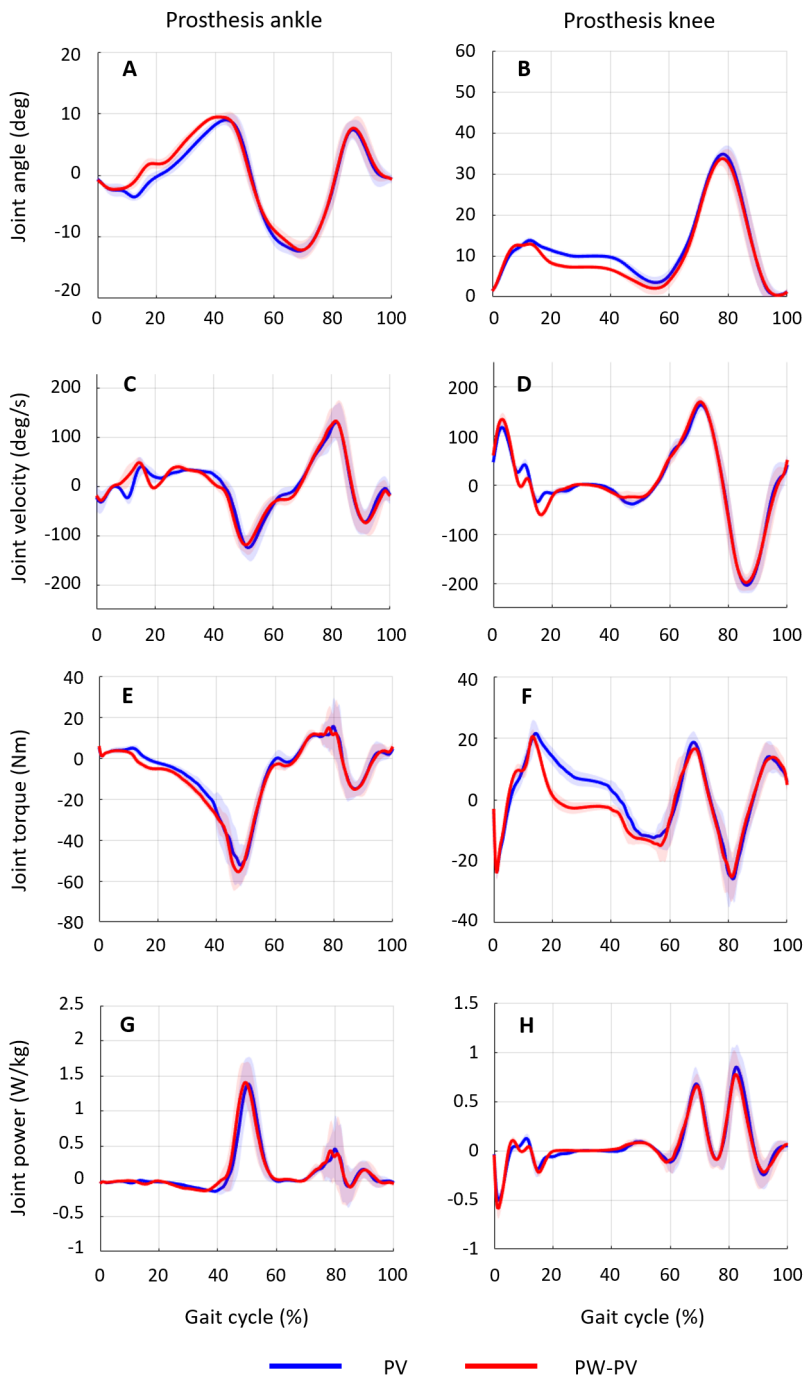
Figure 5.7: Prosthesis-side kinematics/kinetics of the able-bodied subject. (Left) Ankle. (Right) Knee. Solid line and shaded region represent the average of 20 gaits and ±1 SD, respectively. Blue line indicates PV result while red line indicates PW-PV result.

49
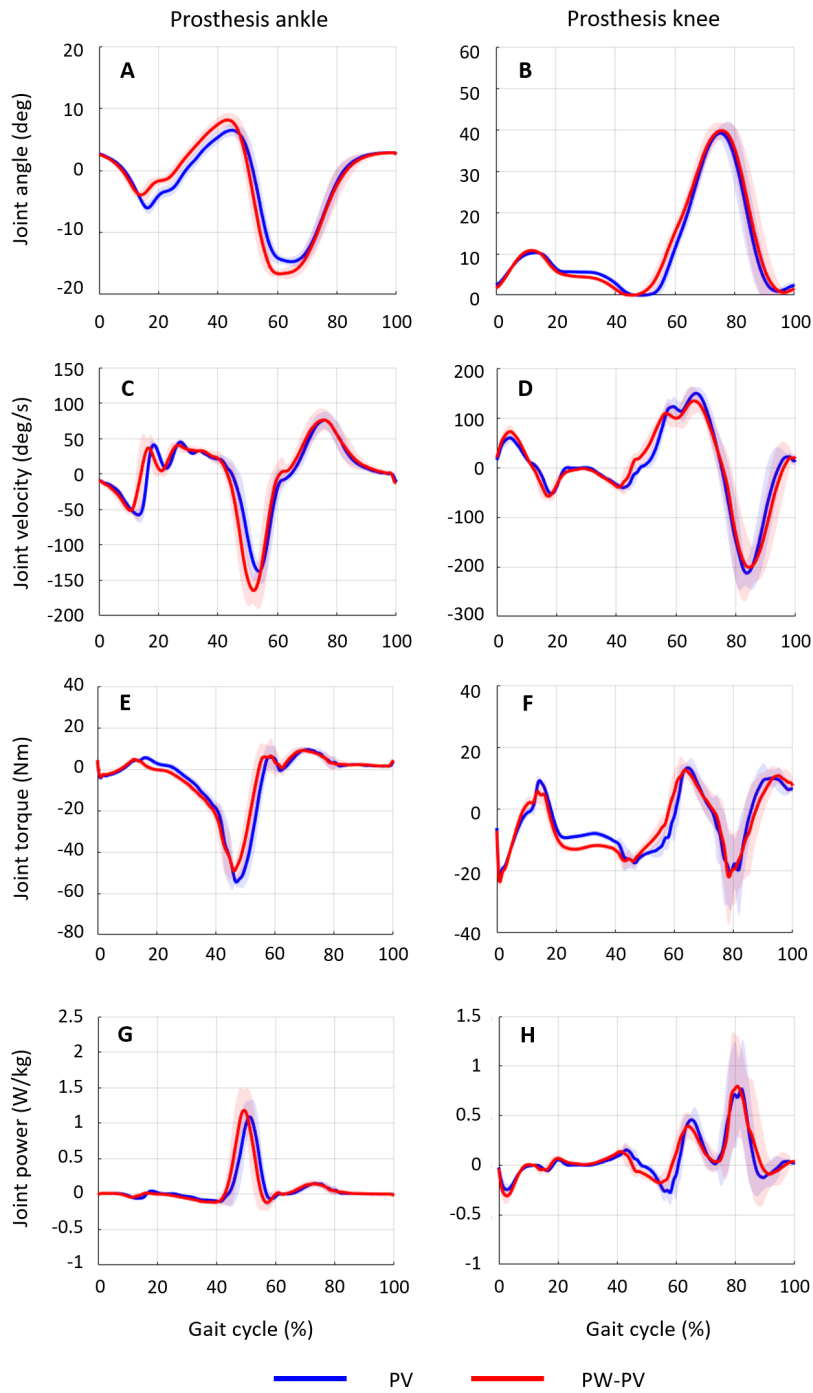
Figure 5.8: Prosthesis-side kinematics/kinetics of the amputee subject. (Left) Ankle. (Right) Knee. Solid line and shaded region represent the average of 20 gaits and ±1 SD, respectively. Blue line indicates PV result while red line indicates PW-PV result.

ankle peak power than PV in Figure 5.8.G (PV: 1.3745±0.1607 vs. PW-PV: 1.5655±0.1566, p=0.035). Earlier ankle peak power was also found with the amputee (PV: 50.72±1.50 vs. PW-PV: 49.12±1.84, p=0.025).
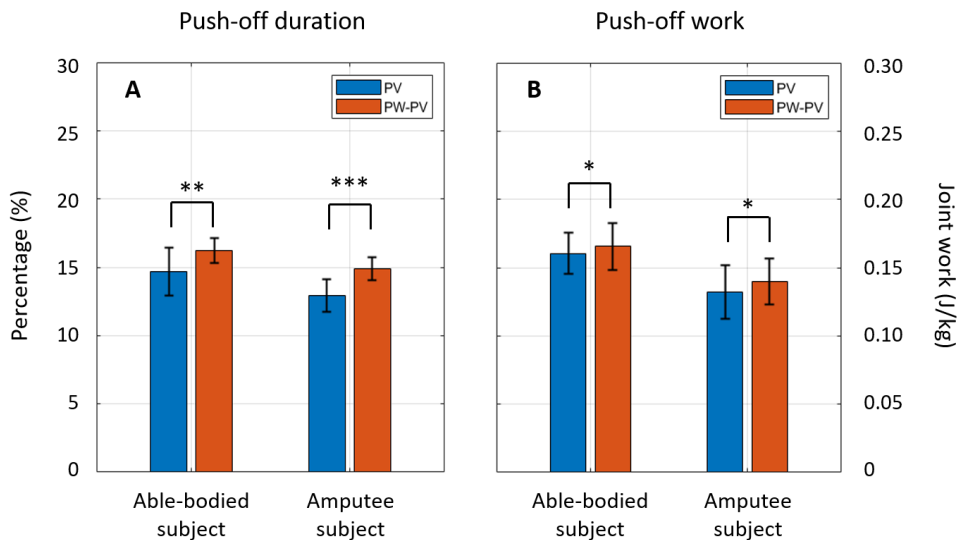
Figure 5.9: Prosthesis-side push-off duration and work. (A) Push-off duration in the percentage. (B) Normalized ankle push-off work. Blue line indicates PV result while red line indicates PW-PV result.

Figures 5.7.G and 5.8.G show a phase called push-off phase that was given a huge positive power. The push-off is significant because this propulsive phase (i.e., during nearly 40–60% of the gait cycle) propels the human forward by providing positive work [119, 120]. The push-off phase accounts for approximately 20% of the gait cycle, according to [119, 120]. As illustrated in Figure 5.9.A, PW-PV resulted in 10.58% and 15.18% longer push-off duration (i.e., closer to 20%) for the able-bodied and amputee subjects, respectively. PW-PV provided 7.33% and 16.95% more ankle push-off work to the able-bodied and amputee subjects, respectively, due to the longer and more timely push-off (see Figure 5.9.B). This is also evident in the ground reaction force (GRF) results shown in Figure 5.10.B. A greater peak GRF can be found when the amputee made a push-off based on PW-PV (p=0.007). No significant difference is found from the intact-side
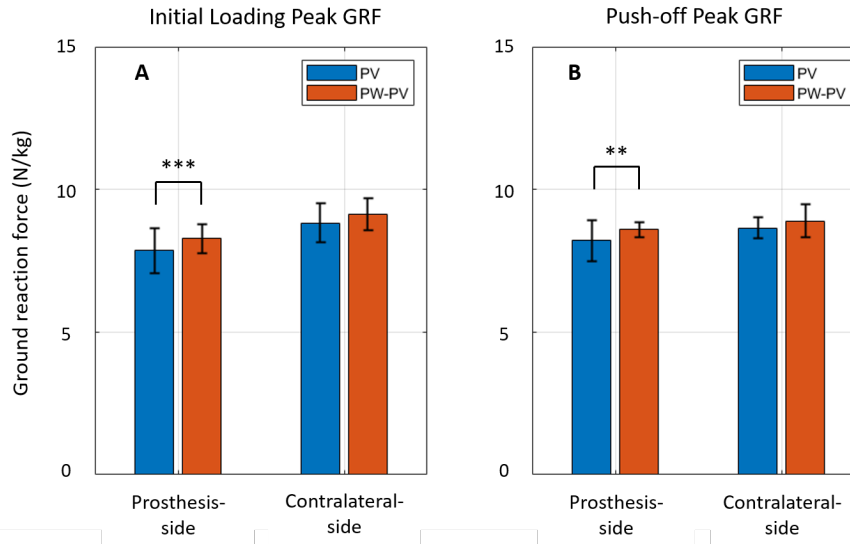
Figure 5.10: Ground reaction force of amputee subject. (A) Initial peak loading GRF (B) Push-off peak GRF. Result of PV is depicted in blue while that of PW-PV is depicted in red.

(i.e., contralateral-side). Figure 5.10.A depicts the initial peak GRF, which was captured when the subject placed her weight on one of her legs following heel-strike. The prosthesis-side has a higher GRF (p=0.001), while the other side has no significant difference. This implies that while walking with PW-PV, the subject put more weight on the prosthesis.

5.2.2 Contralateral-side results

The kinematics of both subjects' contralateral-side limbs are shown in Figure 5.11. Both subjects performed earlier and larger ankle dorsiflexions before push-off with PW-PV (see Figures 5.11.A and 5.11.E). This could be related to the push-off results shown in Figures 5.9.B and 5.10.B. Both subjects benefited from the prosthesis' greater push-off and made faster load transfer on the contralateral side, resulting in earlier and larger ankle dorsiflexions. Figure 5.11.B shows a greater knee flexion during the stance phase in the able-bodied subject. The amputee subject, on the other hand, showed no discernible difference in knee kinematics while exhibiting less ankle plantarflexion during push-off (see Figure 5.11.E).
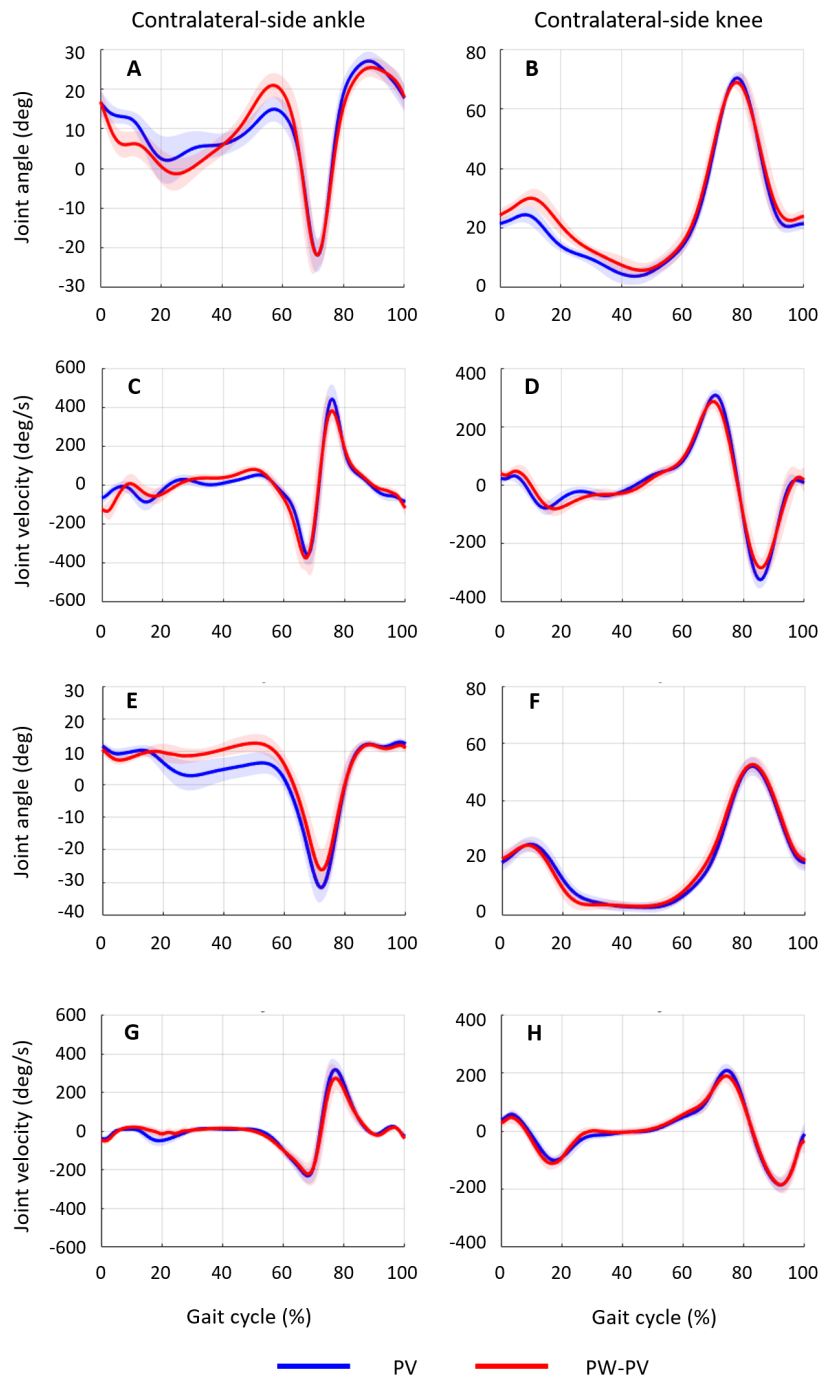
Figure 5.11: Contralateral-side ankle and knee kinematics. (A-D) Able-bodied subject. (E-H) Amputee subject. (Left) Ankle. (Right) Knee. Solid line and shaded region represent the average of 20 gaits and ±1 SD, respectively. Blue line indicates PV result while red line indicates PW-PV result.

5.3 Discussion

Both PV and PW-PV showed high linearity with a small root-mean-square error (RMSE) for both subjects, according to Table 6.1. Even though PW-PV had higher linearity and a lower RMSE than PV, the differences were not statistically significant ($p > 0.05$). Stride time, on the other hand, differs significantly ($p < 0.001$) between methods for both subjects. The stride time is one of the clinically relevant outcome measures used to assess prosthesis users' walking performance [100, 121]. When PW-PV was used, the average stride time was reduced by 3.98% for able-bodied subjects and 4.24% for amputee subjects, respectively. These findings are also related to heel-strike deviation. The temporal difference between the actual heel-strike (i.e., force-plate sensed) and the estimated heel-strike was defined as heel-strike deviation (i.e., when the phase variable is maxed out). PW-PV has smaller deviations from the actual heel-strike than PV for both able-bodied (14.46% reduction, $p=0.033$) and amputee (47.44% reduction, $p=0.003$) subjects.

Table 5.1: Comparison of two methods: PV and PW-PV.

PV method	Able-bodied subject		Amputee subject	
	PV	PW-PV	PV	PW-PV
Linearity (R^2)	0.9921 ± 0.0051	0.9935 ± 0.0040	0.9945 ± 0.0035	0.9962 ± 0.0025
Linearity (RMSE)	$2.14\mathrm{e}^{-3} \pm 5.20\mathrm{e}^{-4}$	$1.97\mathrm{e}^{-3} \pm 5.87\mathrm{e}^{-4}$	$2.15\mathrm{e}^{-3} \pm 6.63\mathrm{e}^{-4}$	$2.15\mathrm{e}^{-3} \pm 5.99\mathrm{e}^{-4}$
Stride time (s)	1.5493 ± 0.0371	1.4900 ± 0.0366	1.6900 ± 0.0303	1.6213 ± 0.0416
Heel-strike error (s)	0.0900 ± 0.0265	0.0741 ± 0.0309	0.1296 ± 0.0456	0.0879 ± 0.0351

We also compare the amputee subject's gaits while using her personal microprocessor-controlled (MPC) prosthesis and the powered prosthesis. The powered prosthesis, as shown in Figure 5.12, has a more human-like gait trend than the MPC prosthesis. The powered prosthesis provided a considerable push-off, resulting in significant plantarflexion as shown in Figure 5.12.A. In contrast,
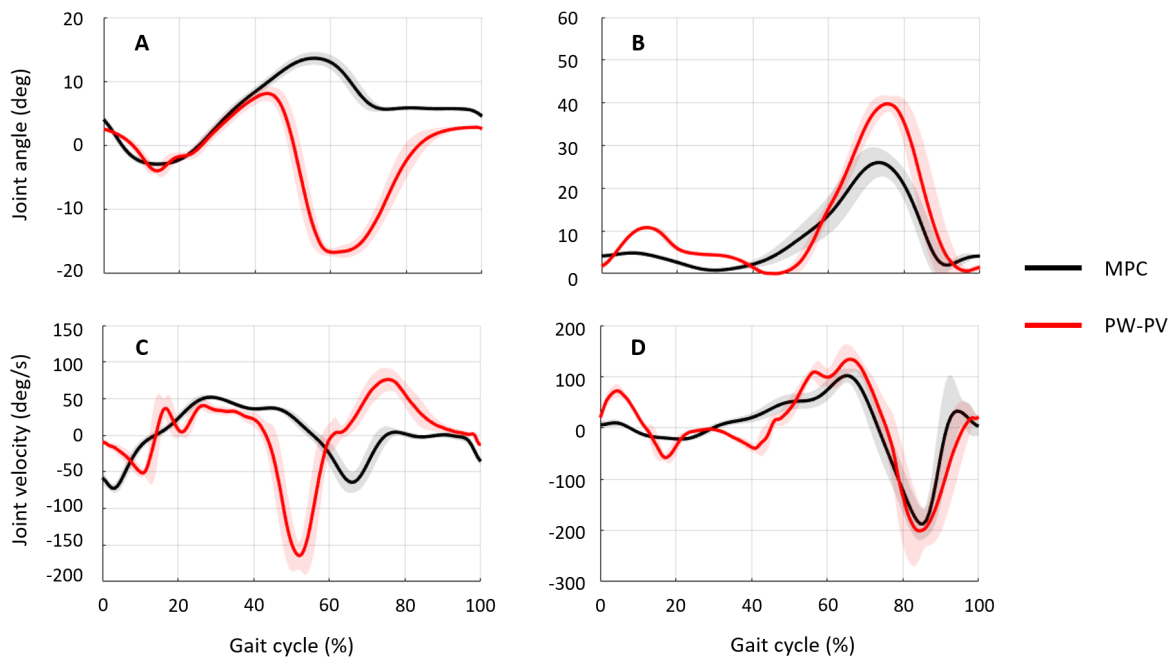
Figure 5.12: Joint kinematics comparison of amputee subject. (Black) MPC prosthesis. (Red) powered prosthesis. Solid line and shaded region represent the average of 20 gaits and ± 1 SD, respectively.

the MPC prosthesis provided a limited push-off, leading to dorsiflexion rather than plantarflexion around 50% of the gait cycle. In the case of the knee joint, both MPC and powered prostheses showed proper knee flexion during the swing phase (see Figure 5.12.B). However, the MPC still has limited knee flexion during the swing phase (less than 30°) compared to the powered prosthesis. Limited range of motion in ankle and knee joints is clearly illustrated in Figure 5.13. To be specific, the powered prosthesis offered approximately six times more ankle plantarflexion than the MPC prosthesis (see Figure 5.13.A). This plantarflexion occurred more than two times faster with the powered prosthesis, shown in Figure 5.13.C. In the case of the knee joint, the powered prosthesis provided 49% more knee flexion compared to the MPC prosthesis (see Figure 5.13.B). The knee joint angular velocities showed similar trends in both the powered and the MPC prostheses, as depicted in Figure 5.13.D.
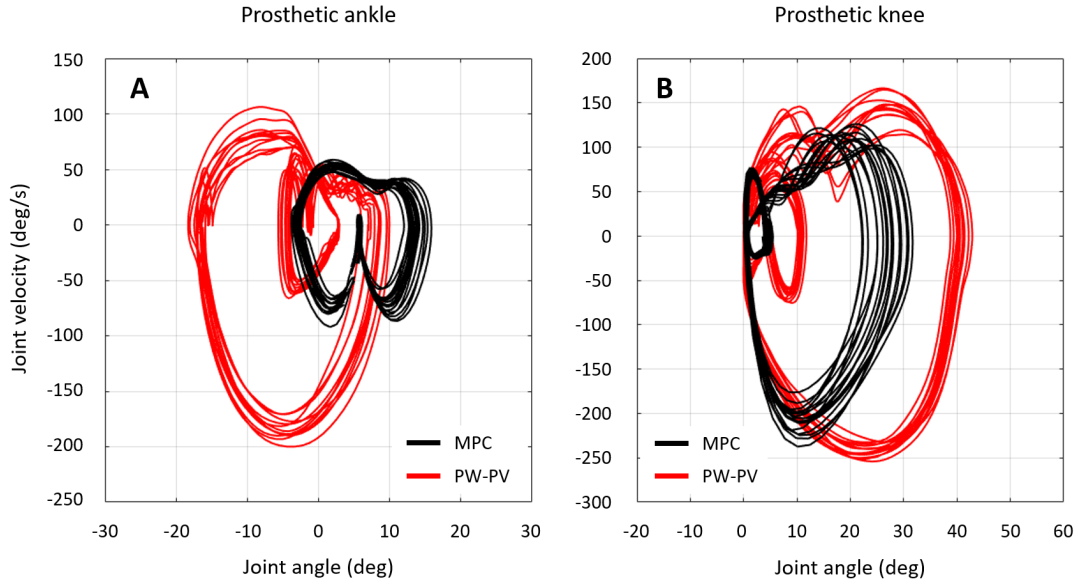
Figure 5.13: (A) Phase portrait of ankle. (B) Phase portrait of knee. (Black) MPC prosthesis. (Red) Powered prosthesis. Solid line and shaded region represent the average of 20 gaits and ± 1 SD, respectively.

5.4 Conclusion

The main focus of this chapter was speed adaptability enhancement when we estimated the user's gait phase. The conventional phase variable (i.e., PV) can adapt to different speeds based on different stride times between heel-strikes, but it cannot reflect variable toe-off timings at different walking speeds. Thus, in this chapter, we aim to reflect toe-off timing in phase variable computation. We propose a new piecewise phase variable (PW-PV) that can be adjusted for different toe-off timings at different walking speeds in order to maximize gait performance. The effects of the piecewise phase variable on joint kinematics, kinetics, and ground reaction forces were measured and analyzed. As a result, the resulting piecewise phase variable showed a faster load transfer with more natural roll-over during walking for both the able-bodied and amputee subjects. This allowed both subjects to have a longer push-off duration and more push-off work while walking. Furthermore, when PW-PV was used, both subjects showed higher ground reaction forces on their prosthesis-side legs, implying that they could trust the prosthesis more. The results of the

proposed method were also compared to those of the microprocessor-controlled (MPC) prosthesis. The proposed method improved push-off and knee flexion over the MPC prosthesis. As a result, we anticipate that by employing the proposed phase variable, we will be able to provide more appropriate and timely assistance with the prosthesis to individuals with varying walking speeds.

6. MACHINE LEARNING-BASED GAIT PHASE ESTIMATION

Researchers attempted to estimate the user gait phase using a learning-based method as data-driven approaches have recently emerged in the field. A linearly interpolated function based on the heel-strike was conventionally used as the ground truth in gait phase estimation model training. However, this labeling method cannot reflect variable toe-off timings at different walking speeds in spite of the importance of toe-off in the gait phase estimation [95, 96]. In this chapter, we propose a new labeling method (i.e., piecewise linear label) that allows the estimator to learn the ground truth based on variable toe-off onset timing at various walking speeds. Using long short-term memory (LSTM), we obtained three different trained models (general, slow, and normal-fast). At four different walking speeds, these models are compared to determine the effect of the piecewise linear label. The primary goal of this chapter is to validate the proposed labeling method for gait phase estimation, as well as to improve the robustness and speed adaptability when estimating the user's gait phase using a learning-based technique.

6.1 Methods

As explained in Section 1.3, when researchers estimate the user gait phase for lower-limb assistive devices such as exoskeletons or prostheses, they commonly use the torso, shank, or thigh information [71, 72, 76, 78]. Regardless of the input dataset chosen by the researchers, they all required heel-strike data measured by a force sensor attached to the heel. This is because the researchers conventionally provide a linear interpolated function based on heel-strikes regardless of walking speeds [71, 72, 76, 78] (red line in Figure 6.1). This linear labeling function, however, cannot reflect variable toe-off timings at different walking speeds, despite the fact that people's toe-off timings vary with speed [95, 96]. We discovered that different toe-off timings at different speeds affect gait phase estimation results [76]. According to [76], it was found that errors increase during mid-stance with greater deviations in slow walking. This could be interpreted as indicating that we may require additional information in model training to reflect varying speeds in order to

improve speed adaptability. A different labeling method could help improve the accuracy of gait phase estimation at different walking speeds. Therefore, we propose a piecewise linear label (blue line in Figure 6.1) for model training to accommodate different toe-off onset timings at various walking speeds in this chapter.
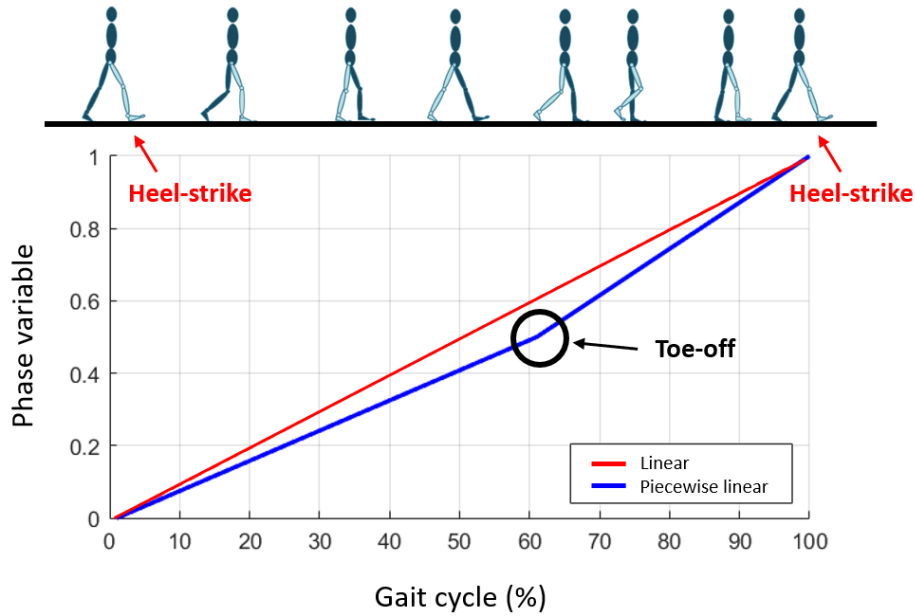
Figure 6.1: Ground truth for gait phase estimation model training. (Red) Linear label based on heel-strike. (Blue) Piecewise linear label based on heel-strike and toe-off.

6.1.1 Dataset

To ensure an adequate size of input data for our model training, we utilized an open-source dataset, which can be found in [122]. This dataset comprised data from 50 healthy subjects (26 male and 24 female) walking on a walkway in five different speed conditions: $0.0 - 0.4$ m/s (C_1), $0.4 - 0.8$ m/s (C_2), $0.8 - 1.2$ m/s (C_3), self-selected speed (C_4) and fast speed (C_5). Individuals' 3D motion data was provided via 52 whole-body reflective markers, allowing us to calculate angular positions and velocities of thigh and torso segments for model training. Furthermore, ground

reaction forces from two force plates were measured and used to estimate heel-strike and toe-off (see Figure 6.2). For markers, the data was sampled at 100 Hz, and for force plates, it was sampled at 1.5 kHz. The data from 42 individuals was chosen at random to be used for model training and validation, while the remaining data from 8 individuals was used for prediction.
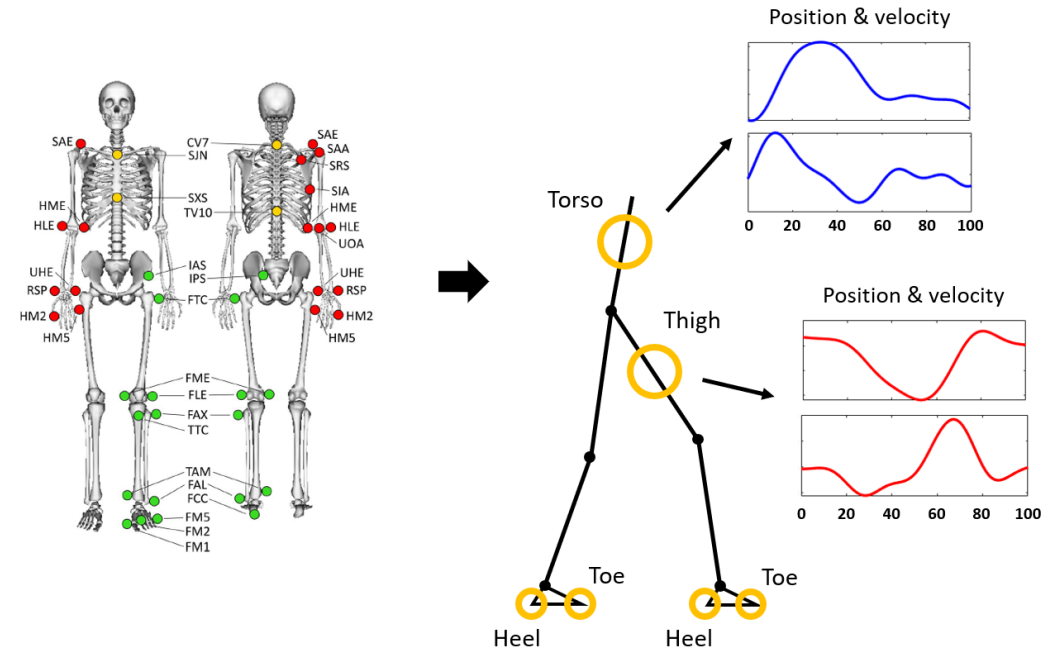
Figure 6.2: Input dataset for the model training. Angular positions and velocities of thigh and torso segments were calculated using 52 whole-body reflective markers. HS and TO were detected using two force plates.

6.1.2 Linear labeling for dataset

Because the human gait cycle is usually defined from heel-strike to subsequent ipsilateral heel-strike, heel-strike is commonly used as a cue of gait initiation [78, 123]. In the training session, we labeled the input dataset based on the heel-strike information using a polar coordinate encoding method [76]. This was because the nominal linear label is vulnerable to discontinuity at heel-strike due to gait initiation (see yellow circle in Figure 6.3), resulting in the undesirable loss (i.e.,

mean-squared error) during model training. We could avoid the undesirable error caused by the discontinuity at heel-strikes by using two independent sinusoidal functions (e.g., sine and cosine) as the ground truth (see Figure 6.3). These sine and cosine functions can be transformed into a linear function bounded in [0,1], which represents the gait cycle.
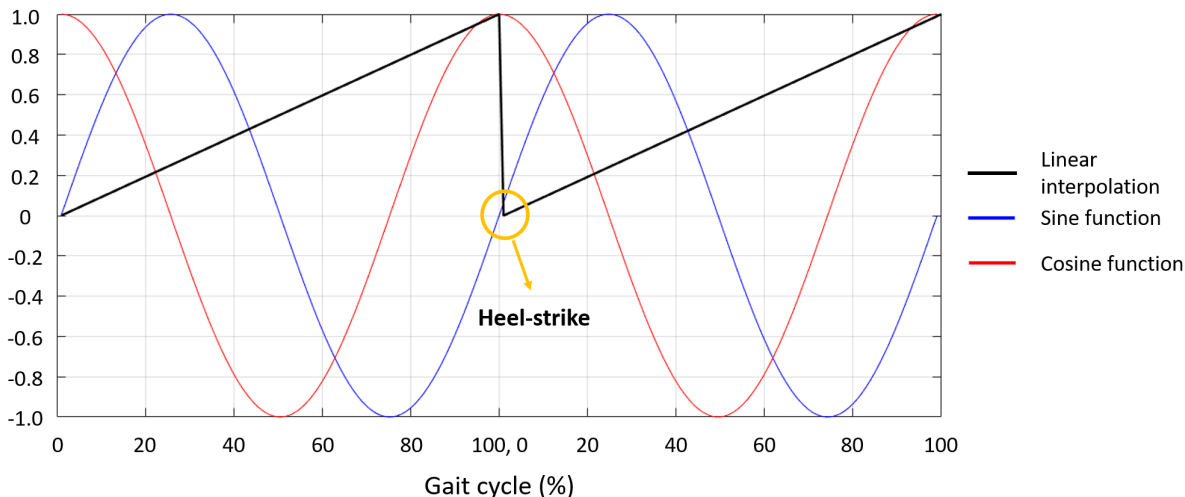
Figure 6.3: A linear interpolation and polar coordinate encoding.

6.1.3 Piecewise linear labeling for dataset

As explained in Section 6.1.2, the linear labeling function is the conventional way to assign the ground truth to the input dataset for the gait phase estimation [71, 72, 76]. Other gait events (e.g., HO and TO) between HS, however, cannot be considered in this case, despite the fact that they vary with walking speed [95, 96]. To take this into account, we propose a piecewise linear label as the ground truth for our model training. In contrast to the linear label, the proposed piecewise linear label is made up of two linear functions that are divided on TO (ϕ_{to}) (see Figure 6.4). To obtain those two linear functions for each phase (i.e., stance and swing), sine and cosine functions are still utilized but with a different period for each phase. As shown in Equation 6.1, the gait progression ($\phi \in [0, 100]$) can be mapped into θ_{st} during stance phase ($\phi < \phi_{to}$) and θ_{sw} during
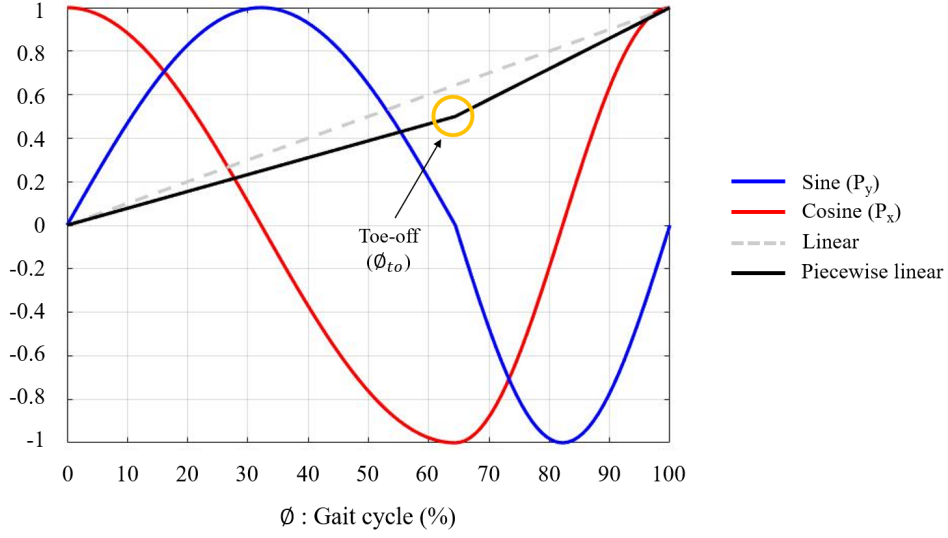
Figure 6.4: Piecewise linear labeling method. Two labels (P_x and P_y) are represented as cosine (Red) and sine (Blue) functions, respectively. Those sinusoidal functions result in a piecewise linear function (Black). A linear function (Gray) is given as a reference.

swing phase ($\phi \geq \phi_{to}$), where $\theta_{st} \in [0, \pi]$ and $\theta_{sw} \in [\pi, 2\pi]$.

$$
\begin{cases}
\theta_{st} = \frac{\phi}{\phi_{to}}\pi & \phi < \phi_{to} \\
\theta_{sw} = \frac{\phi - \phi_{to}}{100 - \phi_{to}}\pi + \pi & \phi \geq \phi_{to}
\end{cases}
\tag{6.1}
$$

Based on θ_{st} and θ_{sw}, the transformation between polar coordinates and cartesian coordinates is utilized to obtain our new labels P_x and P_y. They are represented as continuous sinusoidal functions, which are bounded in [-1,1] (refer to Equation 6.2).

$$
(P_x, P_y) =
\begin{cases}
(\cos\theta_{st}, \sin\theta_{st}) & \phi < \phi_{to} \\
(\cos\theta_{sw}, \sin\theta_{sw}) & \phi \geq \phi_{to}
\end{cases}
\tag{6.2}
$$

The resulting gait phase estimator should be formed as a monotonic and bounded (i.e., [0,1]) function to be used for controlling the assistive devices [59, 74]. Thus, additional transformation is performed based on P_x and P_y as explained in Equations 6.3 and 6.4. We call the resulting $\hat{\tau}$ as a

piecewise linear label in this study.

$$\tau = \frac{1}{2\pi} \operatorname{atan2}(Py, Px) \tag{6.3}$$

$$\hat{\tau} = \begin{cases} \tau & P_y \geq 0 \\ \tau + 1 & P_y < 0 \end{cases} \tag{6.4}$$

6.1.4 Neural network
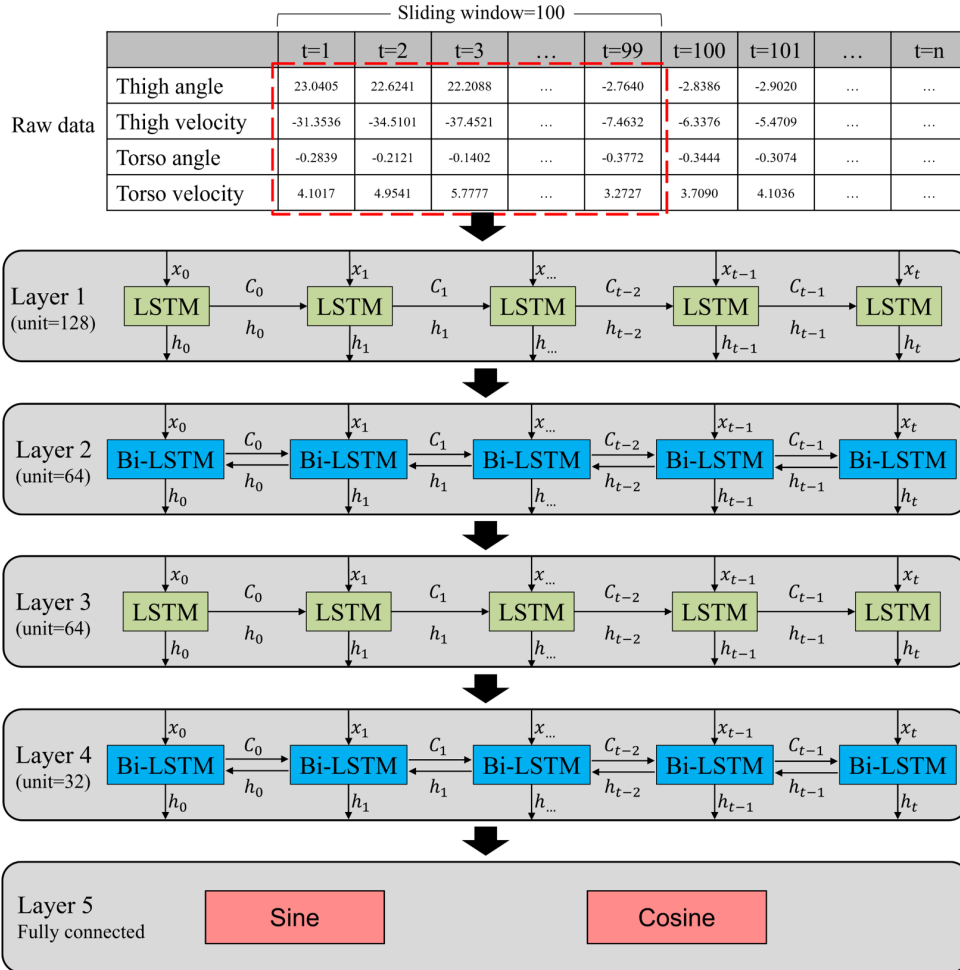
Figure 6.5: Proposed network architecture for gait phase estimation with a linear labeling and a piecewise linear labeling methods.

Long short-term memory (LSTM) was used in this chapter due to its excellent performance with chronological data, such as time series prediction [72, 76, 124]. According to [125], bidirectional LSTM (Bi-LSTM) was also used to achieve both forward and backward learning throughout the training process. This enables the model to learn from both past and future data. For our model, we used a sliding window size of 100. This choice was critical for a successful estimation, but due to the short length of the data obtained, we were unable to avoid a specific upper bound of the window size in this investigation. Figure 6.5 depicts the suggested network architecture. Our network is comprised of five layers, including LSTM and Bi-LSTM. Each layer contains 128, 64, 64, and 32 units, respectively. As shown in Figure 6.5, the current input (x_0) updates the cell state (C_0) and the output (h_0). The cell state updates information based on input data and passes previously learned information to the next block. Layer 5 produces the sine and cosine functions as the outputs. We chose the final value in the sequence to retrieve the gait phase at time t. The Adam optimizer was used to train the network model, and the loss function was set to mean-squared error (MSE) with a batch size of 64. To avoid over-fitting, the model was trained for a maximum of 100 epochs before being stopped if the validation loss did not continue to decrease after 10 epochs. We trained three different models under various speed conditions (e.g., $C_2 - C_5$, C_2, and $C_3 - C_5$). The first model, called general model (GM), trained its model using the broadest range of speed conditions: $C_2 - C_5$. During the training process, the second model (i.e., slow model (SM)) only used slow walking data (C_2), whereas the third model (i.e., normal-fast model (NFM)) used normal-fast speed conditions ($C_3 - C_5$). These models demonstrate the effect of labeling method on various walking speed conditions. It is worth noting that C_1 was left out of our model training because it referred to extremely slow speeds.

6.1.5 Statistical analysis

Statistical analysis was performed using RStudio statistical software (RStudio ver. 1.3.1093) to determine the significant trends in two labeling methods (i.e., linear and piecewise linear) and four speed conditions (i.e., C_2 - C_5). A two-way repeated-measures ANOVA was respectively performed for each trained model (i.e., GM, SM, and NFM) to identify the effects of the labeling

method, walking speed, and their interaction. A Bonferroni post-hoc correction was performed for a multiple comparison. In all analyses, a significance level of 0.05 was used. Statistical significance was denoted as follows: $* = p \leq 0.05$, $** = p \leq 0.01$, $*** = p \leq 0.001$.

6.2 Results

6.2.1 Training results

Each method was evaluated using the mean-square error (MSE). All of the results were trained in the same environment using the proposed networks. According to Figure 6.6, the linear label shows the higher error compare to the piecewise linear label in three trained models: general model (GM), slow model (SM), and normal-fast model (NFM). In the general model, the error was reduced by 39.5% when the piecewise linear label was used ($p < 0.001$). Both the slow and normal-fast models showed significant error reductions with the proposed piecewise linear label; 12.9% reduction in SM, while 40.7% reduction in NFM ($p < 0.001$). This implies that the proposed piecewise linear labeling method improves overall estimation accuracy.
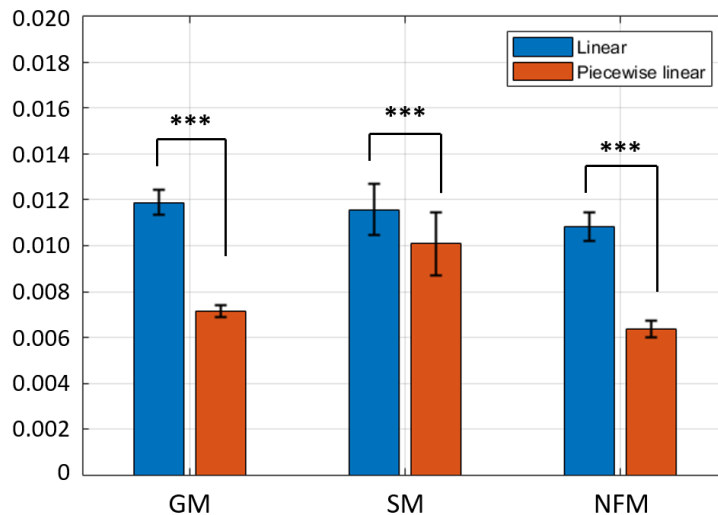
Figure 6.6: Training results of three different trained models: general (GM), slow (SM), and normal-fast model (NFM). Bar colors correspond to two labeling methods: linear, and piecewise linear label. Bar graphs and error bars correspond to mean and ±1 SD.

6.2.2 Prediction results

To evaluate the proposed labeling method, the gait phase prediction was performed based on the eight individual's data at four different walking speeds (i.e., $C_2 - C_5$). We used mean-squared error (MSE) and heel-strike detection error (HSE) to evaluate the proposed method (see Figure 6.7). The mean-squared error (Figure 6.7.A) can be calculated as below.

$$MSE = \frac{1}{n} \sum_{i=1}^{n} (G_i - P_i)^2 \tag{6.5}$$

where n refers to the length of data, while G_i and P_i refer to the ground truth and the predicted value at i^{th} data point. The detection error at heel-strike refers to the difference in time between the actual and predicted heel-strike (see Figure 6.7.B).
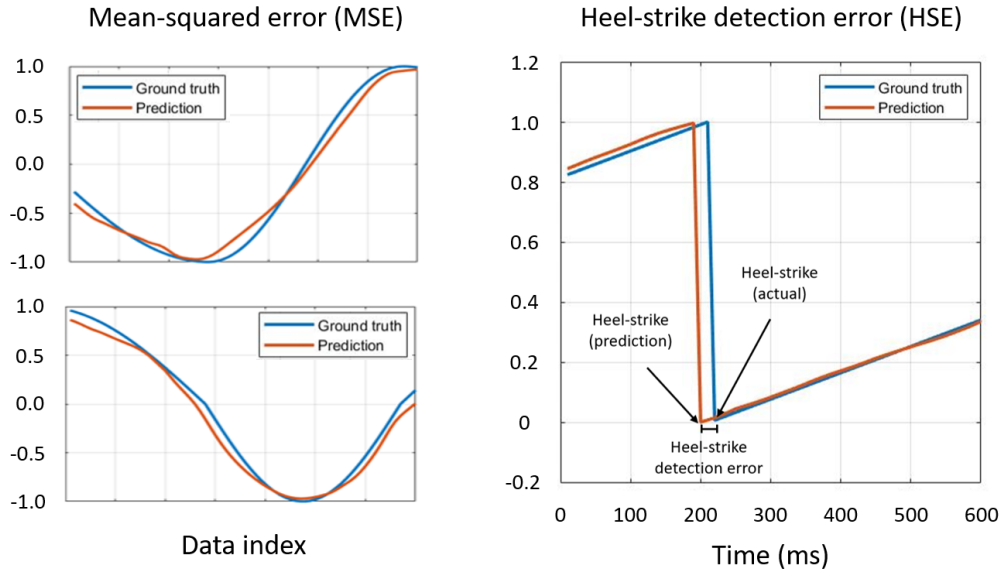
Figure 6.7: Error between prediction and ground truth. (A) Mean-squared error (MSE). (B) Heel-strike detection error (HSE).

The gait phase estimation results (i.e., MSE) of three trained models are illustrated in Figure 6.8. As shown in Figure 6.8.A, the estimation error was significantly reduced across all speed
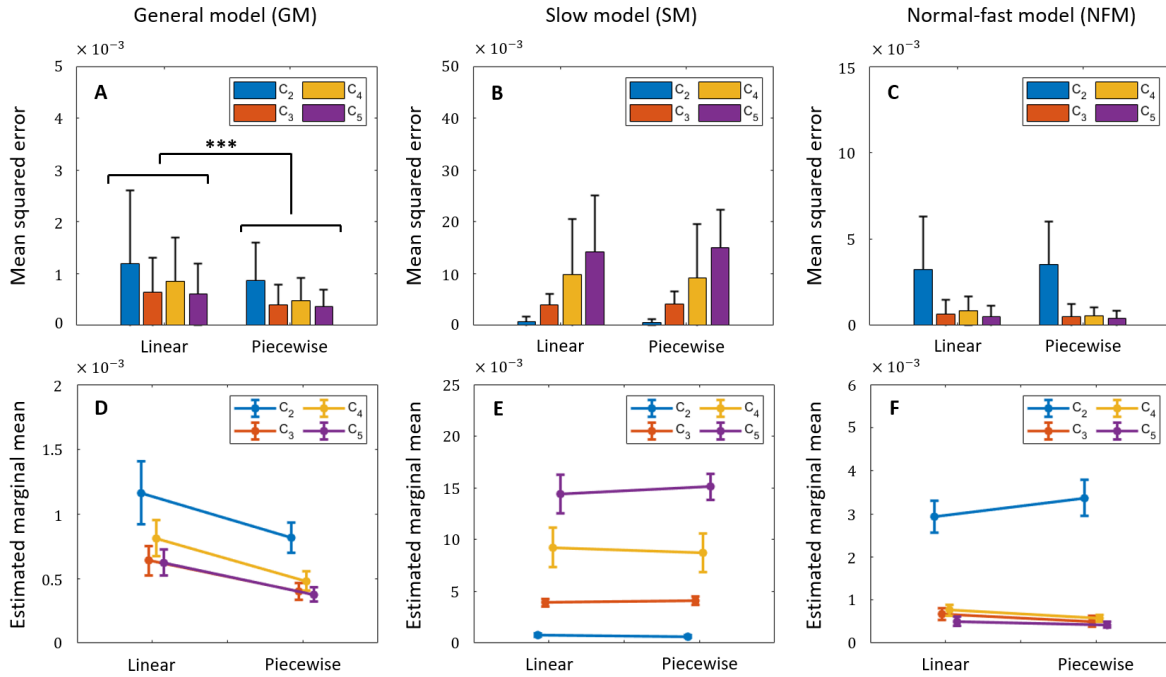
Figure 6.8: Mean-squared error (MSE) between the ground truth and prediction in three trained models: (A) GM, (B) SM, and (C) NFM. The bottom shows the interaction effect between the labeling methods (Linear and Piecewise linear) and the walking speeds ($C_2 - C_5$) in three trained models: (D) GM, (E) SM, and (F) NFM. Bar graphs and error bars correspond to mean and +1 SD. Bar colors correspond to walking speeds: $C_2 - C_5$.

conditions when the piecewise linear label was used in GM ($p < 0.001$). To be more specific, 27.0%, 37.3%, 43.6%, and 39.8% error reductions were found in each speed condition ($C_2 -$ C_5), respectively. The speed condition also showed a significant effect ($p = 0.005$), while there is no interaction effect between the labeling method and the walking speed (see Figure 6.8.D). The slow model revealed no significant difference between the labeling methods ($p = 0.887$), but a significant effect in the speed conditions ($p < 0.001$), depicted in Figure 6.8.B. As the walking speed increased, the error became greater. This was due to the fact that SM was only trained using the slow walking dataset (C_2), which resulted in poor estimation results at faster speeds. No interaction effect was found in Figure 6.8.D. In the case of NFM, there was no main effect of the labeling method (see Figure 6.8.C). The walking speed, however, showed a significant effect ($p < 0.001$). Figure 6.8.C depicted a huge error at the slow speed condition (C_2) compared to the other

speeds ($C_3 - C_5$). This is obvious because the slow walking data was not included while training the NFM. Interestingly, there was an interaction effect between the labeling method and the speed condition in NFM (p = 0.011).
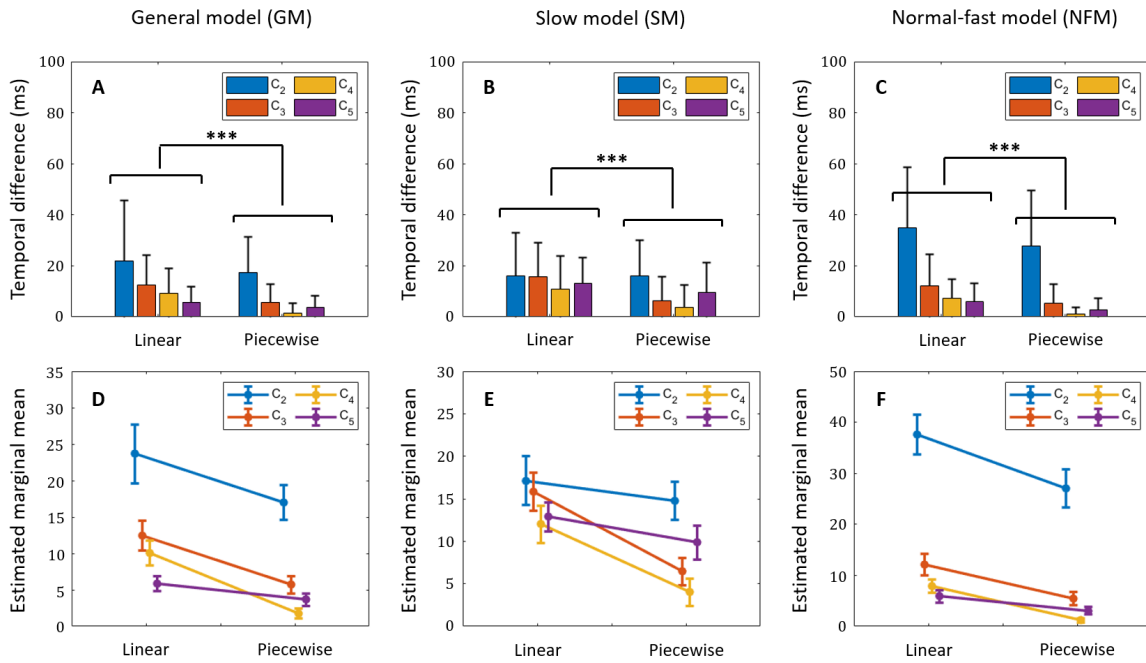
Figure 6.9: Heel-strike detection error (HSE) between the ground truth and prediction in three trained models: (A) GM, (B) SM, and (C) NFM. The bottom shows the interaction effect between the labeling methods (Linear and Piecewise linear) and the walking speeds ($C_2 - C_5$) in three trained models: (D) GM, (E) SM, and (F) NFM. Bar graphs and error bars correspond to mean and +1 SD. Bar colors correspond to walking speeds: $C_2 - C_5$.

The piecewise linear labeling method showed a significantly higher accuracy in the heel-strike detection for three trained models, depicted in Figures 6.9.A-C (GM: p = 0.001, SM: p < 0.001, NFM: p < 0.001). In GM, the heel-strike detection error (HSE) was reduced by 20.6%, 54.0%, 83.2%, and 38.4% for each walking speed with the piecewise linear label (see Figure 6.9.A). In the case of SM, there was no significant effect of labeling method in C_2, but 59.5%, 67.1%, and 25.8% of HSE reduction were found with the piecewise linear label in $C_3 - C_5$, respectively (see Figure 6.9.B). Figure 6.9.C shows the HSE results of NFM. A great error reduction can be found when

Table 6.1: Mean-squared error (MSE) results, when $C_3 - C_5$ was excluded in SM and C_2 was excluded in NFM.

	Mean-squared error (MSE)	
	Linear	Piecewise linear
SM (C_2)	0.7908 $\pm$ 0.9014 E-03	0.6453 $\pm$ 0.5794 E-03
NFM (C_3)	0.6784 $\pm$ 0.8096 E-03	0.5041 $\pm$ 0.7399 E-03
NFM (C_4)	0.8417 $\pm$ 0.8144 E-03	0.5585 $\pm$ 0.4861 E-03
NFM (C_5)	0.5076 $\pm$ 0.6326 E-03	0.4076 $\pm$ 0.4252 E-03

the piecewise linear labeling method was used (C_2: 20.0%, C_3: 55.3%, C_4: 85.7%, C_5: 51.1% reduced). According to the given two-way repeated-measures ANOVA, there was an apparent effect of the walking speed for all three models (GM: p < 0.001, SM: p = 0.001, NFM: p < 0.001). However, no interaction effect between the label and the speed condition was found in three models (see Figures 6.9.D-F).

6.3 Discussion

According to Figures. 6.8.B and C, the labeling method showed no significant effect on the gait phase estimation for the slow model and the normal-fast model. However, these results may be affected by incomparably large errors derived from $C_3 - C_5$ in SM, and derived from C_2 in NFM. To be more specific, $C_3 - C_5$ showed 5.6, 13.2, 20.4 times more errors compared to C_2 in SM (Fig. 6.8.B). In the case of NFM, C_2 showed approximately 6 times more errors compared to $C_3 - C_5$ (Fig. 6.8.C). These large errors were obviously induced because $C_3 - C_5$ and C_2 were excluded for the slow model training and the normal-fast model training, respectively. Table 6.1 shows the MSE result of C_2 in SM and that of $C_3 - C_5$ in NFM. In these results, the piecewise linear labeling achieved a 18.4% error reduction in SM, and 25.7%, 33.6%, 19.7% error reduction at C_3, C_4, C_5 in NFM, respectively (SM: p < 0.001, NFM: p < 0.001). This implies that when we focus on C_2 result of SM and $C_3 - C_5$ result of NFM, we could find the significant effect of the labeling method.

Among the three trained models (i.e., GM, SM, and NFM), GM showed the best performance in general. Across four given speed conditions, GM achieved the smallest mean squared error

in estimating the user's gait phase and the best detection of the heel-strike (see Figures. 6.8 and 6.9). With the piecewise label, both prediction and heel-strike detection errors are surprisingly reduced across all walking speeds in Figures 6.8.A and 6.9.A. This implies that the inclusion of toe-off timing information in model training improves accuracy in gait phase estimation. Even though there was a relatively high error at slow speed in Figure 6.9.A, their values were less than 35 ms at most (i.e., 17.50±13.84 ms). Seeing that the maximum temporal error is comparable to the short-latency response time of the human lower-limb reflex pathway (i.e., $\simeq$ 40-50 ms) [126], those errors are acceptable to be used for heel-strike detection. Note that the temporal error of heel-strike detection is less than 15 ms when C_2 results are excluded.

As we mentioned in Section 6.1.4, we did not have much choice in the size of the sliding window for our model training. Since the chosen dataset was collected on a walkway, it contained relatively short time-series data (compared to treadmill walking), including only a single gait cycle at most. We considered an alternative dataset, but the selected dataset contained an abundant number of subjects, which guaranteed to show individuals' variability. The chosen window size may affect the estimation accuracy, but we obtained sufficiently high accuracy in our estimation. To be fair with validating this claim, we implemented the same window size (i.e., 100) to our previous model [76] and compared its training results (i.e., MSE) to this study. As a result, there was no significant difference between them ([76]: 1.10E-02 vs. this study: 1.19E-02), thereby alleviating the concern about the window size.

In future work, the authors plan to develop a user-adaptive gait phase estimator for enhancing an individual's gait trait adaptability. This is important for providing user-specific control of wearable devices based on user-specific gait estimation. This is because all individuals have their own gait traits, and considering these traits is expected to give a better estimation of the individual. Also, we plan to implement a convolutional neural network (CNN) with LSTM to obtain faster estimation. The proposed method will be implemented to control a custom-built powered prosthesis. The authors have controlled the powered prosthesis using a phase variable, deriving from the user's thigh motion [74]. Unlike the phase variable, a learning-based gait phase estimation utilized a

plentiful dataset, so we could expect improved robustness, leading to more stable control of the prosthesis. Furthermore, estimating the user gait phase in different ambulation modes (e.g., ramp ascent/descent and stair ascent/descent) is important when we use the prosthesis in an overground situation. Thus, we plan to develop a terrain-adaptive gait phase estimator for the lower-limb prosthesis.

6.4 Conclusion

A linearly interpolated function has been commonly used as the ground truth in gait phase estimation using machine learning. This function can estimate the user's gait phase at various speeds, but it cannot account for variable toe-off timings at various walking speeds. In this study, we newly proposed a piecewise linear labeling method in the model training to enhance speed adaptability for gait phase estimation. This let the estimator learn the new ground truth based on variable toe-off timing at different walking speeds. The proposed idea was compared to the conventional linear labeling method at four different walking speeds. Consequently, at various walking speeds, the gait phase prediction results were more accurate with the proposed label. Furthermore, the proposed labeling method improved heel-strike detection for gait initiation. As a result, this study suggests the proposed piecewise linear label could enhance the speed-adaptability, thereby improving the accuracy of gait phase estimation at various walking speeds.

7. CONCLUSION

The goal of this dissertation was to develop an adaptive gait phase estimation for different users and walking speeds. First, we focused on improving user adaptability for gait phase estimation. To adapt to an individual's walking traits while estimating their gait phase, a phase-shifting method was proposed. Human data show that people have a cosine-like trend in their thigh segment movement while walking, which can be used to estimate their walking progression. However, it has been demonstrated that they are prone to having different thigh phase-shifts in their walking. Adopting this information resulted in improved heel detection and linearity of phase variables across the gait cycle. The proposed phase-shifting phase variable also resulted in more consistent walking. Second, we worked on improving the gait phase estimator's speed adaptability. To accomplish this, we proposed a piecewise phase variable that, when computed, can use variable toe-off timings at different walking speeds. While walking with the prosthesis, this allows the prosthesis to provide a more timely and effective push-off. As a result, the proposed phase variable resulted in faster load transfer during walking, as well as longer push-off duration and more push-off work. Furthermore, when the proposed method was used, all of the subjects showed higher ground reaction forces on their prosthesis-side legs with PW-PV, implying that they had more trust in the prosthesis. A machine-learning approach was also used to estimate the user's gait phase at different speeds. At different walking speeds, people have different onsets of heel-off or toe-off. To improve speed change adaptability based on variable toe-off timings, we proposed a new labeling method (i.e., piecewise linear label) for gait phase estimation. The estimator was able to learn the new ground truth based on variable toe-off timings at different walking speeds as a result of this. Consequently, higher accuracy was achieved in the prediction results at various walking speeds. This dissertation, therefore, introduces new methods that could improve user adaptability and speeds when estimating the user's gait phase while walking.

REFERENCES

[1] "Ottobock aqualine waterproof passive prosthesis." Accessed on: Dec. 2, 2021. [Online]. Available: "https://www.ottobockus.com/products/aqualine-waterproof-above-knee-system/".

[2] "Ottobock c-leg above knee prosthetic leg." Accessed on: Dec. 2, 2021. [Online]. Available: "http://www.ottobockus.com/C-Leg.html".

[3] "Rheo knee." Accessed on: Dec. 2, 2021. [Online]. Available: "https://www.ossur.com/en-us/prosthetics/knees/rheo-knee".

[4] F. Sup, H. A. Varol, J. Mitchell, T. J. Withrow, and M. Goldfarb, "Preliminary evaluations of a self-contained anthropomorphic transfemoral prosthesis," *IEEE/ASME Transactions on Mechatronics*, vol. 14, no. 6, pp. 667–676, 2009.

[5] B. E. Lawson, H. A. Varol, A. Huff, E. Erdemir, and M. Goldfarb, "Control of stair ascent and descent with a powered transfemoral prosthesis," *IEEE Transactions on Neural Systems and Rehabilitation Engineering*, vol. 21, no. 3, pp. 466–473, 2012.

[6] B. E. Lawson and M. Goldfarb, "Impedance & admittance-based coordination control strategies for robotic lower limb prostheses," *Mechanical Engineering Magazine Select Articles*, vol. 136, no. 09, pp. S12–S17, 2014.

[7] H. Zhao, J. Horn, J. Reher, V. Paredes, and A. D. Ames, "Multicontact locomotion on transfemoral prostheses via hybrid system models and optimization-based control," *IEEE Transactions on Automation Science and Engineering*, vol. 13, no. 2, pp. 502–513, 2016.

[8] V. Azimi, T. Shu, H. Zhao, E. Ambrose, A. D. Ames, and D. Simon, "Robust control of a powered transfemoral prosthesis device with experimental verification," in *2017 American Control Conference (ACC)*, pp. 517–522, IEEE, 2017.

[9] D. Quintero, D. J. Villarreal, and R. D. Gregg, "Preliminary experiments with a unified controller for a powered knee-ankle prosthetic leg across walking speeds," in *2016 IEEE/RSJ International Conference on Intelligent Robots and Systems (IROS)*, pp. 5427–5433, IEEE, 2016.

[10] T. Elery, S. Rezazadeh, C. Nesler, and R. D. Gregg, "Design and validation of a powered knee–ankle prosthesis with high-torque, low-impedance actuators," *IEEE Transactions on Robotics*, vol. 36, no. 6, pp. 1649–1668, 2020.

[11] N. Thatte, N. Srinivasan, and H. Geyer, "Real-time reactive trip avoidance for powered transfemoral prostheses," *Robotics Systems and Sciences (RSS)*, 2019.

[12] J. Lee, H. L. Bartlett, and M. Goldfarb, "Design of a semi-powered stance-control swing-assist transfemoral prosthesis," *IEEE/ASME Transactions on Mechatronics*, 2019.

[13] H. L. Bartlett, B. Lawson, and M. Goldfarb, "Design, control, and preliminary assessment of a multifunctional semi-powered ankle prosthesis," *IEEE/ASME Transactions on Mechatronics*, 2019.

[14] M. Tran, L. Gabert, M. Cempini, and T. Lenzi, "A lightweight, efficient fully powered knee prosthesis with actively variable transmission," *IEEE Robotics and Automation Letters*, vol. 4, no. 2, pp. 1186–1193, 2019.

[15] L. Gabert, S. Hood, M. Tran, M. Cempini, and T. Lenzi, "A compact, lightweight robotic ankle-foot prosthesis: Featuring a powered polycentric design," *IEEE robotics & automation magazine*, vol. 27, no. 1, pp. 87–102, 2020.

[16] S. H. Collins and A. D. Kuo, "Recycling energy to restore impaired ankle function during human walking," *PLoS One*, vol. 5, no. 2, p. e9307, 2010.

[17] K. Ziegler-Graham, E. J. MacKenzie, P. L. Ephraim, T. G. Travison, and R. Brookmeyer, "Estimating the prevalence of limb loss in the united states: 2005 to 2050," *Archives of Physical Medicine and Rehabilitation*, vol. 89, no. 3, pp. 422–429, 2008.

[18] L. D. Patti Ephraim, "People with amputation speak out with the amputee coalition of america (ACA)," Accessed on: Dec. 2, 2021. [Online]. Available: "https://www.amputee-coalition.org".

[19] "Amputee statistics you ought to know." Accessed on: Dec. 2, 2021. [Online]. Available: "https://advancedamputees.com/amputee-statistics-you-ought-know".

[20] "Effects of amputation." Accessed on: Dec. 2, 2021. [Online]. Available: "http://www.seriousinjurylaw.co.uk/other-serious-claims/amputation/effects-of-amputation".

[21] W. C. Miller, A. B. Deathe, M. Speechley, and J. Koval, "The influence of falling, fear of falling, and balance confidence on prosthetic mobility and social activity among individuals with a lower extremity amputation," *Archives of Physical Medicine and Rehabilitation*, vol. 82, no. 9, pp. 1238–1244, 2001.

[22] C. Gauthier-Gagnon, M.-C. Grisé, and D. Potvin, "Enabling factors related to prosthetic use by people with transtibial and transfemoral amputation," *Archives of Physical Medicine and Rehabilitation*, vol. 80, no. 6, pp. 706–713, 1999.

[23] L. A. Talbot, R. J. Musiol, E. K. Witham, and E. J. Metter, "Falls in young, middle-aged and older community dwelling adults: perceived cause, environmental factors and injury," *BMC Public Health*, vol. 5, no. 1, pp. 1–9, 2005.

[24] R. E. Seroussi, A. Gitter, J. M. Czerniecki, and K. Weaver, "Mechanical work adaptations of above-knee amputee ambulation," *Archives of Physical Medicine and Rehabilitation*, vol. 77, no. 11, pp. 1209–1214, 1996.

[25] T. Pohjolainen, H. Alaranta, and M. Kärkäinen, "Prosthetic use and functional and social outcome following major lower limb amputation," *Prosthetics and Orthotics International*, vol. 14, no. 2, pp. 75–79, 1990.

[26] "Classification of lower limb amputation." Accessed on: Dec. 2, 2021. [Online]. Available: "http://www.cdha.nshealth.ca /amputee-rehabilitation-musculoskeletal-program/patient-family-information/lower-limb-amputations".

[27] D. G. Smith, "The transfemoral amputation level, part 1," 2004. Accessed on: Dec. 2, 2021. [Online]. Available: "http://www.amputee-coalition.org /resources/transfemoral-amputation-part-1".

[28] T. R. Dillingham, L. E. Pezzin, and E. J. MacKenzie, "Limb amputation and limb deficiency: epidemiology and recent trends in the united states," *Southern Medical Journal*, vol. 95, no. 8, pp. 875–884, 2002.

[29] C. Walker, R. Ingram, M. Hullin, and S. McCreath, "Lower limb amputation following injury: a survey of long-term functional outcome," *Injury*, vol. 25, no. 6, pp. 387–392, 1994.

[30] M. Jones, J. Steel, G. Bashford, and I. Davidson, "Static versus dynamic prosthetic weight bearing in elderly trans-tibial amputees," *Prosthetics and Orthotics International*, vol. 21, no. 2, pp. 100–106, 1997.

[31] B. J. Hafner, J. E. Sanders, J. Czerniecki, and J. Fergason, "Energy storage and return prostheses: does patient perception correlate with biomechanical analysis?," *Clinical Biomechanics*, vol. 17, no. 5, pp. 325–344, 2002.

[32] A. E. Minetti, C. Moia, G. S. Roi, D. Susta, and G. Ferretti, "Energy cost of walking and running at extreme uphill and downhill slopes," *Journal of Applied Physiology*, vol. 93, no. 3, pp. 1039–1046, 2002.

[33] R. Riener, M. Rabuffetti, and C. Frigo, "Stair ascent and descent at different inclinations," *Gait & Posture*, vol. 15, no. 1, pp. 32–44, 2002.

[34] S. M. Reid, S. K. Lynn, R. P. Musselman, and P. A. Costigan, "Knee biomechanics of alternate stair ambulation patterns," *Medicine and Science in Sports and Exercise*, vol. 39, no. 11, pp. 2005–2011, 2007.

[35] R. Gailey, K. Allen, J. Castles, J. Kucharik, and M. Roeder, "Review of secondary physical conditions associated with lower-limb amputation and long-term prosthesis use," *Journal of Rehabilitation Research & Development*, vol. 45, no. 1, pp. 15–30, 2008.

[36] C. Jayaraman, S. Hoppe-Ludwig, S. Deems-Dluhy, M. McGuire, C. Mummidisetty, R. Siegal, A. Naef, B. E. Lawson, M. Goldfarb, K. E. Gordon, *et al.*, "Impact of powered knee-ankle prosthesis on low back muscle mechanics in transfemoral amputees: A case series," *Frontiers in Neuroscience*, vol. 12, p. 134, 2018.

[37] P. F. Pasquina, P. R. Bryant, M. E. Huang, T. L. Roberts, V. S. Nelson, and K. M. Flood, "Advances in amputee care," *Archives of Physical Medicine and Rehabilitation*, vol. 87, no. 3, pp. 34–43, 2006.

[38] H. Zhao, J. Reher, J. Horn, V. Paredes, and A. D. Ames, "Realization of nonlinear real-time optimization based controllers on self-contained transfemoral prosthesis," in *ACM/IEEE 6th International Conference on Cyber-Physical Systems*, pp. 130–138, ACM, 2015.

[39] F. Sup, A. Bohara, and M. Goldfarb, "Design and control of a powered transfemoral prosthesis," *The International Journal of Robotics Research*, vol. 27, no. 2, pp. 263–273, 2008.

[40] R. D. Gregg, T. Lenzi, L. J. Hargrove, and J. W. Sensinger, "Virtual constraint control of a powered prosthetic leg: From simulation to experiments with transfemoral amputees," *IEEE Transactions on Robotics*, vol. 30, no. 6, pp. 1455–1471, 2014.

[41] F. Sup, H. A. Varol, and M. Goldfarb, "Upslope walking with a powered knee and ankle prosthesis: initial results with an amputee subject," *IEEE Transactions on Neural Systems and Rehabilitation Engineering*, vol. 19, no. 1, pp. 71–78, 2011.

[42] V. Paredes, W. Hong, S. Patrick, and P. Hur, "Upslope walking with transfemoral prosthesis using optimization based spline generation," in *2016 IEEE/RSJ International Conference on Intelligent Robots and Systems (IROS)*, pp. 3204–3211, IEEE, 2016.

[43] W. Hong, V. Paredes, K. Chao, S. Patrick, and P. Hur, "Consolidated control framework to control a powered transfemoral prosthesis over inclined terrain conditions," in *2019 International Conference on Robotics and Automation (ICRA)*, pp. 2838–2844, IEEE, 2019.

[44] H. Zhao, J. Reher, J. Horn, V. Paredes, and A. D. Ames, "Realization of stair ascent and motion transitions on prostheses utilizing optimization-based control and intent recognition," in *2015 IEEE International Conference on Rehabilitation Robotics (ICORR)*, pp. 265–270, IEEE, 2015.

[45] B. E. Lawson, H. A. Varol, F. Sup, and M. Goldfarb, "Stumble detection and classification for an intelligent transfemoral prosthesis," in *2010 32nd Annual International Conference of the IEEE Engineering in Medicine and Biology Society (EMBC)*, pp. 511–514, IEEE, 2010.

[46] N. Thatte and H. Geyer, "Toward balance recovery with leg prostheses using neuromuscular model control," *IEEE Transactions on Biomedical Engineering*, vol. 63, no. 5, pp. 904–913, 2015.

[47] A. M. Simon, K. A. Ingraham, N. P. Fey, S. B. Finucane, R. D. Lipschutz, A. J. Young, and L. J. Hargrove, "Configuring a powered knee and ankle prosthesis for transfemoral amputees within five specific ambulation modes," *PloS One*, vol. 9, no. 6, p. e99387, 2014.

[48] H. Huang, D. L. Crouch, M. Liu, G. S. Sawicki, and D. Wang, "A cyber expert system for auto-tuning powered prosthesis impedance control parameters," *Annals of Biomedical Engineering*, vol. 44, no. 5, pp. 1613–1624, 2016.

[49] K. Bhakta, J. Camargo, and A. J. Young, "Control and experimental validation of a powered knee and ankle prosthetic device," in *ASME 2018 Dynamic Systems and Control Conference*, American Society of Mechanical Engineers Digital Collection, 2018.

[50] H. A. Varol, F. Sup, and M. Goldfarb, "Powered sit-to-stand and assistive stand-to-sit framework for a powered transfemoral prosthesis," in *2009 IEEE International Conference on Rehabilitation Robotics (ICORR)*, pp. 645–651, IEEE, 2009.

[51] L.-X. Wang and J. M. Mendel, "Generating fuzzy rules by learning from examples," *IEEE Transactions on Systems, Man, and Cybernetics*, vol. 22, no. 6, pp. 1414–1427, 1992.

[52] A. D. Ames, "First steps toward automatically generating bipedal robotic walking from human data," in *Robot Motion and Control 2011*, pp. 89–116, Springer, 2012.

[53] H. Zhao, E. Ambrose, and A. D. Ames, "Preliminary results on energy efficient 3d prosthetic walking with a powered compliant transfemoral prosthesis," in *2017 IEEE International Conference on Robotics and Automation (ICRA)*, pp. 1140–1147, IEEE, 2017.

[54] A. E. Martin and R. D. Gregg, "Hybrid invariance and stability of a feedback linearizing controller for powered prostheses," in *2015 American Control Conference (ACC)*, pp. 4670–4676, IEEE, 2015.

[55] D. Quintero, A. E. Martin, and R. D. Gregg, "Unifying the gait cycle in the control of a powered prosthetic leg," in *2015 IEEE International Conference on Rehabilitation Robotics (ICORR)*, pp. 289–294, IEEE, 2015.

[56] K. A. Hamed and R. D. Gregg, "Decentralized feedback controllers for exponential stabilization of hybrid periodic orbits: Application to robotic walking," in *2016 American Control Conference (ACC)*, pp. 4793–4800, IEEE, 2016.

[57] D. J. Villarreal, D. Quintero, and R. D. Gregg, "Piecewise and unified phase variables in the control of a powered prosthetic leg," in *2017 IEEE International Conference on Rehabilitation Robotics (ICORR)*, pp. 1425–1430, IEEE, 2017.

[58] D. J. Villarreal, H. A. Poonawala, and R. D. Gregg, "A robust parameterization of human gait patterns across phase-shifting perturbations," *IEEE Transactions on Neural Systems and Rehabilitation Engineering*, vol. 25, no. 3, pp. 265–278, 2016.

[59] D. Quintero, D. J. Villarreal, D. J. Lambert, S. Kapp, and R. D. Gregg, "Continuous-phase control of a powered knee–ankle prosthesis: Amputee experiments across speeds and inclines," *IEEE Transactions on Robotics*, vol. 34, no. 3, pp. 686–701, 2018.

[60] S. Rezazadeh, D. Quintero, N. Divekar, E. Reznick, L. Gray, and R. D. Gregg, "A phase variable approach for improved rhythmic and non-rhythmic control of a powered knee-ankle prosthesis," *IEEE Access*, vol. 7, pp. 109840–109855, 2019.

[61] N. Thatte and H. Geyer, "Towards local reflexive control of a powered transfemoral prosthesis for robust amputee push and trip recovery," in *2014 IEEE/RSJ International Conference on Intelligent Robots and Systems (IROS)*, pp. 2069–2074, IEEE, 2014.

[62] T. Lenzi, M. Cempini, L. J. Hargrove, and T. A. Kuiken, "Design, development, and validation of a lightweight nonbackdrivable robotic ankle prosthesis," *IEEE/ASME Transactions on Mechatronics*, vol. 24, no. 2, pp. 471–482, 2019.

[63] N. Anil Kumar, W. Hong, and P. Hur, "Impedance control of a transfemoral prosthesis using continuously varying ankle impedances and multiple equilibria," in *2020 IEEE International Conference on Robotics and Automation (ICRA)*, pp. 1755–1761, IEEE, 2020.

[64] R. Desai and H. Geyer, "Robust swing leg placement under large disturbances," in *2012 IEEE International Conference on Robotics and Biomimetics (ROBIO)*, pp. 265–270, IEEE, 2012.

[65] R. Desai and H. Geyer, "Muscle-reflex control of robust swing leg placement," in *2013 IEEE International Conference on Robotics and Automation (ICRA)*, pp. 2169–2174, IEEE, 2013.

[66] H. Geyer and H. Herr, "A muscle-reflex model that encodes principles of legged mechanics produces human walking dynamics and muscle activities," *IEEE Transactions on Neural Systems and Rehabilitation Engineering*, vol. 18, no. 3, pp. 263–273, 2010.

[67] T. Lenzi, M. Cempini, L. Hargrove, and T. Kuiken, "Design, development, and testing of a lightweight hybrid robotic knee prosthesis," *The International Journal of Robotics Research*, vol. 37, no. 8, pp. 953–976, 2018.

[68] A. D. Segal, K. E. Zelik, G. K. Klute, D. C. Morgenroth, M. E. Hahn, M. S. Orendurff, P. G. Adamczyk, S. H. Collins, A. D. Kuo, and J. M. Czerniecki, "The effects of a controlled en-

ergy storage and return prototype prosthetic foot on transtibial amputee ambulation," *Human Movement Science*, vol. 31, no. 4, pp. 918–931, 2012.

[69] K. E. Zelik, S. H. Collins, P. G. Adamczyk, A. D. Segal, G. K. Klute, D. C. Morgenroth, M. E. Hahn, M. S. Orendurff, J. M. Czerniecki, and A. D. Kuo, "Systematic variation of prosthetic foot spring affects center-of-mass mechanics and metabolic cost during walking," *IEEE Transactions on Neural Systems and Rehabilitation Engineering*, vol. 19, no. 4, pp. 411–419, 2011.

[70] C. Buesing, G. Fisch, M. O'Donnell, I. Shahidi, L. Thomas, C. K. Mummidisetty, K. J. Williams, H. Takahashi, W. Z. Rymer, and A. Jayaraman, "Effects of a wearable exoskeleton stride management assist system (sma®) on spatiotemporal gait characteristics in individuals after stroke: a randomized controlled trial," *Journal of Neuroengineering and Rehabilitation*, vol. 12, no. 1, pp. 1–14, 2015.

[71] K. Seo, Y. J. Park, J. Lee, S. Hyung, M. Lee, J. Kim, H. Choi, and Y. Shim, "Rnn-based on-line continuous gait phase estimation from shank-mounted imus to control ankle exoskeletons," in *2019 IEEE International Conference on Rehabilitation Robotics (ICORR)*, pp. 809–815, 2019.

[72] I. Kang, P. Kunapuli, and A. J. Young, "Real-time neural network-based gait phase estimation using a robotic hip exoskeleton," *IEEE Transactions on Medical Robotics and Bionics*, vol. 2, pp. 28–37, 2019.

[73] G. S. Sawicki, O. N. Beck, I. Kang, and A. J. Young, "The exoskeleton expansion: improving walking and running economy," *Journal of NeuroEngineering and Rehabilitation*, vol. 17, no. 1, pp. 1–9, 2020.

[74] W. Hong, N. Anil Kumar, and P. Hur, "A phase-shifting based human gait phase estimation for powered transfemoral prostheses," *IEEE Robotics and Automation Letters*, vol. 6, no. 3, pp. 5113–5120, 2021.

[75] H. T. T. Vu, F. Gomez, P. Cherelle, D. Lefeber, A. Nowé, and B. Vanderborght, "Ed-fnn: A new deep learning algorithm to detect percentage of the gait cycle for powered prostheses," *Sensors*, vol. 18, no. 7, p. 2389, 2018.

[76] J. Lee, W. Hong, and P. Hur, "Continuous gait phase estimation using lstm for robotic transfemoral prosthesis across walking speeds," *IEEE Transactions on Neural Systems and Rehabilitation Engineering*, 2021.

[77] B. Zhang, M. Zhou, W. Xu, *et al.*, "An adaptive framework of real-time continuous gait phase variable estimation for lower-limb wearable robots," *Robotics and Autonomous Systems*, vol. 143, p. 103842, 2021.

[78] H. T. T. Vu, D. Dong, H.-L. Cao, T. Verstraten, D. Lefeber, B. Vanderborght, and J. Geeroms, "A review of gait phase detection algorithms for lower limb prostheses," *Sensors*, vol. 20, no. 14, p. 3972, 2020.

[79] J. M. Jasiewicz, J. H. Allum, J. W. Middleton, A. Barriskill, P. Condie, B. Purcell, and R. C. T. Li, "Gait event detection using linear accelerometers or angular velocity transducers in able-bodied and spinal-cord injured individuals," *Gait & Posture*, vol. 24, no. 4, pp. 502–509, 2006.

[80] E. Allseits, J. Lučarević, R. Gailey, V. Agrawal, I. Gaunaurd, and C. Bennett, "The development and concurrent validity of a real-time algorithm for temporal gait analysis using inertial measurement units," *Journal of Biomechanics*, vol. 55, pp. 27–33, 2017.

[81] D. Kotiadis, H. J. Hermens, and P. H. Veltink, "Inertial gait phase detection for control of a drop foot stimulator: Inertial sensing for gait phase detection," *Medical Engineering & Physics*, vol. 32, no. 4, pp. 287–297, 2010.

[82] A. Mannini, V. Genovese, and A. M. Sabatini, "Online decoding of hidden markov models for gait event detection using foot-mounted gyroscopes," *IEEE Journal of Biomedical and Health Informatics*, vol. 18, no. 4, pp. 1122–1130, 2013.

[83] N. Abaid, P. Cappa, E. Palermo, M. Petrarca, and M. Porfiri, "Gait detection in children with and without hemiplegia using single-axis wearable gyroscopes," *PloS One*, vol. 8, no. 9, p. e73152, 2013.

[84] J. Bae and M. Tomizuka, "Gait phase analysis based on a hidden markov model," *Mechatronics*, vol. 21, no. 6, pp. 961–970, 2011.

[85] E. J. Rouse, L. J. Hargrove, E. J. Perreault, and T. A. Kuiken, "Estimation of human ankle impedance during the stance phase of walking," *IEEE Transactions on Neural Systems and Rehabilitation Engineering*, vol. 22, no. 4, pp. 870–878, 2014.

[86] H. Lee, E. J. Rouse, and H. I. Krebs, "Summary of human ankle mechanical impedance during walking," *IEEE Journal of Translational Engineering in Health and Medicine*, vol. 4, pp. 1–7, 2016.

[87] A. L. Shorter and E. J. Rouse, "Mechanical Impedance of the Ankle during the Terminal Stance Phase of Walking," *IEEE Transactions on Neural Systems and Rehabilitation Engineering*, vol. 26, no. 1, pp. 135–143, 2018.

[88] M. A. Holgate, T. G. Sugar, and A. W. Bohler, "A novel control algorithm for wearable robotics using phase plane invariants," in *2009 IEEE International Conference on Robotics and Automation (ICRA)*, pp. 3845–3850, IEEE, 2009.

[89] D. J. Villarreal and R. D. Gregg, "A survey of phase variable candidates of human locomotion," in *2014 36th Annual International Conference of the IEEE Engineering in Medicine and Biology Society (EMBC)*, pp. 4017–4021, IEEE, 2014.

[90] W. Hong, "Transfemoral prosthesis control for inclined walking using impedance control and bezier polynomial based optimization," Master's thesis, Texas A&M University, College Station, TX, USA, 2017.

[91] D. J. Villarreal and R. D. Gregg, "Unified phase variables of relative degree two for human locomotion," in *2016 38th Annual International Conference of the IEEE Engineering in Medicine and Biology Society (EMBC)*, pp. 6262–6267, IEEE, 2016.

[92] J. Mendez, S. Hood, A. Gunnel, and T. Lenzi, "Powered knee and ankle prosthesis with indirect volitional swing control enables level-ground walking and crossing over obstacles," *Science Robotics*, vol. 5, no. 44, 2020.

[93] F. Weigand, J. Zeiss, M. Grimmer, and U. Konigorski, "A novel approach for gait phase estimation for different locomotion modes using kinematic shank information," *IFAC-PapersOnLine*, vol. 53, no. 2, pp. 8697–8703, 2020.

[94] C. L. Vaughan, B. L. Davis, and J. C. OConnor, "Dynamics of human gait," 1999.

[95] Y. Liu, K. Lu, S. Yan, M. Sun, D. K. Lester, and K. Zhang, "Gait phase varies over velocities," *Gait & Posture*, vol. 39, no. 2, pp. 756–760, 2014.

[96] F. Hebenstreit, A. Leibold, S. Krinner, G. Welsch, M. Lochmann, and B. M. Eskofier, "Effect of walking speed on gait sub phase durations," *Human Movement Science*, vol. 43, pp. 118–124, 2015.

[97] "Robot operating system (ROS)." Accessed on: Dec. 2, 2021. [Online]. Available: "https://www.ros.org/".

[98] R. P. Kumar, J. Yoon, G. Kim, *et al.*, "The simplest passive dynamic walking model with toed feet: a parametric study," *Robotica*, vol. 27, no. 5, pp. 701–713, 2009.

[99] N. P. Fey, G. K. Klute, and R. R. Neptune, "Optimization of prosthetic foot stiffness to reduce metabolic cost and intact knee loading during below-knee amputee walking: a theoretical study," *Journal of Biomechanical Engineering*, vol. 134, no. 11, p. 111005, 2012.

[100] E. C. Honert, G. Bastas, and K. E. Zelik, "Effect of toe joint stiffness and toe shape on walking biomechanics," *Bioinspiration & Biomimetics*, vol. 13, no. 6, p. 066007, 2018.

[101] H.-J. Um, H.-S. Kim, W. Hong, H.-S. Kim, and P. Hur, "Design of 3d printable prosthetic foot to implement nonlinear stiffness behavior of human toe joint based on finite element analysis," *Scientific Reports*, vol. 11, no. 1, pp. 1–11, 2021.

[102] J. Zhu, Q. Wang, and L. Wang, "On the design of a powered transtibial prosthesis with stiffness adaptable ankle and toe joints," *IEEE Transactions on Industrial Electronics*, vol. 61, no. 9, pp. 4797–4807, 2013.

[103] D. A. Winter, *Biomechanics and Motor Control of Human Movement*. Wiley, 4 ed., 2009.

[104] N. Anil Kumar, W. Hong, and P. Hur, "Control of a transfemoral prosthesis on sloped terrain using continuous and nonlinear impedance parameters," in *2021 IEEE International Conference on Robotics and Automation (ICRA)*, pp. 3219–3225, IEEE, 2021.

[105] E. J. Rouse, L. J. Hargrove, E. J. Perreault, and T. A. Kuiken, "Estimation of human ankle impedance during walking using the perturberator robot," in *Biomedical Robotics and Biomechatronics (BioRob), 2012 4th IEEE RAS & EMBS International Conference on*, pp. 373–378, IEEE, 2012.

[106] K. R. Embry, D. J. Villarreal, R. L. Macaluso, and R. D. Gregg, "Modeling the kinematics of human locomotion over continuously varying speeds and inclines," *IEEE Transactions on Neural Systems and Rehabilitation Engineering*, vol. 26, no. 12, pp. 2342–2350, 2018.

[107] S. Hood, M. K. Ishmael, A. Gunnell, K. Foreman, and T. Lenzi, "A kinematic and kinetic dataset of 18 above-knee amputees walking at various speeds," *Scientific Data*, vol. 7, no. 1, pp. 1–8, 2020.

[108] W. Hong, "The supplemental video for the treadmill walking results with a powered transfemoral prosthesis using the phase-shifting method." `https://youtu.be/6JlfXk8XPRk`.

[109] A. Wolf, J. B. Swift, H. L. Swinney, and J. A. Vastano, "Determining lyapunov exponents from a time series," *Physica D: Nonlinear Phenomena*, vol. 16, no. 3, pp. 285–317, 1985.

[110] A. H. Nayfeh and B. Balachandran, *Applied nonlinear dynamics: analytical, computational, and experimental methods*. John Wiley & Sons, 2008.

[111] J. B. Dingwell and J. P. Cusumano, "Nonlinear time series analysis of normal and patho-logical human walking," *Chaos: An Interdisciplinary Journal of Nonlinear Science*, vol. 10, no. 4, pp. 848–863, 2000.

[112] J. B. Dingwell and L. C. Marin, "Kinematic variability and local dynamic stability of upper body motions when walking at different speeds," *Journal of Biomechanics*, vol. 39, no. 3, pp. 444–452, 2006.

[113] H. Kantz and T. Schreiber, *Nonlinear time series analysis*, vol. 7. Cambridge university press, 2004.

[114] R. Hegger, H. Kantz, and T. Schreiber, "Practical implementation of nonlinear time series methods: The tisean package," *Chaos: An Interdisciplinary Journal of Nonlinear Science*, vol. 9, no. 2, pp. 413–435, 1999.

[115] L. M. Silva and N. Stergiou, "The basics of gait analysis," *Biomechanics and Gait Analysis*.

[116] M. Perc, "The dynamics of human gait," *European Journal of Physics*, vol. 26, no. 3, p. 525, 2005.

[117] C. A. Fukuchi, R. K. Fukuchi, and M. Duarte, "A public dataset of overground and treadmill walking kinematics and kinetics in healthy individuals," *PeerJ*, vol. 6, p. e4640, 2018.

[118] J. Camargo, A. Ramanathan, W. Flanagan, and A. Young, "A comprehensive, open-source dataset of lower limb biomechanics in multiple conditions of stairs, ramps, and level-ground ambulation and transitions," *Journal of Biomechanics*, vol. 119, p. 110320, 2021.

[119] K. E. Zelik and A. D. Kuo, "Human walking isn't all hard work: evidence of soft tissue contributions to energy dissipation and return," *Journal of Experimental Biology*, vol. 213, no. 24, pp. 4257–4264, 2010.

[120] K. E. Zelik, K. Z. Takahashi, and G. S. Sawicki, "Six degree-of-freedom analysis of hip, knee, ankle and foot provides updated understanding of biomechanical work during human walking," *The Journal of Experimental Biology*, vol. 218, no. 6, pp. 876–886, 2015.

[121] M. J. Highsmith, B. W. Schulz, S. Hart-Hughes, G. A. Latlief, and S. L. Phillips, "Differences in the spatiotemporal parameters of transtibial and transfemoral amputee gait," *JPO: Journal of Prosthetics and Orthotics*, vol. 22, no. 1, pp. 26–30, 2010.

[122] C. Schreiber and F. Moissenet, "A multimodal dataset of human gait at different walking speeds established on injury-free adult participants," *Scientific Data*, vol. 6, no. 1, pp. 1–7, 2019.

[123] J. Taborri, E. Palermo, S. Rossi, and P. Cappa, "Gait partitioning methods: A systematic review," *Sensors*, vol. 16, no. 1, p. 66, 2016.

[124] J. S. S. Hochreiter, "Long short-term memory," *Neural Computation*, vol. 9, no. 8, pp. 1735–1780, 1997.

[125] J. S. A. Graves, "Framewise phoneme classification with bidirectional lstm and other neural network architectures," *Neural Networks*, vol. 18, no. 5–6, pp. 602–610, 2005.

[126] E. Scholz, H. Diener, J. Noth, H. Friedemann, J. Dichgans, and M. Bacher, "Medium and long latency emg responses in leg muscles: Parkinson's disease.," *Journal of Neurology, Neurosurgery & Psychiatry*, vol. 50, no. 1, pp. 66–70, 1987.